Technische Universität München
Wissenschaftszentrum Weihenstephan für Ernährung, Landnutzung und Umwelt

Lehrstuhl für Molekulare Ernährungsmedizin

Novel experimental strategies to assess the interplay between white adipocyte mitochondrial bioenergetics and systemic glucose homeostasis in C57BL/6 mice

Theresa Schöttl

Vollständiger Abdruck der von der Fakultät Wissenschaftszentrum Weihenstephan für Ernährung, Landnutzung und Umwelt der Technischen Universität München zur Erlangung des akademischen Grades eines

Doktors der Naturwissenschaften

genehmigten Dissertation.

Vorsitzende:	Univ.-Prof. Dr. H. Daniel
Prüfer der Dissertation:	1. Univ.-Prof. Dr. M. Klingenspor
	2. Univ.-Prof. Dr. D. Haller

Die Dissertation wurde am 03.09.2015 bei der Technischen Universität München eingereicht und durch die Fakultät Wissenschaftszentrum Weihenstephan für Ernährung, Landnutzung und Umwelt am 18.12.2015 angenommen.

TABLE OF CONTENT

GLOSSARY OF TERMS

GENERAL TERMS

AF	Adipocyte fraction
Anti A	Antimycin A
ADP	Adenosine diphosphate
ANOVA	Analysis of variance
ATP	Adenosine triphosphate
AUC	Area under the curve
(i)BAT	(Interscapular) Brown adipose tissue
BSA (-faf)	Bovine serum albumin (-fatty acid free)
CD	Control diet
(mt/n)DNA	Mitochondrial/nuclear deoxyribonucleic acid
DTNB	5,5'dithiobis(2-nitrobenzoic) acid
ELISA	Enzyme linked immunosorbent assay
ETC	Electron transport chain
FELASA	Federation of European Laboratory Animal Science Associations
FCCP	Carbonyl cyanide 4-(trifluoromethoxy) phenylhydrazone
H&E	Hematoxylin and eosin
HFD	High-fat diet
HF-recovery	High-fat diet recovery
HRP	Horseradish peroxidase
IRS-1	Insulin receptor substrate 1
NMR	Nuclear magnetic resonance
oGTT	Oral glucose tolerance test
Oligo	Oligomycin
OXPHOS	Oxidative phosphorylation
(qRT-)PCR	Quantitative real-time polymerase chain reaction
PEF	Phytoestrogen-free chow
POS	Polarographic oxygen sensor
(c)RCR	(Cell) Respiratory control ratio
ROS	Reactive oxygen species
Rot	Rotenone
RT	Room temperature
SD	Standard deviation
SDS-PAGE	Sodium dodecyl sulfate polyacrylamide gel electrophoresis

SKM	Skeletal muscle
SVF	Stromal vascular fraction
TAM	Tamoxifen
TCA cycle	Tricarboxylic acid cycle
mtUPR	Mitochondrial unfolded protein response
T2DM	Type 2 diabetes mellitus
(i/ps/e)WAT	(Posterior subcutaneous/inguinal/epididymal) white adipose tissue
XF96	XF96 Extracellular Flux Analyzer, Seahorse Bioscience
Wt	Wildtype

ENZYMES, GENES, HORMONES, RECEPTORS, TRANSCRIPTION FACTORS, ETC.

AdipoQ	Adiponectin
aP2	Adipocyte protein 2
CEBP	CCAAT-enhancer-binding protein
CHOP	C/EBP homologous protein
ClpP	Caseinolytic peptidase
CoA	Coenzyme A
Cre	Causes recombination
CS	Citrate synthase
GLUT4	Glucose transporter type 4
HSP	Heat shock protein
Hspd1	Heat shock 60kDa protein 1
JNK	C-Jun N-terminal kinase
loxP	Locus of crossover in P1 bacteriophage
Mc4r	Melanocortin-4 receptor
Retn	Resistin
PKR	Double-stranded RNA-activated protein kinase
TFAM	Mitochondrial transcription factor A
UCP1	Uncoupling protein 1

ABSTRACT

Obesity-related type 2 diabetes mellitus is a major global health burden. The mechanisms triggering the development of impaired glucose tolerance, insulin resistance and finally type 2 diabetes mellitus, however, are still not fully understood. Impaired mitochondrial function in white adipocytes is currently debated as a causative factor in this context. The discussion was initiated by a series of human und rodent obesity studies showing simultaneous occurrence of altered mitochondria in white adipose tissue, or isolated adipocytes, and impaired glucose tolerance. The mere fact that obesity is often accompanied by both impaired glucose homeostasis and reduced white adipocyte mitochondrial function, however, does not prove causality between both phenomena. Therefore, in this PhD thesis, the interrelation between white adipocyte mitochondrial function and systemic glucose homeostasis was analyzed.

In a first approach, using a novel protocol for detailed characterization of white adipocyte mitochondrial respiration, a key parameter of mitochondrial function, a higher respiratory capacity in adipocytes of subcutaneous fat compared to adipocytes of intraabdominal fat was observed in C57Bl/6N mice. Further, feeding these mice a high-fat diet for one week caused reduction in white adipocyte mitochondrial capacity. This limitation was more pronounced in intraabdominal as compared to subcutaneous adipocytes, and was paralleled by systemic glucose intolerance. Thus, the elevated metabolic risk associated with excessive intraabdominal versus subcutaneous white adipose tissue was indeed associated with differences in mitochondrial respiratory function between these types of body fat.

In a second approach, using four different mouse models of profound obesity with either normal or impaired glucose tolerance, reduced white adipocyte mitochondrial respiratory capacity was identified as a hallmark of excessive body fat. Consistently, a greater limitation was observed for intraabdominal versus subcutaneous adipocytes. Notably, white adipocyte mitochondrial impairment was demonstrated in both glucose tolerant and glucose intolerant obese mice, thus occurred irrespective of the glucose tolerance status.

In another approach, using inducible Cre-LoxP recombination technology, adipocyte-specific knockout of the mitochondrial matrix chaperonin heat shock protein 60 resulted in massively impaired mitochondrial function. This manipulation of mitochondrial physiology caused systemic glucose intolerance.

Altogether, marked differences in mitochondrial respiratory capacity of intraabdominal versus subcutaneous white adipocytes were revealed both in the lean state, as well as their divergent susceptibility to high dietary fat intake or elevated body fat. As a key finding, impaired respiratory capacity in white adipocytes turned out to be a general hallmark of weight gain and obesity, but not sufficient to affect systemic glucose homeostasis. Beyond respiratory capacity, however, massive generic impairment of white adipocyte mitochondrial functionality by disturbed proteostasis represents a potential risk and trigger for systemic glucose intolerance.

ZUSAMMENFASSUNG

Der Adipositas-assoziierte Typ 2 Diabetes mellitus hat sich zu einer erheblichen globalen Gesundheitsbelastung entwickelt. Die Mechanismen der Pathogenese dieser Erkrankung sind jedoch noch weitgehend ungeklärt. Derzeit wird eine Beeinträchtigung der Mitochondrienfunktion in weißen Adipozyten als ein kausaler Faktor in diesem Zusammenhang diskutiert. Die Grundlage für diese Debatte liefern zahlreiche Studien an fettleibigen Menschen und Nagetiermodellen, welche sowohl Veränderungen in den Mitochondrien im weißen Fettgewebe, als auch eine Beeinträchtigung der Glukosehomöostase aufzeigen. Die alleinige Tatsache, dass beide Parameter wiederholt parallel auftreten rechtfertigt jedoch noch keinen Rückschluss über einen möglichen kausalen Zusammenhang. Der Fokus dieser Doktorarbeit liegt entsprechend auf der Aufklärung des Einflusses der Mitochondrienfunktion in weißen Adipozyten auf die systemische Glukosehomöostase.

Basierend auf einem neu etablierten Protokoll zur Charakterisierung der respiratorischen Kapazität in Fettzellen, der Schlüsselfunktion der Mitochondrien, wurde zunächst herausgefunden, dass Adipozyten aus Subkutanfett von C57Bl/6N Mäusen über eine deutlich höhere respiratorische Kapazität verfügen als Adipozyten aus Intraabdominalfett. Zusätzlich konnte erarbeitet werden, dass eine einwöchige Fütterung dieser Mäuse mit einer Hochfett-Diät eine Reduktion der mitochondrialen respiratorischen Kapazität in Adipozyten beider Fettgewebstypen bewirkt. Verglichen mit Adipozyten aus Subkutanfett war das Ausmaß der Beeinträchtigung in Adipozyten aus Intraabdominalfett größer. Ferner wurde eine verminderte orale Glukosetoleranz festgestellt. Tatsächlich war zu diesem Zeitpunkt das metabolische Risiko, das mit erhöhtem Intraabdominalfett verbunden wird, mit einer reduzierten mitochondrialen Atmungskapazität dieses Körperfetttyps assoziiert.

An vier verschiedenen Mausmodellen für Fettleibigkeit, jeweils zwei mit normaler, sowie gestörter oraler Glukosetoleranz, konnte gezeigt werden, dass eine Reduktion der mitochondrialen Atmungskapazität eine generelle Begleiterscheinung von erhöhtem Körperfett darstellt. Wiederum war die Reduktion der mitochondrialen Kapazität in Adipozyten aus Intraabdominalfett stärker ausgeprägt als in Adipozyten aus Subkutanfett. Von höchstem Stellenwert ist hier, dass diese mitochondriale Einschränkung sowohl in Mäusen mit normaler, als auch mit verminderter oraler Glukosetoleranz auftrat. Demnach ist eine Reduktion der mitochondrialen Kapazität unabhängig vom Auftreten einer gestörten Glukosehomöostase.

In einem weiteren Ansatz wurde gezielt in die Mitochondrienphysiologie weißer Fettzellen eingegriffen, um schließlich die Folgen einer Störung der Mitochondrienfunktion für die Glukosehomöostase zu erforschen. Ein induzierbares, gewebsspezifisches Cre-loxP Rekombinations-Systems wurde angewandt, um die Expression des mitochondrialen Chaperonins Hitzeschockprotein 60 in Adipozyten auszuschalten. Letztlich konnte gezeigt werden, dass eine massive Beeinträchtigung der Mitochondrienphysiologie in Adipozyten in einer verminderten systemischen Glukosetoleranz resultiert.

Zusammenfassend zeigt diese Arbeit deutliche Unterschiede in der Mitochondrienfunktion zwischen subkutanen und intraabdominalen Adipozyten, sowohl bei schlanken, aus auch bei fettleibigen Mäusen. Bei jeder Form von Gewichtszunahme und Fettleibigkeit kommt es zu einer Reduktion der respiratorischen Kapazität in Adipozyten. Die mit Fettleibigkeit assoziierte Störung der Glukosehomöostase entwickelt sich jedoch unabhängig von dieser Art der mitochondrialen Veränderung. Eine schwere, nicht-spezifische Beeinträchtigung der Mitochondrienphysiologie, über die Funktion der respiratorischen Kapazität hinaus, ist dagegen als potentieller Auslöser von Glukoseintoleranz zu bewerten.

1 INTRODUCTION

"Corpulence is not only a disease itself, but the harbinger of others."
(Hippocrates, c. 460 – c. 370 BC).

In this sense, obesity-related type 2 diabetes mellitus (T2DM) has advanced to one of the major global health burdens affecting people of all ages in low-, middle-, as well as high-income countries. Currently around 310 million people suffer from T2DM and its complications. This number, as well as T2DM related death, will rise dramatically during the next years (WHO, 2015). Despite those tremendous costs on human health, the mechanisms causing systemic glucose intolerance, insulin resistance, and finally T2DM are still not fully understood (Rowe & Arany, 2014). Fueled by the obesity and T2DM epidemic, research interests are increasingly focusing on a clear understanding of white adipose tissue (WAT) biology in health and disease (Rosen & Spiegelman, 2014). On this basis, the present PhD project was initiated in order to clarify the impact of white adipocyte mitochondrial function on systemic glucose homeostasis.

1.1 WHITE ADIPOSE TISSUE IS A COMPLEX ORGAN

1.1.1 MORE THAN FUEL STORAGE- THE METABOLIC IMPACT OF WAT

WAT is now recognized as a highly dynamic and complex metabolic organ, but has not always been. Until the mid-20th century, WAT was simply thought to form a connective tissue containing lipid droplets - without any further metabolic meaning. The view on its metabolic impact improved when WAT was recognized as the body's long-term energy storage depot, with the ability to adapt lipogenesis and lipolysis to the bodys feeding state (Rosen & Spiegelman, 2014). A major breakthrough came in 1994 with the discovery of leptin as an adipocyte-derived hormone directed to brain, identifying WAT as an endocrine organ, with a key role in energy homeostasis regulation (Zhang *et al.*, 1994; Trayhurn & Beattie, 2001; Rosen & Spiegelman, 2014). Since then, several hundred WAT-derived bioactive secretory molecules, the majority of which are peptide hormones collectively referred to as adipokines, and their autocrine, paracrine, and endocrine effects have been identified and described (Fasshauer & Blüher, 2015). To our current understanding, WAT, far beyond the ancient paradigms, integrates an array of homeostatic processes on the systemic level (Trayhurn & Beattie, 2001; Rosen & Spiegelman, 2014). These include, among others, appetite and satiety control, energy expenditure, fat distribution, and insulin secretion and sensitivity (Blüher, 2012; Fasshauer & Blüher, 2015). Thus, WAT is a major regulator of nutritional, energy, and glucose homeostasis (Rosen & Spiegelman, 2014). The outstanding importance of WAT physiology for systemic metabolic health is highlighted by several

pathophysiological states of WAT associated with impaired glucose homeostasis including both loss (lipoatrophy, lipodystrophy) and excessive accumulation (obesity) of WAT, and lack of specific adipokines (leptin and adiponectin) (Garthwaite *et al.*, 1980; Shimomura *et al.*, 1998; Pajvani *et al.*, 2005; Nawrocki *et al.*, 2006; Kim *et al.*, 2007; Kless *et al.*, 2015).

1.1.2 SUBCUTANEOUS VERSUS VISCERAL - DIFFERENT TYPES OF WHITE ADIPOSE TISSUE

WAT is organized in multiple specific depots which are, according to their anatomical localization, either categorized to subcutaneous or visceral (also referred to as intraabdominal) (Cinti, 2012). While accumulation of extensive visceral fat mass represents an established risk factor for the development of metabolic diseases like insulin resistance and T2DM, large amounts of subcutaneous fat mass are metabolically unproblematic or even inversely associated with metabolic risk (Vague, 1956; Fox *et al.*, 2007; Hocking *et al.*, 2008; Tran *et al.*, 2008; Bjorndal *et al.*, 2011; Lee *et al.*, 2013; Hocking *et al.*, 2015). A wide range of physiological differences between the two types of white fat have been recognized, and are intensely discussed in the context of divergent metabolic risk (Montague & O'Rahilly, 2000). These include, among others, a higher rate of lipolysis in visceral than in subcutaneous fat (Richelsen *et al.*, 1991; Hellmer *et al.*, 1992), and differences in expression and secretion of adipokines (Alessi *et al.*, 1997; Montague *et al.*, 1997; Fried *et al.*, 1998). It has often been suggested that individual innervation and relation to the circulation could account for the divergent metabolic risk of visceral versus subcutaneous fat. The most prominent example is the venous system of the visceral fat depot that flows into the portal circulation flooding the liver with its products (Rosen & Spiegelman, 2014). Several lines of evidence, however, support that cell intrinsic mechanisms determine the depot-specific differences in adipocyte biology; gene expression, differentiation properties, and responses to environmental and genetic factors differ greatly between adipocyte precursor cells of subcutaneous and visceral fat (Macotela *et al.*, 2012). Very recently, a major ontogenetic difference has been uncovered between adipocytes of both origins (Chau *et al.*, 2014). Studies on regional WAT-transplantation validated this hypothesis: Implanting subcutaneous fat into the visceral cavity lowers body weight and body fat mass, and improves glucose tolerance, whereas transplantation of visceral fat does not (Hocking et al., 2008; Tran et al., 2008; Hocking et al., 2015). Thus, it is highly likely that cell-autonomeous differences account for the divergent metabolic risk associated with visceral versus subcutaneous fat (Rosen & Spiegelman, 2014).

1.1.3 MATURE WHITE ADIPOCYTES ARE THE PRIMARY CELL TYPE OF WAT

Mature lipid-laden white adipocytes constitute the primary cell type of WAT and clearly dominate the histological picture (Müller *et al.*, 2015). Lipid storage within the adipocyte varies greatly, and depends on physiological or pathological circumstances (Le Lay *et al.*,

2001). In times of negative energy balance, fatty acids are released from the lipid store, causing reduction of adipocyte size, and transferred to non-adipose tissues in need of energy. In times of positive energy balance, adipocyte lipid uptake, esterification, and storage, cause an increase in cell size and allow expansion of the adipose organ (Rutkowski *et al.*, 2015). Finally, adipocyte hypertrophy is the main cause for fat mass increase in obesity (Jo *et al.*, 2009), and has been associated with major alterations in cellular physiology, as well as systemic metabolic complications (Le Lay et al., 2001). Hypertrophic adipocytes are insulin resistant, indicated by reduced glucose transporter type 4 (GLUT4) trafficking to the plasma membrane, finally resulting in diminished insulin-dependent glucose uptake (Kim *et al.*, 2015). Lack of downstream effects of insulin signaling results in unregulated adipocyte lipolysis and ectopic lipid accumulation, aggravating whole body insulin resistance (Rutkowski et al., 2015). Besides, massively hypertrophic adipocytes were reported to show markedly altered adipokine secretion patterns (Skurk *et al.*, 2007). Altogether, several alterations in adipocyte biology and systemic glucose homeostasis have been associated with adipocyte hypertrophy– but the (cell-intrinsic) mechanisms determining these alterations remain to be elucidated.

1.2 MITOCHONDRIA ARE CENTRAL TO WHITE ADIPOCYTE PHYSIOLOGY

Intact mitochondrial function is essential for many different pathways in the adipocyte (Figure 1-1). First, mitochondria are crucial for ATP generation by oxidative phosphorylation (OXPHOS) to supply the cell with energy. Additional functions include the production and detoxification of reactive oxygen species (ROS), regulation of apoptosis, turnover of metabolites, synthesis of Fe-S clusters, regulation of calcium concentration in both cytoplasm and mitochondrial matrix and many more (Brand & Nicholls, 2011; Stehling *et al.*, 2014). In addition to these general functions, mitochondria fulfill adipocyte specific tasks (Forner *et al.*, 2009). ROS generated by complex III of the respiratory chain is needed to induce adipocyte differentiation. Concordantly, treatment of mesenchymal stem cells with mitochondrial targeted antioxidants inhibited differentiation into mature adipocytes (Tormos *et al.*, 2011). Further, adipocyte differentiation is inhibited upon impairment of OXPHOS by complex I blockade (Lu *et al.*, 2010). Next, proper mitochondrial function is crucial for lipogenesis (De Pauw *et al.*, 2009). On the one hand, mitochondria must provide “additional” ATP to supply highly energy-consuming lipogenic processes, while maintaining regular cellular activity (Lu et al., 2010). On the other hand, adipocytes must generate glycerol 3-phosphate for triglyceride synthesis and this is covered by a glyceroneogenic pathway and mitochondrial anaplerosis (Franckhauser *et al.*, 2002; Olswang *et al.*, 2002; De Pauw et al., 2009). Besides their role in lipogenesis, white adipocyte mitochondria are also essential for fatty acid degradation subsequent to lipolysis, indicated by the fact that the enzymes involved in beta-

oxidation are localized in the mitochondrial matrix (De Pauw et al., 2009). Notably, there is also evidence for an essential role of mitochondrial integrity for the production and secretion of adipokines. Consequently, mitochondrial impairment reduces adiponectin synthesis and secretion (Koh *et al.*, 2007; Frizzell *et al.*, 2009; Jeon *et al.*, 2012).

Taken together, the integration of mitochondria in numerous aspects of adipocyte physiology demonstrates the requirement of proper mitochondrial functioning for cellular, as well as systemic glucose homeostasis.

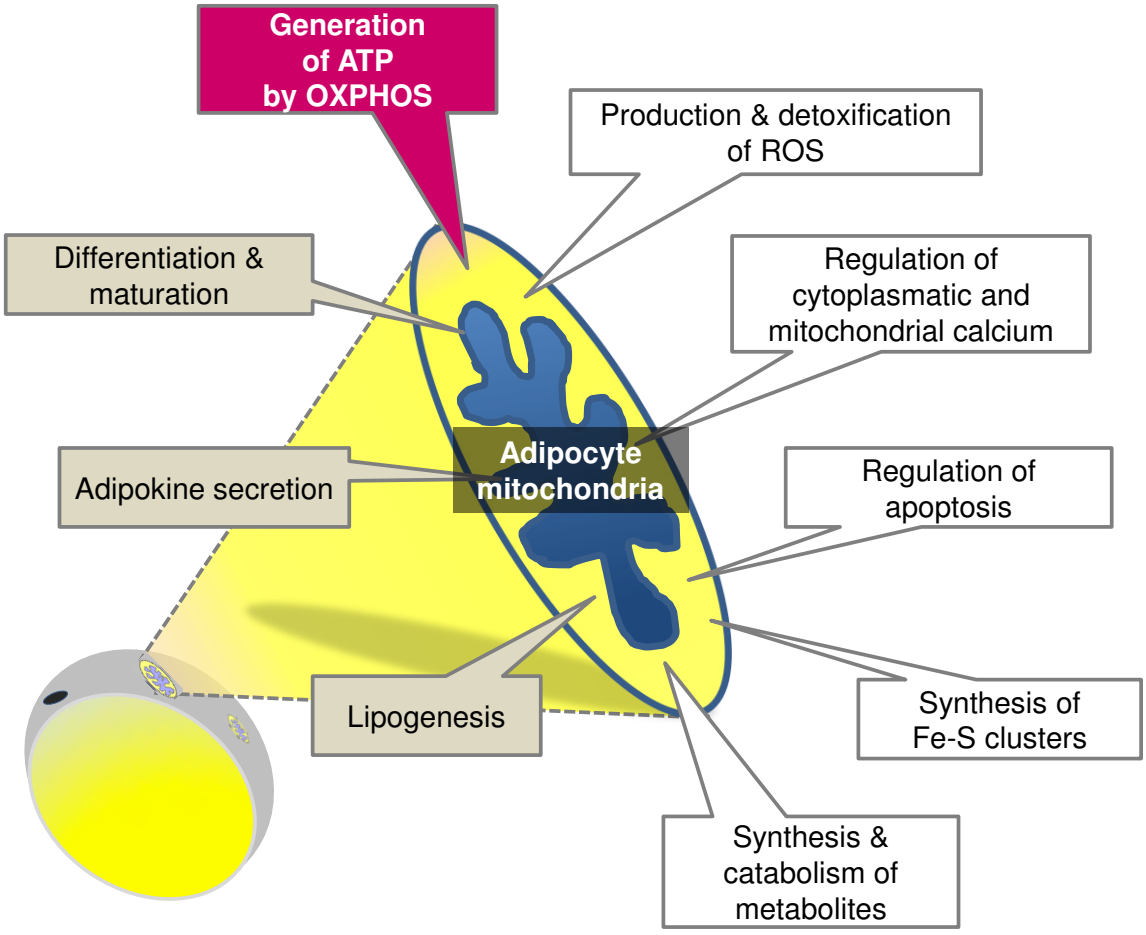

Figure 1-1. Mitochondrial functions in white adipocytes.
In addition to the requirement for general cellular physiology, mitochondria are essential for special aspects of adipocyte biology.
Pink background: ATP production by oxidative phosphorylation (OXPHOS) is commonly defined as the main function of mitochondria. White background: Further general mitochondrial functions. Grey background: Particular mitochondrial functions in white adipocyte physiology.
Abbreviations: ATP Adenosine triphosphate, OXPHOS oxidative phosphorylation, ROS reactive oxygen species.
(Franckhauser et al., 2002; Olswang et al., 2002; Koh et al., 2007; De Pauw et al., 2009; Frizzell et al., 2009; Lu et al., 2010; Brand & Nicholls, 2011; Tormos et al., 2011; Jeon et al., 2012; Stehling et al., 2014).

1.3 WHITE ADIPOCYTE MITOCHONDRIA ARE AFFECTED BY OBESITY

In 1989, mitochondrial oxygen consumption in human WAT has been demonstrated to be negatively related to total body fat (Hallgren *et al.*, 1989). Years before the discovery of WAT as an endocrine organ and its influence on the metabolism of other organs, these results were not discussed in a systemic context. In 2004, Wilson-Fritch *et al.* initiated the discussion about a potential link between mitochondrial capacity in white adipocytes and systemic metabolic health. First, they reported that, relative to cell volume, mitochondrial mass was reduced in adipocytes of obese and glucose intolerant $Lep^{ob/ob}$ versus lean and healthy control mice. Second, treating those mice with the insulin sensitizer rosiglitazone normalized blood glucose levels and at the same time increased mitochondrial biogenesis in white adipocytes. Based on these data, it has been suggested that mitochondrial capacity in white adipocytes may be related to whole-body glucose homeostasis and insulin sensitivity (Wilson-Fritch *et al.*, 2004). These findings induced a surge of further investigation on obesity-associated changes of white adipocyte (or total WAT) mitochondria and their relation to systemic glucose homeostasis, both in humans and rodent models. Meanwhile, numerous studies have demonstrated reduced mitochondrial biogenesis and abundance, gene transcripts encoding mitochondrial proteins, mitochondrial proteins, and different aspects of mitochondrial functionality in WAT or isolated adipocytes of obese and/or type 2 diabetic humans and rodents (Hallgren et al., 1989; Wilson-Fritch et al., 2004; Bogacka *et al.*, 2005; Choo *et al.*, 2006; Dahlman *et al.*, 2006; Valerio *et al.*, 2006; Kaaman *et al.*, 2007; Rong *et al.*, 2007; Sutherland *et al.*, 2008; Lindinger *et al.*, 2010; Yehuda-Shnaidman *et al.*, 2010; Christe *et al.*, 2013; Wang *et al.*, 2014; Fischer *et al.*, 2015). Downregulation of mitochondrial functioning represents an early response to high-fat diet feeding, that continuously deteriorates during prolonged high-fat diet exposure (Derous et al., 2015). In conclusion, these studies indubitably figured out that weight gain and obesity cause profound alterations in adipocyte or WAT mitochondria. It has not been clarified, however, whether white adipocyte mitochondrial defects are involved in the development of systemic glucose intolerance in obesity. The re-emerging question is whether impaired white adipocyte mitochondria are cause or consequence of the glucose intolerant phenotype associated with obesity (Rong et al., 2007; Pardo *et al.*, 2011; Kusminski & Scherer, 2012; Ryu *et al.*, 2013; Vernochet *et al.*, 2014). Possibly, they are not at all related to glucose tolerance, but are simply a phenomenon of excessive body fat. Beyond that, it has not been addressed whether differences in mitochondrial function in anatomical distinct fat – visceral/intraabdominal and subcutaneous – are contributing to the divergent metabolic risk associated with those distinct types of body fat.

1.4 AIMS OF THE PHD THESIS

The primary task of the present PhD project was to assess the impact of white adipocyte mitochondrial bioenergetics on systemic glucose homeostasis. C57Bl/6 mice, lean and healthy, as well as metabolically challenged by either high-fat diet feeding or genetic mutations affecting energy homeostasis or mitochondrial function served as experimental model system. A protocol for comprehensive functional analysis of white adipocyte mitochondria, including state-of-the-art respirometry of intact and permeabilized adipocytes, as well as isolated mitochondria, was established to clarify the following research questions:

(1) **CHAPTER I** – Is the divergent metabolic risk of excessive visceral/intraabdominal versus subcutaneous fat predetermined by a difference in mitochondrial function in white adipocytes from these types of body fat?

(2) **CHAPTER II** – Are alterations in white adipocyte mitochondrial respiratory function a specific phenomenon of obesity, glucose intolerance, or both? In case of the latter, is impaired adipocyte mitochondrial OXPHOS capacity a causative factor for the development of systemic glucose intolerance?

(3) **CHAPTER III** – What are the consequences of targeted disturbance of white adipocyte mitochondrial function on systemic glucose homeostasis?

In summary, the studies performed in the scope of this PhD project unprecedentedly characterized white adipocyte mitochondrial OXPHOS function of mice in different metabolic conditions. Profound differences in OXPHOS capacity of visceral/intraabdominal versus subcutaneous white adipocytes were revealed both in the lean state, as well as their divergent susceptibility to weight gain and obesity. Furthermore, these studies demonstrated that limitations in OXPHOS capacity solely are not sufficient to trigger the development of glucose intolerance. Finally, beyond OXPHOS impairment, massive and generic disturbance of white adipocyte mitochondria represents a potential risk and trigger for systemic glucose intolerance.

2 METHODOLOGY TO ASSESS WHITE ADIPOCYTE MITOCHONDRIAL BIOENERGETICS

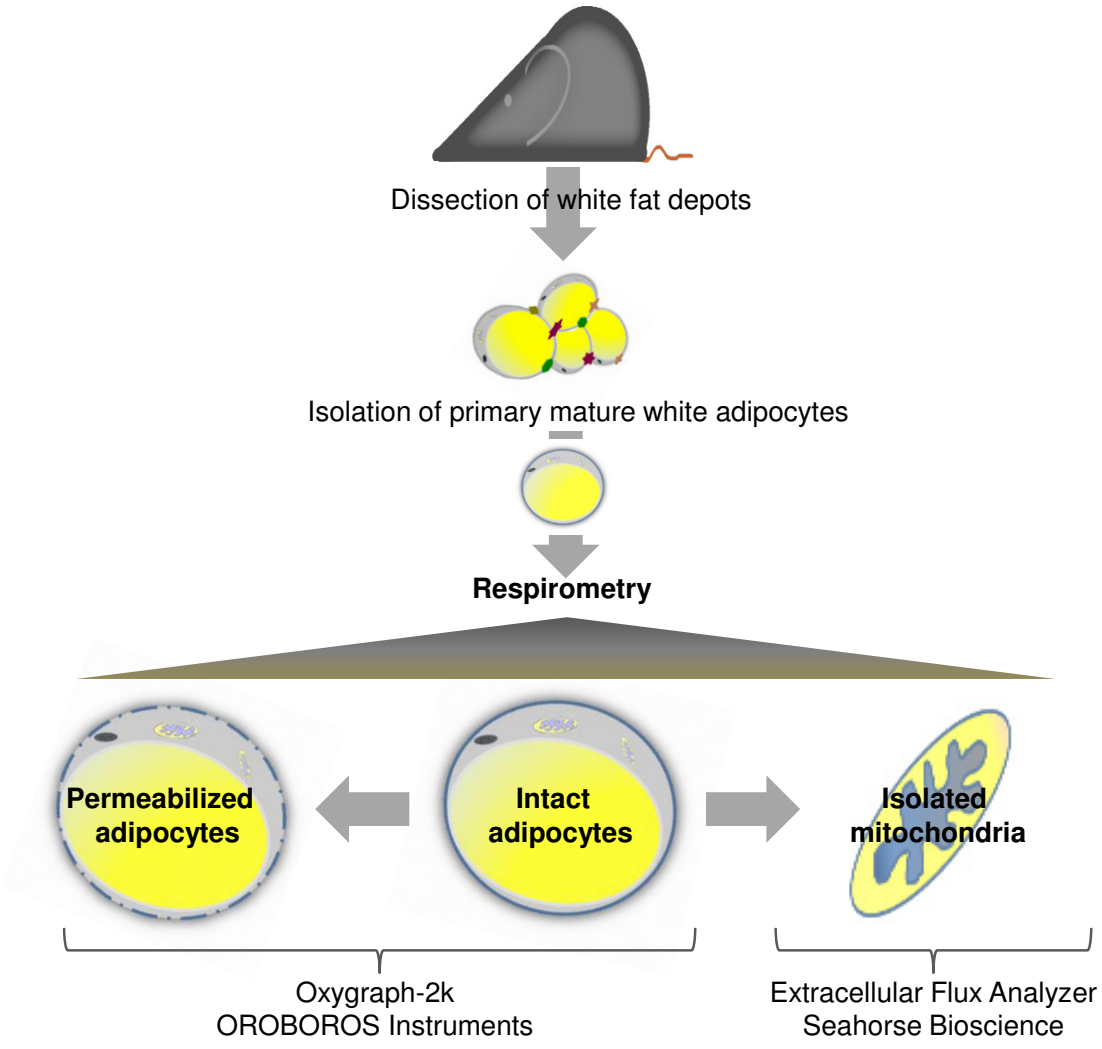

The cornerstone of the present PhD project was to establish a guideline for comprehensive characterization of white adipocyte mitochondrial bioenergetics. Recent technologies were applied to analyze mitochondrial respiration on three different levels, in intact adipocytes, in permeabilized adipocytes, as well as in isolated adipocyte mitochondria. Each approach has its strengths and weaknesses (Brand & Nicholls, 2011) (Figure 2-1), but the three approaches complement each other ideally. For isolated mitochondria additional techniques were applied to extend bioenergetic characterization by further parameters of mitochondrial functionality.

The established experimental design allows generating detailed bioenergetic fingerprints and is described in detail in this chapter[1]. Defects in mitochondrial bioenergetics can be dissected into alterations in mitochondrial mass per cell, alterations in organellar functionality itself, and alterations on the level of electron transport chain complexes.

	Intact adipocytes		**Permeabilized** adipocytes		**Isolated** mitochondria	
	Strengths	**Weaknesses**	**Strengths**	**Weaknesses**	**Strengths**	**Weaknesses**
Physiol. relevance, technical issues	Highest physiological relevance due to unaltered cellular environment.	Several substrates are cell-impermeant. Not all important respiratory states can be assessed.	All stimulators and inhibitors can be used, all substances reach mitochondria, all respiratory states can be assessed.		All stimulators and inhibitors can be used. No influence of cytosolic/ nuclear factors. Best method to study mechanisms.	No cellular context. Effects by loss of mitochondrial dynamcis.
Mitochondrial integrity	Mitochondrial dynamics are preserved. No damage of mitochondria.		No damage of mitochondria due to isolation.	Damage of mitochondria by permeabilization reagent possible.		Damage during isolation possible.
Data normalization		Challenge to find an appropriate normalization method– results depend on normalization to DNA, mitochondrial content, etc.		Challenge to find an appropriate normalization method– results depend on normalization to DNA, mitochondrial content, etc.	Values can be easily normalized to mitochondrial protein.	

Figure 2-1. Assessing mitochondrial bioenergetics in white adipocytes - strengths and weaknesses of different approaches (contents were adopted from (Brand & Nicholls, 2011)).

[1] Further methods and protocols, as well as detailed information on mouse models, mouse phenotyping, experimental diets, and statistics applied in this work are demonstrated in the appendix. Besides, all chemicals, enzymes, antibodies, equipment and material, and kit systems used are listed there.

2.1 CHARACTERIZATION OF PRIMARY MATURE WHITE ADIPOCYTES

2.1.1 DISSECTION OF WHITE ADIPOSE TISSUE DEPOTS

The posterior-subcutaneous (comprising gluteal, inguinal, and dorsolumbar fat depots) and the epididymal fat pads were chosen as representatives for subcutaneous and intraabdominal fat, respectively. Fat depots were dissected according to Cinti et *al.* (Cinti, 2002) (Figure 2-2). Large blood vessels were removed before fat depots underwent further processing.

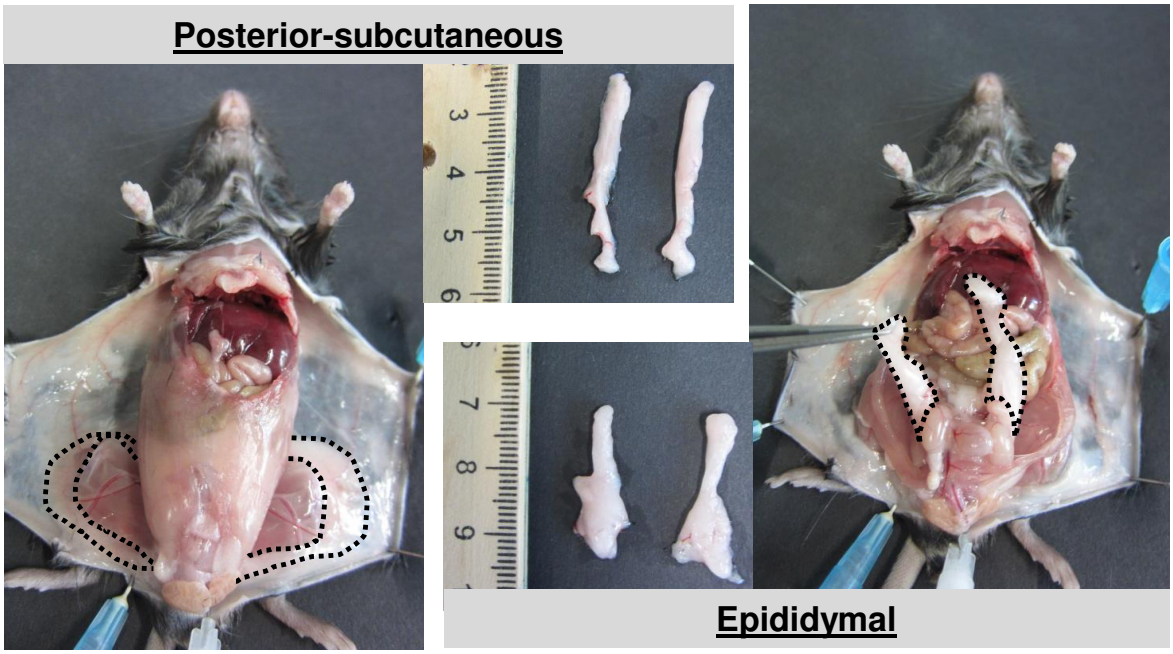

Figure 2-2. Dissection of posterior-subcutaneous and epididymal fat depots.
Demonstrated are respective fat depots in a male, 12 weeks old, chow diet fed C57Bl/6N mouse (indicated by the dotted line; sizes are indicated by centimeter scales).

2.1.2 ISOLATION OF MATURE WHITE ADIPOCYTES FROM ADIPOSE TISSUE

Total WAT was digested by collagenase and the resulting fat-suspension was centrifuged to separate mature white adipocytes from blood and cells of the stromal vascular fraction (Kanneganti & Dixit, 2012) (Figure 2-3).

Immediately after dissection, fat depots were transferred into WAT-digestion buffer (10 ml per fat depot) and minced by scissors (Figure 2-3A). For subsequent analyses on adipocytes (cellular level), fat depots of individual mice were used. For subsequent analyses on adipocyte mitochondria (organellar level), due to the low mitochondrial yield per ml adipocyte suspension, fat depots of 8-12 mice were combined. The adipose-suspension was transferred into a falcon tube (15 ml tubes for single fat depots, 50 ml tubes for pooled fat

depots) and gently shaken at 37 °C (Wisd laboratory instruments, 150 rpm, guidance values: inguinal fat 30 minutes, epididymal fat 20 minutes. Figure 2-3B). Still aggregated particles were manually disrupted using a pasteur pipette (PLASTIBRAND). Lymph nodes and undigested tissue were removed by filtering the solution through a 250 µM nylon gauze (Schwegmann Filtrations-Technik, Figure 2-3C). After low speed centrifugation (300g, 2 min, RT, Figure 2-3D), mature adipocytes accumulated on top of the liquid phase (Figure 2-3E). WAT-digestion buffer containing blood and cells of the stromal vascular fraction were withdrawn (Figure 2-3G). For following experiments except protein isolation, adipocytes were washed once with standard STE and twice with STE-BSA. For subsequent protein isolation, all washing steps were conducted with standard STE buffer (to avoid protein contamination by BSA).

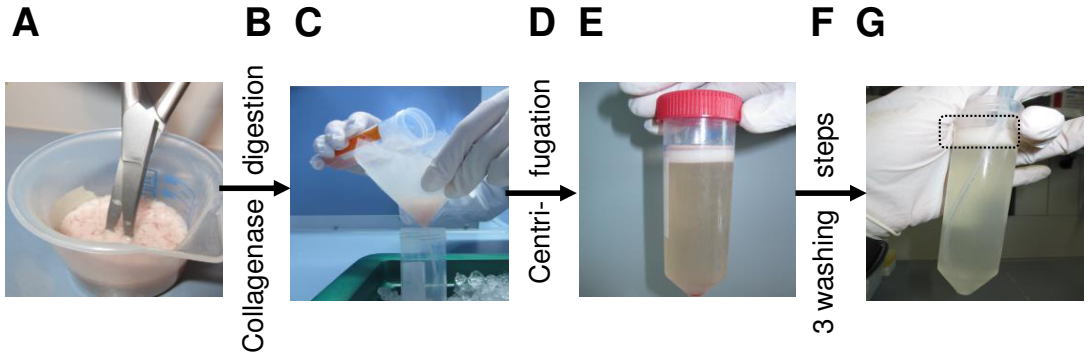

Figure 2-3. Isolation of mature white adipocytes from white adipose tissue depots.
(A) After dissection, fat depots were transferred into WAT-digestion buffer, minced by scissors, transferred into a falcon tube, and **(B)** digested by collagenase. **(C)** Afterwards, the fat suspension was filtered through a nylon mesh. **(D)** Low spin centrifugation allowed separation of **(E)** mature adipocytes (white top phase) from buffer (brownish liquid phase) and cells of the stromal vascular fraction (red pellet). **(F)** Adipocytes were further purified by three washing steps. **(G)** Purified adipocytes (indicated by the dotted line) were used for bioenergetic characterization, etc.

WAT-digestion buffer	1 mg/ml collagenase A in 1 x Hank's Balanced Salt Solution, 4% BSA
Standard STE buffer	250 mM sucrose, 5 mM TRIS, 2 mM EGTA, pH=7.4 at 4°C
STE-BSA buffer	Standard STE buffer containing 4% essentially fatty acid-free BSA

2.1.3 MEASUREMENT OF MITOCHONDRIAL OXYGEN CONSUMPTION IN INTACT AND PERMEABILIZED WHITE ADIPOCYTES

Oxygen consumption of adipocytes was assessed amperometrically using the Oxygraph-2k (OROBOROS INSTRUMENTS). The polarographic oxygen sensor (OroboPOS) represents the core of the high-resolution respirometry system and is based on a clark-type electrode. The OroboPOS comprises a gold cathode which is polarized negatively to a silver anode (-0.8V). A saturated potassium chloride solution allows connection of the electrodes.

Molecular oxygen diffuses from the incubation chamber through a semipermeable teflon membrane and becomes reduced at the cathode (Pesta & Gnaiger, 2012). The anode becomes oxidized. Overall electrochemical process that occurs is:

Cathode: $O_2 + 2H_2O + 4e^- \rightarrow 4\ OH^-$

Anode: $4\ Ag + 4\ Cl - 4e^- \rightarrow 4\ AgCl$

The electrical current is directly proportional to the oxygen partial pressure (pO_2) inside the incubation chamber (Pesta & Gnaiger, 2012). DatLab software (OROBOROS INSTRUMENTS, version 6) allows on-line data acquisition and analysis after a current-to-voltage conversion, amplification, and an analog-digital conversion.

pO_2 is converted to oxygen concentration [µM], with regard to the oxygen solubility of the respiration buffer (Pesta & Gnaiger, 2012). Chamber assembly, OroboPOS service, membrane mounting, and instrumental background correction were performed as described in the manufacturer's protocol. Two-point OroboPOS calibration was conducted with air-saturated respiration buffer (MIR05, 100% oxygen, ~ 183 nmol O_2/ml) and zero oxygen by sodium dithionite addition.

Assay preparation

100 µl of adipocyte suspension in STE-BSA were added to 2 ml mitochondrial respiration buffer (MIR05) using a cut pipette tip. The chamber was closed, the stirrer speed set to 750 rpm, and the temperature to 37°C.

***Intact adipocytes** – assay procedure*

For oxygen consumption measurements of intact adipocytes, pyruvate and malate was injected and basal cellular respiration was recorded (Figure 2-4). Oligomycin was injected and proton leak respiration was assessed. Titration of carbonyl cyanide 4-(trifluoromethoxy) phenylhydrazone (FCCP) was performed for measuring maximal cellular respiration rates. Non-mitochondrial oxygen consumption was determined by addition of antimycin A and subtracted from the other respiratory states. Spare respiratory capacity (Equation 2-1) and cell respiratory control ratio (cRCR) were calculated (Equation 2-2) to judge mitochondrial function. After the measurements were finished, adipocytes (in MIR05 buffer) were transferred into 15 ml falcon tubes and stored at -20°C until further use (quantification of DNA).

$$Spare\ respiratory\ capacity = max - basal \quad (2\text{-}1)$$

$$cRCR = \frac{oxygen\ consumption\ in\ presence\ of\ FCCP}{oxygen\ consumption\ in\ presence\ of\ oligomycin} = \frac{maximal}{basal} \quad (2\text{-}2)$$

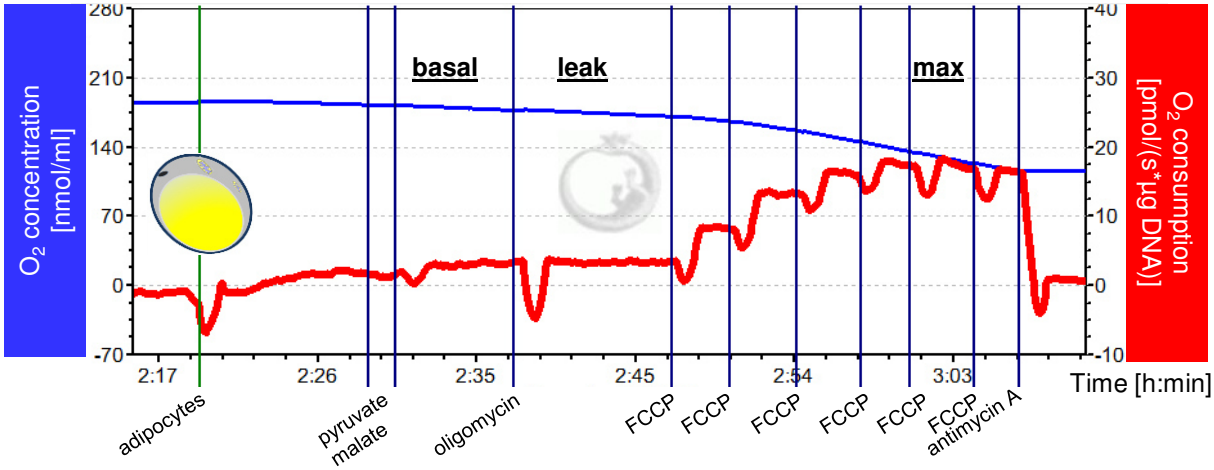

Figure 2-4. Representative on-line oxygen consumption measurement of intact white adipocytes using the Oxygraph-2k.
The blue graph reflects oxygen concentration in the incubation chamber, the red graph reports normalized oxygen consumption. The green vertical mark indicates addition of adipocytes. Injection of stimulators or inhibitors of the respiratory chain are indicated by blue vertical marks. States: basal = oxygen consumption determined by proton leak and ATP production; leak= proton leak driven oxygen consumption after ATP-synthase blockade by oligomycin, max= maximal respiratory capacity achieved by titration of the chemical uncoupler FCCP. Afterwards, all values are corrected for non-mitochondrial background determined by inhibition of electron flow at complex III through antimycin A.

Digitonin-permeabilized adipocytes *– assay procedure*

Adipocyte plasma membranes were permeabilized by digitonin (Figure 2-5). The working concentration of 2 µM was adopted from a publication of Kraunsøe *et al*. Pilot experiments using a range from 0–10 µM identified that this concentration enables optimal permeabilization of adipocytes in biopsies, without leading to cell damage (Kraunsoe *et al*., 2010). State 4 respiration was induced by succinate. Rotenone was added to block reverse electron flow. Injection of ADP induced phosphorylating state 3 respiration. ATP production was inhibited by oligomycin (state 4o). Titration of FCCP was performed for measuring maximal cellular respiration rates (state 3u). Terminology of respiratory states refers to Brand and Nicholls (Brand & Nicholls, 2011). Non-mitochondrial background was assessed in presence of antimycin A and subtracted from the other respiratory states. As marker for mitochondrial function and integrity, respiratory control ratio (RCR) was calculated (Equation 2-3). As for intact cells, adipocytes in MIR05 buffer were transferred into 15 ml falcon tubes and stored at -20°C until assignment for DNA quantification.

$$RCR = \frac{oxygen\ consumption\ in\ presence\ of\ substrate\ and\ ADP}{oxygen\ consumption\ in\ presence\ of\ oligomycin} = \frac{state\ 3}{state\ 4o} \qquad (2\text{-}3)$$

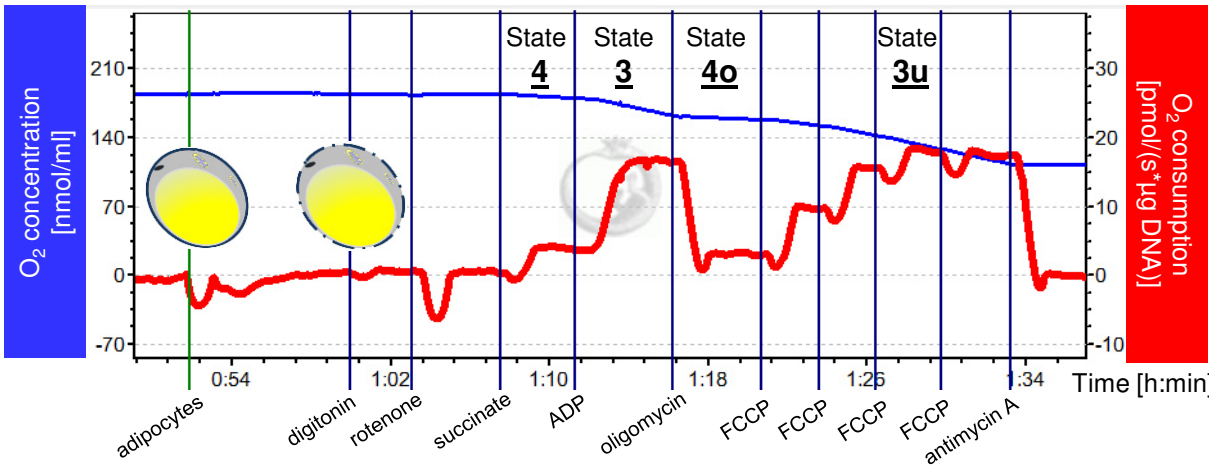

Figure 2-5. Representative on-line oxygen consumption measurement of digitonin permeabilized white adipocytes using the Oxygraph-2k.
The blue graph reflects oxygen concentration in the incubation chamber, the red graph reports normalized oxygen consumption. The green vertical mark illustrates addition of adipocytes. Injection of stimulators or inhibitors of the respiratory chain are indicated by blue vertical marks. States: state 4 = substrate driven respiration (complex II substrate succinate with blockade of reverse electron flow by rotenone; state 3 = phosphorylating respiration in presence of substrate and ADP; state 4o = proton leak respiration after ATP-synthase blockade by oligomycin, state 3u = maximal uncoupled respiration achieved by titration of the chemical uncoupler FCCP. Afterwards, all values are corrected for non-mitochondrial background determined by inhibition of electron flow at complex III through antimycin A.

KCL electrolyte	1M KCL in H_2O
Sodium dithionite solution	10 mM $Na_2S_2O_4$ in phosphate buffer (44 mM Na_2HPO_4 * 2 H_2O, 5.9 mM NaH_2PO_4 * H_2O, ph 8.0, as described by OROBOROS INSTRUMENTS)
MIR05 buffer	110 mM Sucrose, 60 mM potassium lactobionate, 0.5 mM EGTA, 3 mM $MgCl_2$ * $6H_2O$, 20 mM taurine, 10 mM KH_2PO_4, 20 mM HEPES, 1g/l BSA-essentially fatty acid free, pH 7.1 with 5 N KOH at 30°C, as described by OROBOROS INSTRUMENTS
Final concentrations	Substrates: 5 mM succinate (+ 2 µM rotenone), 5 mM pyruvate + 5 mM malate, 5 mM ADP Inhibitors: 2.5 µg/ml oligomycin, 4 µM antimycin A, Others: 2 µM digitonin, 0.5 µM titration steps of FCCP

Combination of both approaches, respirometry of intact and permeabilized adipocytes, allows comprehensive determination of mitochondrial bioenergetics on the cellular level with special regard to the ATP generating machinery.

Normalization of oxygen consumption to DNA

Oxygen consumption of adipocytes was normalized to genomic DNA (gDNA) content by quantitative real-time polymerase chain reaction (qRT-PCR), allowing data presentation as [pmol O_2/(s*µg DNA)].

Adipocyte samples stored at -20°C were thawed on ice. After vigorous vortexing, 100 µl adipocyte suspension were transferred into a 1.5 ml tube and diluted 1:5 in lysis buffer.

Samples were digested for 1h at 65°C under agitation (1,000 rpm). Proteinase K was inactivated at 95°C for 10 min. Samples were put on ice and 2.25 volumes phenol:chloroform:isoamyl alcohol (25:24:1) were added. After vortexing and phase separation by centrifugation at 16,000g for 5 min, the hydrophilic phase containing nucleic acids was directly employed to qRT-PCR analysis according to Table 2-1. Primers were targeted 5' to the resistin (*Retn*) gene. DNA concentrations were calculated with due regard to dilution factors referring to a mouse gDNA standard series of known concentrations.

Table 2-1. DNA quantification by qRT-PCR for normalization of oxygen consumption measurements.

qRT-PCR mix (one reaction)		**qRT-PCR program**			
Substance	**Volume [µl]**	**Step**	**Temperature [°C]**	**Time [s]**	**Cycles**
SensiMix SYBR No-ROX	6.25	Initialization	97	420	
Forward primer [5 pmol/µl]	0.625	Denaturing	97	10	45
Reverse primer [5 pmol/µl]	0.625	Annealing	59	15	
Nuclease-free water	4	Elongation	72	20	
Genomic DNA extract	1	Cooling	4	∞	

Forward primer 5'-ACCTCTCTTGGGGTCAGATGT-3'
Reverse primer 5'-CTGGGTATTAGCTCCTGTCCC-3'
Primers were designed by Dr. Christoph Hoffmann

Lysis buffer: 10 mM TRIS in H_2O - pH 8.3 with 6 N HCL, 50 mM KCL, 0.45% Nonidet P-40, 0.45% Tween 20, 0.2 mg/ml Proteinase K

2.1.4 DETERMINATION OF MITOCHONDRIAL MASS

Determination of mitochondrial abundance represents an important factor in the quantitative assessment of cellular or tissue oxidative capacity. Here, activity of tricarboxylic acid (TCA) cycle enzyme citrate synthase (CS) and mitochondrial DNA abundance were chosen as surrogate measures for mitochondrial content.

Determination of citrate synthase activity

CS catalyzes the initial reaction of the TCA by formation of citrate from acetyl-CoA and oxaloacetate thereby releasing coenzyme A (CoA). Thiol-groups of CoA cleave 5,5'dithiobis(2-nitrobenzoic) acid (DTNB) in the CS-assay medium releasing yellow NTB^{2-}.
The reaction can be quantified spectrophotometrically by measuring absorbance at 412 nm.
Adipocyte suspensions were diluted 1:25 in CS-lysis buffer to a final volume of 400 µl and homogenized using an Ultra-Turrax (30 sec. level 2, IKA). For one reaction 10 µl of adipocyte homogenates or CS-lysis buffer for negative control were mixed with 240 µl CS-assay medium. Measurements were performed in duplicates at 30°C in a 96-well microplate format (Greiner, microplate reader TECAN). After a forerun period of 5 kinetic cycles à 1 min 50 µl oxaloacetate solution were injected to initiate CS activity. Measurements were continued for 10 kinetic cycles. CS activity of adipocyte suspensions was calculated according to Equation 2-4.

$$CS\ activity\ [U/\mu g\ DNA] = \frac{(slope\ after\ oxaloacetate - slope\ before\ oxaloacetate) * DF}{extinction\ coefficient\ of\ DTNB * path\ length\ of\ plate * \mu g\ DNA} \quad (2\text{-}4)$$

(CS = citrate synthase, DF = dilution factor (30),
extinction coefficient of DTNB = 13.6 ml * µmol^{-1} * cm^{-1} (Alexson & Nedergaard, 1988), path length of plate filled with 300 µl suspension = 0.75 cm. DNA concentrations were determined as described in 2.2.4.)

CS-lysis buffer	MIR05 buffer, 1% Tween 20
MIR05 buffer	110 mM Sucrose, 60 mM potassium lactobionate, 0.5 mM EGTA, 3 mM $MgCl_2$ * $6H_2O$, 20 mM taurine, 10 mM KH_2PO_4, 20 mM Hepes, 1g/l BSA-essentially fatty acid free, pH 7.1 with 5 N KOH at 30°C, as described by OROBOROS INSTRUMENTS
CS-assay medium	100 mM TRIS, 1 mM EDTA, 1 mM $MgCl_2$, 0.1 mM DTNB (freshly added) 0.36 mM Acetyl-CoA (freshly added), pH 8.2
Final concentrations	Substrates: 0.5 mM oxaloacetate

Quantification of mitochondrial genome copy number

Mitochondrial DNA was related to nuclear DNA as marker for mitochondrial content of cells or tissues as established by Dr. Tobias Fromme (TU München). This method is based on qRT-PCR with primers targeting sequences exclusively in either the mitochondrial or the nuclear genome.

DNA was isolated from snap-frozen adipocytes (40 µl) using the Wizard® SV Genomic DNA Purification System following the manufacturer's protocol. DNA yield was measured spectrophotometrically (TECAN) and diluted to a concentration of 25 ng/µl in nuclease-free water. The qRT-PCR was performed in a Roche LightCycler®480 (96-well format). Measurements were performed in technical duplicates. PCR amplification was quantified by specific probes (Roche) (Table 2-2). Mitochondrial or nuclear DNA content, respectively, were calculated for every replicate separately according to Equation 2-5. Finally, means of technical replicates were determined to calculate the ratio of mitochondrial DNA to nuclear DNA.

$$DNA\ [arbitrary\ units] = \frac{10^6}{2^{Cp}} \qquad (2\text{-}5)$$

(with C_p = crossing point-PCR-cycle; indicates the cycle at which amplification-related fluorescence exceeds background).

Table 2-2. Quantification of mitochondrial genome copy number by qRT-PCR.

qRT-PCR Mix (one reaction)		**qRT-PCR Program**			
Substance	**Volume [µl]**	**Step**	**Temperature [°C]**	**Time [s]**	**Cycles**
2x Mastermix (LightCycler®480 ProbesMaster, Roche	5.0	Initialization	95	300	
Forward primer [20 µmol/l]	0.2	Denaturing	95	10	
Reverse primer [20 µmol/l]	0.2	Annealing	60	20	
Probe	0.2				45
Nuclease free water	0.4	Elongation	72	2	
DNA [25 ng/µl]	4	Final elongation	72	180	
∑	10				

Target: Mitochondrial genome
Forward primer: 5'-CAAATTTACCCGCTACTCAACTC-3'
Reverse primer: 5'-GCTATAATTTTTCGTATTTGTGTTTGG-3'
Location chrM: 4343+4452; probe no. 101, Universal Probe Library, Roche - Cat. No. 04692195001.

Target: Nuclear genome
Forward primer: 5'-TTTACAGGATCTCCAAGATTCAGA-3'
Reverse primer: 5'-GATCACCCCATGTGAACAAA-3'
Location chr8: 1000128+31000199; probe no 26, Universal Probe Library, Roche - Cat. No. 04687574001.

2.2 CHARACTERIZATION OF ISOLATED MITOCHONDRIA

2.2.1 ISOLATION OF MITOCHONDRIA FROM WHITE ADIPOCYTES

Isolation of mitochondria from white adipocytes is based on homogenization followed by differential centrifugation (Figure 2-6). The homogenate is separated according to differences in size and density of cellular components.

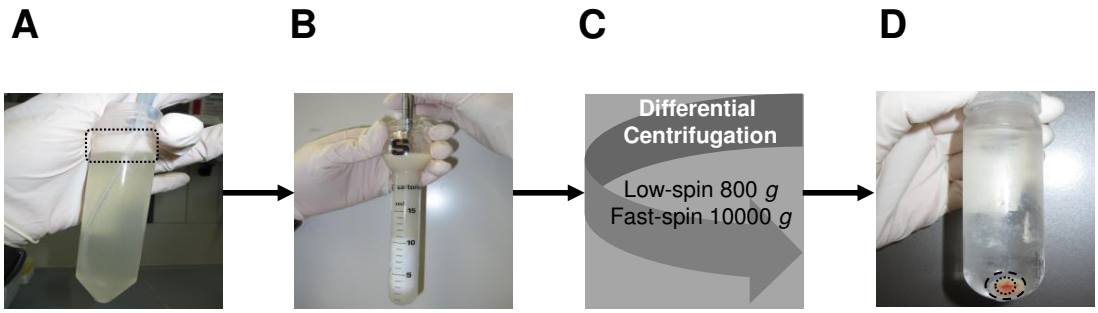

Figure 2-6. Isolation of mitochondria from white adipocytes by homogenization and subsequent differential centrifugation.
(A) After several washing procedures, floating white adipocytes (indicated by the dashed line) are transferred to a **(B)** glass-teflon homogenizer: adipocytes are carefully homogenized by 5 rotating strokes. **(C)** Low-spin and following fast-spin centrifugation allow isolation of mitochondria from the adipocyte homogenate. **(D)** Finally, mitochondria, indicated by the brownish part of the pellet (dashed line) are resuspended in KHE buffer for further analysis. Red apparent blood contaminations of the pellet, indicated by the central dotted line, are discarded.

Procedures were conducted using ice-cold equipment and buffers. Freshly isolated adipocytes were transferred into a 15-ml glass-teflon homogenizer (Sartorius), filled up to 15 ml with STE-BSA, and homogenized manually by 5 rotating strokes (Figure 2-6A and B). Homogenates were transferred into a 40-ml centrifuge tube, filled with STE-BSA up to 30 ml and centrifuged at 800g and 4°C for 10 min (Figure 2-6C). The top layer (fat, still intact adipocytes) was returned into the homogenizer, the middle phase (buffer including organelles) was transferred into a new 40-ml centrifuge tube and the pellet (cell debris and nuclei) was discarded. In order to enhance mitochondrial yield, homogenization of the top layer and subsequent low-spin centrifugation was repeated as described. Afterwards, the middle phase of both low-spin runs was centrifuged at 10,000g and 4°C for 10 min. The supernatant was discarded and mitochondria, forming the pellet (Figure 2-6D), were carefully resuspended in 30 ml STE-BSA using a common paint brush. For further purification of mitochondria, fast-spin centrifugation was repeated once. Again, the supernatant was discarded and the pellet was resuspended in 210 µl KHE buffer. Purified mitochondria were transferred into a 1.5 µl tube using a cut pipette tip.

2.2.2 DETERMINATION OF MITOCHONDRIAL PROTEIN CONCENTRATION

Protein concentrations of mitochondrial suspensions were determined in a 96-well format using a commercial Bradford assay kit (Carl Roth, all procedures according to manufacturer's

instructions). Therefore, mitochondria were diluted 1:200 in KHE buffer. Measurements were performed in technical duplicates. Protein concentrations were calculated referring to a standard series (0-0.1 mg/ml BSA in KHE buffer). Values were corrected for KHE-BSA-dependent absorbance.

2.2.3 BIOENERGETIC PROFILING

Bioenergetic profiles of isolated white adipocyte mitochondria were ascertained using the Seahorse *XF96* Extracellular Flux Analyzer. Based on a 96 well microplate-cartridge system, this technique enables measuring oxygen consumption of mitochondria via fluorescent sensors (Figure 2-7) (Ferrick *et al.*, 2008). Multiple technical and biological replicates can be assessed within one measurement by simultaneously using very small amounts of mitochondria (Rogers *et al.*, 2011). Basic parameters were adopted from a protocol developed for respirometry of liver mitochondria using the *XF24* (Rogers et al., 2011).

Assay preparation

Cartridges were hydrated overnight in a non-CO_2 incubator at 37°C using the *XF96* Calibrant solution (200 µl per well). *XF96*-PS cell culture plates were coated with collagen. All media and compounds were warmed to 37ºC in a water bath.

Assay procedure

Isolated white adipocyte mitochondria were seeded in collagen coated *XF96*-PS cell culture plates (5 µg mitochondrial protein per well, diluted in 20 µl KHE buffer containing substrate: succinate/rotenone or pyruvate/malate or palmitoyl-L-carnitine/malate; Figure 2-7A). By centrifugation (Eppendorf 5804 R) at 2,000g for 20 min at 4°C, mitochondria were attached to the bottom of the plate. After mitochondria acclimatized to RT for 5 min, 180 µl KHE buffer containing substrate (see above) were added. Mitochondria were incubated for 30 min in the *XF* incubator at 37°C before the measurement was started.

Measurements were performed in 8 technical replicates. First, mitochondrial oxygen consumption was measured in the presence of substrate only (state 4, Figure 2-7B). ADP was injected to promote maximal phosphorylating respiration (state 3). ATP-synthase was inhibited by addition of oligomycin. Remaining oxygen consumption is defined as basal proton leak (state 4o). The chemical uncoupler FCCP was injected to assess maximal uncoupled respiration (state 3u). Finally, mitochondrial electron flow was inhibited by antimycin A and rotenone. Remaining non-OXPHOS background was subtracted from values of the other conditions. Oxygen consumption rates were calculated by plotting oxygen concentration (nmoles O_2) versus time (min), using the original (gain) fixed algorithm of the *XF* Software, and normalized to mitochondrial content [nmol/(min*mg protein)]. Respiratory

control ratios were ascertained by dividing oxygen consumption during state 3 respiration by oxygen consumption during state 4o respiration (Equation 2-2).
The standard assay protocol is demonstrated in appendix 6.5.

KHE buffer	120 mM KCL, 5 mM KH_2PO_4, 3 mM HEPES, 1 mM EGTA, 0.5% BSA essentially fatty acid free, pH 7.2 with KOH at RT
Final concentrations	Substrates: 5 mM succinate (+ 2 µM rotenone), 5 mM pyruvate + 5 mM malate, 40 µM palmitoyl-L-carnitine + 5 mM malate, 6 mM ADP Inhibitors: 2.5 µg/ml oligomycin, 4 µM antimycin A Others: 4 µM FCCP

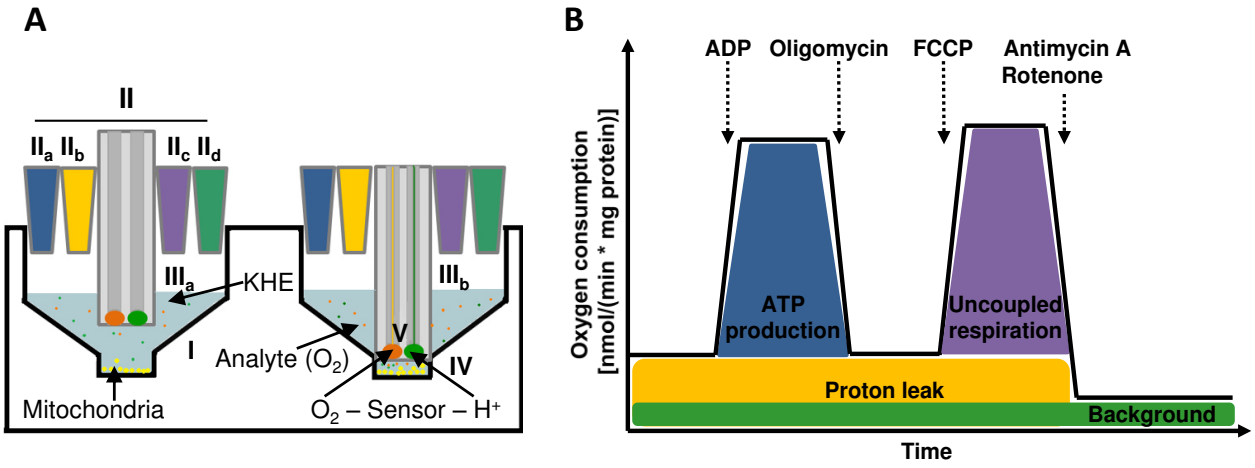

Figure 2-7. Schematic illustration of *XF96* mircoplate based respirometry.
(A) I) Collagen coated *XF96* cell culture microplates. II) Four drug delivery ports in the cartridge allow successive delivery of IIa) ADP IIb) Oligomycin IIc) FCCP IId) Antimycin A/rotenone. IIIa/b) Vertically flexible sensor sleeves create IV) a transient microchamber. V) Fluorophores measure O_2 concentration (and H^+, measure for glycolysis in cellular systems).
(B) Bioenergetic profile of isolated mitochondria including proton leak, ATP production, uncoupled respiration and non-mitochondrial background.
Main features of this illustration were adopted from the manufacturers protocol and (Ferrick *et al.*, 2008).

2.2.4 QUANTIFICATION OF MITOCHONDRIAL ROS METABOLISM

Mitochondrial H_2O_2 efflux, a surrogate measure for mitochondrial ROS metabolism, was assessed using Amplex® Red fluorescence. In presence of horseradish peroxidase (HRP), non-fluorescent and colorless Amplex® Red (10-acetyl-3, 7-dihydroxyphenoxazine) reacts 1:1 stoichiometrically with H_2O_2, resulting in red fluorescent resorufin (Zhou *et al.*, 1997; Schlieve *et al.*, 2006).
Measurements were performed in duplicates at 37°C in a 96-well microplate format (Greiner, microplate reader TECAN, excitation wavelength 560 nm, emission wavelength 590 nm).

For each well, 20 µg mitochondrial protein were diluted in 200 µl ROS medium. Ten kinetic cycles (à 1min) were recorded before induction of state 4 respiration by substrate injection, and state 3 respiration by substrate and ADP injection. Fluorescence intensity was recorded for 20 further kinetic cycles. H_2O_2 efflux was calculated according to Equation 2-6 using a standard series of known H_2O_2 concentrations and expressed as [pmol H_2O_2/(min*mg mitochondrial protein)].

$$H_2O_2\ efflux\ [\frac{pmol}{min} * mg\ protein] = \frac{slope_{substrate}\left[\frac{RFU}{min}\right] - slope_{no\ substrate}\left[\frac{RFU}{min}\right]}{slope_{standard}\left[\frac{RFU}{min}\right] * m_{mitochondria}\,[mg]} \quad (2\text{-}6)$$

(RFU = relative fluorescence units)

ROS medium	KHE buffer, 4 U/ml SOD, 2 U/ml HRP, 100 µM Amplex® Red
KHE buffer	see 2.3.2
Final concentrations	Substrates: 6 mM succinate (+ 4 µM rotenone), 5 mM pyruvate + 5mM malate, 2 mM ADP Standard curve: 0, 200, 400, 600, 800 and 1,000 pmol H_2O_2

2.2.5 ASSESSMENT OF MITOCHONDRIAL MEMBRANE POTENTIAL

Safranin O is a cationic membrane-permeant fluorescent dye widely used for assessment of changes in mitochondrial membrane potential ($\Delta\Psi_m$) (Akerman & Wikstrom, 1976; Eriksson *et al.*, 1998; Zago *et al.*, 2000; Perevoshchikova *et al.*, 2009; Toime & Brand, 2010; Lionetti *et al.*, 2014). Induction of electrical potentials across the mitochondrial membrane leads to accumulation of dye molecules within the organelle (Akerman & Wikstrom, 1976), resulting in a quenched fluorescence signal.

Measurements were performed in duplicates at 37°C in a 96-well microplate format (Greiner, microplate reader TECAN**,** excitation wavelength 495 nm, emission wavelength 586 nm). For each well 20 µg mitochondrial protein were suspended in 100 µl safranin O-medium. A forerun period of 15 kinetic cycles (à 1 min) was measured to allow signal stabilization. Then, 10 kinetic cycles of state 4 respiration induced by substrate injection were recorded. FCCP was injected to induce state 3u respiration and collapse of membrane potential. Fluorescence was again recorded for 10 kinetic cycles. Due to considerable inter-experiment variation in the overall fluorescence level, fluorescence intensity was normalized to percentage of maximal fluorescence during state 3u (100%). Fluorescence signal intensity differences between state 4 and state 3u respiration can be translated as capability of mitochondria to build up $\Delta\Psi_m$.

Safranin O-medium	KHE buffer, safranin O 8 µM
KHE buffer	see 2.3.2
Final concentrations	Substrates: 5 mM succinate (+ rotenone 2 µM), 5 mM pyruvate + 5mM malate, Others: 2 µM FCCP

Altogether, this array of methods on intact adipocytes, permeablized adipocytes, and isolated mitochondria allows detailed characterization of white adipocyte mitochondrial bioenergetics, as well as further aspects of mitochondrial functionality. In addition, total WAT specimen, isolated white adipocytes, and isolated mitochondria can be used for various other experiments (compare appendix), as immunoblot analysis, proteomics, etc.

3 PUBLICATIONS AND MANUSCRIPTS

CHAPTER I - WHITE ADIPOCYTE MITOCHONDRIAL BIOENERGETICS IN SUBCUTANEOUS VERSUS INTRAABDOMINAL FAT

"Limited mitochondrial capacity of visceral versus subcutaneous white adipocytes in male C57BL/6N mice"

Theresa Schöttl, Lisa Kappler, Katharina Braun, Tobias Fromme, Martin Klingenspor

Endocrinology, 2015 Mar;156(3):923-33.[2]

Personal contribution: Theresa Schöttl designed the study, performed the experiments, analyzed data, prepared figures, and wrote and revised the manuscript.

CHAPTER II - OBESITY MEDIATED ALTERATIONS IN WHITE ADIPOCYTE MITOCHONDRIAL BIOENERGETICS AND THEIR RELATION TO SYSTEMIC GLUCOSE HOMEOSTASIS

"Limited OXPHOS capacity in white adipocytes is a hallmark of obesity in laboratory mice irrespective of the glucose tolerance status"

Theresa Schöttl, Lisa Kappler, Tobias Fromme, Martin Klingenspor

Molecular Metabolism, 2015 Jul 21 [Epub ahead of print][3]

Personal contribution: Theresa Schöttl designed the study, performed the experiments, analyzed data, prepared figures, and wrote and revised the manuscript.

CHAPTER III - SYSTEMIC CONSEQUENCES OF IMPAIRED WHITE ADIPOCYTE MITOCHONDRIAL FUNCTION

"Ablation of mitochondrial heat shock protein 60 in adipocytes causes systemic glucose intolerance in laboratory mice"

Theresa Schöttl*, Katharina Braun*, Emanuel Berger, Tobias Fromme, Dirk Haller, Martin Klingenspor

*both authors contributed equally to this study; manuscript for submission

Personal contribution: Theresa Schöttl planned and designed the study, established the methods required, assisted during experiments, analyzed data, prepared the figures, and wrote the manuscript.

Univ.-Prof. Dr. Martin Klingenspor (Supervisor)
Chair of Molecular Nutritional Medicine

[2] Letter of approval is shown in appendix 6.6.1.
[3] Letter of approval is shown in appendix 6.6.2.

CHAPTER I

"WHITE ADIPOCYTE MITOCHONDRIAL BIOENERGETICS IN SUBCUTANEOUS VERSUS INTRAABDOMINAL FAT"

ENDOCRINOLOGY, 2015 MAR;156(3):923-33.

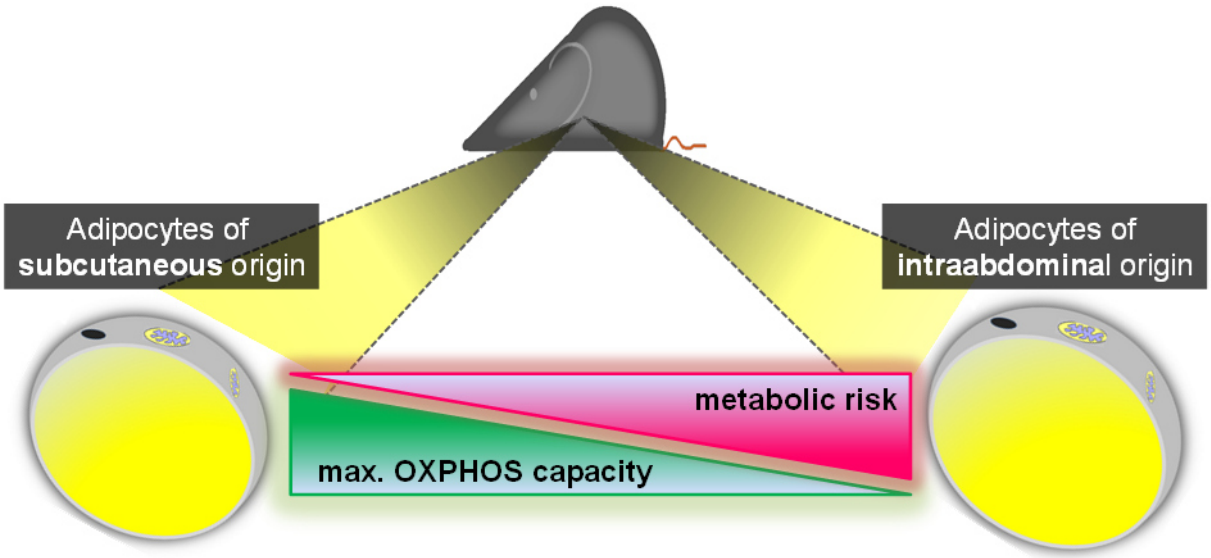

Limited Mitochondrial Capacity of Visceral Versus Subcutaneous White Adipocytes in Male C57BL/6N Mice

Theresa Schöttl, Lisa Kappler, Katharina Braun, Tobias Fromme, and Martin Klingenspor

Molecular Nutritional Medicine, Technische Universität München, Else Kröner Fresenius Center for Nutritional Medicine, 85350 Freising, Germany

Accumulation of visceral fat is associated with metabolic risk whereas excessive amounts of peripheral fat are considered less problematic. At the same time, altered white adipocyte mitochondrial bioenergetics has been implicated in the pathogenesis of insulin resistance and type 2 diabetes. We therefore investigated whether the metabolic risk of visceral vs peripheral fat coincides with a difference in mitochondrial capacity of white adipocytes. We assessed bioenergetic parameters of subcutaneous inguinal and visceral epididymal white adipocytes from male C57BL/6N mice employing a comprehensive respirometry setup of intact and permeabilized adipocytes as well as isolated mitochondria. Inguinal adipocytes clearly featured a higher respiratory capacity attributable to increased mitochondrial respiratory chain content compared with epididymal adipocytes. The lower capacity of mitochondria from epididymal adipocytes was accompanied by an increased generation of reactive oxygen species per oxygen consumed. Feeding a high-fat diet (HFD) for 1 week reduced white adipocyte mitochondrial capacity, with stronger effects in epididymal when compared with inguinal adipocytes. This was accompanied by impaired body glucose homeostasis. Therefore, the limited bioenergetic performance combined with the proportionally higher generation of reactive oxygen species of visceral adipocytes could be seen as a candidate mechanism mediating the elevated metabolic risk associated with this fat depot. **(*Endocrinology* 156: 923–933, 2015)**

Obesity is a well-known risk factor for numerous pathologies including insulin resistance, type 2 diabetes, hypertension and dyslipidemia, together forming the core of the metabolic syndrome (1–3). Although obesity in general is defined as an excess of body fat, not all adipose tissue depots seem to contribute to this increased risk to the same extent. Already in 1956, Jean Vagues pioneering work suggested a phenomenon later confirmed in multiple ways: Although even large amounts of subcutaneous (sc) fat are unproblematic for metabolic health, extensive visceral fat is an established risk factor for insulin resistance and type 2 diabetes (1, 4–7). Intra-abdominal transplantation of sc fat even ameliorates metabolic health, whereas transplantation of visceral fat does not (5, 6).

These fascinating observations led to intense research aiming to elucidate the underlying mechanisms (8–12). Comparisons on the level of cell physiology revealed a wide range of differences between the anatomically distinct white adipose tissues (13). To only name a few, stimulated lipolysis is higher in visceral than in sc fat (14, 15), the expression pattern of adipokines differs (16–18) and of note, it has been proposed that sc and visceral adipocytes have a different developmental origin (19). Thus, in contrast with the opposing view of adipose tissue forming a single organ with a multidepot organization (20–22), it has been suggested that each single fat depot should be regarded a separate mini-organ (19).

ISSN Print 0013-7227 ISSN Online 1945-7170
Printed in U.S.A.

Received August 14, 2014. Accepted December 22, 2014.
First Published Online December 30, 2014

Abbreviations: AUC, area under the curve; CD, control diet; COX IV, cytochrome c oxidase subunit 4; cRCR, cellular respiratory control ratio; CS, citrate synthase; faf, fatty acid free; FCCP, carbonyl cyanide 4-(trifluoromethoxy) phenylhydrazone; HFD, high-fat diet; HSP60, heat shock protein 60; mtDNA, mitochondrial DNA; nDNA, nuclear DNA; NDUFB8, NADH dehydrogenase [ubiquinone] 1 beta subcomplex subunit 8, mitochondrial; OXPHOS, oxidative phosphorylation; RCR, respiratory control ratio; SOD2, superoxide dismutase 2; sc, subcutaneous; VDAC, voltage-dependent anion channel.

Importantly, studies in both mice and men uncovered a correlation between impaired white adipocyte mitochondrial function and the deranged glucose homeostasis accompanying obesity (23–28). However, these data are mainly based on surrogate measures like mitochondrial DNA abundance, mitochondrial mRNA and protein levels, electron microscopy or citrate synthase activity measurements. State of the art functional analyses of white adipocyte mitochondrial bioenergetics are rather scarce in this context. In addition, often only a single depot is investigated and extrapolated to the entirety of body fat.

In this study, we characterized mitochondrial bioenergetics of murine sc inguinal and visceral epididymal white adipocytes with an unprecedented array of state-of-the-art methodology including respirometry of intact and permeabilized adipocytes as well as isolated mitochondria. We specifically isolated mature white adipocytes to exclude all effects of other celltypes resident in adipose tissue. We here demonstrate a higher respiratory capacity of inguinal compared with epididymal adipocytes. This finding holds true on the level of intact adipocytes, permeabilized adipocytes and isolated mitochondria.

In a next step we analyzed mitochondrial function of both types of adipocytes after high-fat diet feeding for 1 week. This resulted in a reduction of white adipocyte mitochondrial capacity. Of note, the limitation was more pronounced in epididymal when compared with inguinal adipocytes and was accompanied by impaired whole body glucose homeostasis. Thus, the limited bioenergetic capacity of adipocytes from visceral fat may be part of the elevated metabolic risk associated with this fat depot.

Materials and Methods

Mice

General

Experiments were performed on 12-weeks-old male wildtype C57BL/6N mice (Charles River, Sulzfeld, Germany), which were housed in groups in a specific pathogen-free environment on a 12:12-h light-dark photocycle at 22°C with ad libitum access to water and food (CHOW, type M-Z, Ssniff; Soest, Germany). This study is in accordance with the German animal welfare law and with permission of the government of Upper Bavaria (Regierung von Oberbayern, reference No. Az. 55.2.1.54–2532–148–13).

High-fat diet feeding.

At the age of 7 weeks wildtype C57BL/6N mice were switched from CHOW to a purified research control diet (CD, 12 kJ% fat, SS745-E702, Ssniff, Soest, Germany). After acclimatization for 1 week mice were matched by body weight into a CD and a high-fat diet (HFD) group (48 kJ% fat SS745-E712; Ssniff, Soest, Germany). Feeding was conducted for 1 week.

Body weight and body composition

Body weight was measured before and after the HFD vs CD feeding trial. Body composition was measured with nuclear magnetic resonance spectroscopy (minispec LF50H TD-nuclear magnetic resonance [NMR] analyzer, Bruker Biospin, Rheinstetten, Germany) at the end of the feeding period.

Oral glucose tolerance test

After a fasting period of 6 hours, mice received 2.66 mg glucose per [(lean mass + 0.2 fat mass) g] by single oral gavage (29). Blood glucose was monitored before and 15, 30, 60, and 90 minutes after gavage. Total area under the curve (AUC) was calculated as measure for glucose tolerance.

Tissue dissection and isolation of adipocytes

Mice were killed by carbon dioxide exposure and exsanguination. Inguinal (posterior sc) and epididymal fat depots were dissected and weighed. Visible blood vessels were removed. For experiments on isolated mitochondria, inguinal and epididymal fat depots from 15 mice were pooled separately and minced into small pieces. For measurements on intact or permeabilized adipocytes, fat depots of individual mice were used.

Mature adipocytes were separated from other cell types by collagenase-digestion (Type A, Roche Applied Science, Penzberg, Germany; 1 g/L in Hank's Balanced Salt Solution [14025–092, Gibco, Life Technologies, Darmstadt, Germany]) containing 4% BSA) at 37°C in a shaking incubator (WiseCube WIS-20, Wisd laboratory instruments, Witeg, Wertheim, Germany, 150 rpm), filtering through a 250-μM nylon gauze and subsequent low-spin centrifugation (300× *g*, 2 min, RT). Floating mature adipocytes were washed twice with STE buffer (250 mM Sucrose, 5 mM Tris and 2 mM EGTA, pH 7.4 at 4°C) containing 4% BSA. Washing steps were repeated two times more with STE containing 4% essentially fatty-acid free (faf) BSA. Floating adipocytes were stored in STE on ice until the respective respirometry measurements were performed ($\leq$ 4 h).

Histology

Paraffin-embedded adipose tissue samples were sliced into 5-μm sections, mounted, and stained with hematoxylin and eosin. Cell diameters were analyzed in fat depots of six mice each with five independent histological sections. Adipocyte size was determined using a macro specifically developed for automated image analysis of adipose tissue (WimAdipose, Wimasis GmbH; Munich, Germany).

Respirometry of adipocytes

Oxygen consumption of adipocytes was measured with high-resolution respirometry (Oxygraph-2k, OROBOROS INSTRUMENTS; Innsbruck, Austria). Adipocyte suspension (100 μL) was pipetted into 2 mL mitochondrial respiration medium (MIR05). The stirrer speed was set to 750 rpm.

For oxygen consumption measurements of intact adipocytes, pyruvate (5mM) was injected and basal cellular respiration was

doi: 10.1210/en.2014-1689

recorded. Proton leak respiration was assessed by addition of oligomycin (2 μg/mL). Titration of carbonyl cyanide 4-(trifluoromethoxy) phenylhydrazone (FCCP, 0.5-μM steps) was performed for measuring maximal cellular respiration rates. Nonmitochondrial oxygen consumption determined in the presence of antimycin A (2.5μM) was subtracted from the other respiratory states. Spare respiratory capacity was calculated by subtracting basal from maximal oxygen consumption rates. For mitochondrial integrity control, cellular respiratory control ratio (cRCR) was calculated as the ratio of maximal to leak oxygen consumption.

For oxygen consumption measurements of permeabilized adipocytes, 2μM digitonin was added. State 4 respiration was measured in the presence of succinate/rotenone (5mM/2μM). By addition of ADP (5mM), phosphorylating state 3 was induced. ATP synthase was inhibited by oligomycin (2 μg/mL) (state 4o). Titration of FCCP (0.5-μM steps) was performed for measuring maximal cellular respiration rates (state 3u). Nonmitochondrial oxygen consumption was determined in presence of antimycin A (2.5μM) and subtracted from the other respiratory states. Respiratory control ratio (RCR) was calculated dividing state 3 by state 4o respiration.

Cellular DNA quantification

DNA content of adipocyte suspensions was quantified by quantitative PCR targeting a unique region of genomic DNA (promotor resistin). Samples were diluted 1:5 in digestion buffer (50mM KCL, 0.45% Nonidet P-40, 0.45% Tween 20, 0.2 mg/mL Proteinase K) and incubated for 1 hour at 65°C under agitation (1000 rpm). Proteinase K was inactivated at 95°C for 10 minutes and 2.25 volumes phenol:chloroform:isoamyl alcohol (25:24:1, Carl Roth GmbH & Co. KG; Karlsruhe, Germany) were added. After phase separation by centrifugation at 16 000× *g* for 10 minutes the hydrophilic phase was used for qPCR (Roche Lightcycler 480 II;Roche, Basel, Switzerland) using a commercial premix (SensiMix No-Rox; Bioline; London, United Kingdom). Primers (fw 5′-ACCTCTCTTGGGGTCAG ATGT-3′, rev 5′-CTGGGTATTAGCTCCTGTCCC-3′) were synthesized by a commericial provider (Eurofins Genomics, Ebersberg, Germany). DNA concentrations were determined by comparison with a mouse gDNA standard dilution series of known concentration.

Quantification of mtDNA

DNA was isolated from adipocytes using the Wizard SV Genomic DNA Purification System (A 2360, Promega, Fitchburg, WI, USA). Yield was quantified spectrophotometrically (TECAN Infinite M200, NanoQuant, Tecan Group Ltd., Männedorf, Switzerland). DNA were amplified with specific primers (nuclear: fw 5′-TTTACAGGATCTCCAAGATTCAGA-3′, rev 5′-GATCACCCCATGTGAACAAA-3′; mitochondrial: fw 5′-CAAATTTACCCGCTACTCAACTC-3′, rev 5-′GCTATAATT TTTCGTATTTGTGTTTGG-3′). Quantification of PCR amplification was achieved by specific probes (Universal ProbeLibrary, Roche; nuclear no 26, Cat. No. 04687574001; mitochondrial No. 101, Cat. No. 04692195001).

Citrate synthase activity

Adipocyte suspensions containing 1% Tween 20 were homogenized (ULTRA-TURRAX, IKA; Staufen, Germany) and diluted 1:25 in reaction buffer (100mM Tris, 1mM $MgCl_2$, 1mM EGTA, 0.1mM DTNB [Ellman's reagent, 5,5′-dithiobis-(2-nitrobenzoic acid], 3.6mM acetyl coenzyme A; pH 8.2). Absorption was measured at 30°C and 412 nm with a microplate reader (TECAN Infinite M200, Tecan Group Ltd.) for 5 minutes before oxaloacetate (0.5mM) was injected. Data were recorded for 10 minutes. Enzyme activity (μmol/min*mg protein) was calculated on the basis of the absorption change before and after injection of oxaloacetate with respect to dilution factor, extinction coefficient of DTNB, and path length of the plate.

Isolation of mitochondria

Mitochondria were isolated from mature adipocytes by homogenization and differential centrifugation. All steps were conducted at 4°C or on ice. Adipocytes were transferred into a glass-teflon homogenizer (15 mL), filled with STE to 15 mL, and manually disrupted by five rotating strokes. The homogenate was transferred to a 40-mL centrifuge tube, filled with STE buffer containing 4% BSA-faf, and centrifuged for 10 minutes at 800× *g*. Supernatant was transferred to a second tube and centrifuged for 10 minutes at 10 000× *g*, whereas the pellet was homogenized and centrifuged for 10 minutes at 800× *g* once more. Again, the supernatant was transferred to a new centrifuge tube and centrifuged for 10min at 10 000× *g*. Supernatants of both fast spins were discarded, the pellets were resuspended in KHE ((120 mM KCL, 5 mM KH_2PO_4, 3 mM HEPES, 1 mM EGTA, 0.5% BSA-faf, pH=7.2) buffer and combined in a single centrifuge tube. The fast spin was repeated. Again, supernatant was discarded and the mitochondrial pellet resuspended in KHE.

Quantification of mitochondrial protein

Protein concentration of mitochondrial suspensions was determined by the Bradford method. Mitochondrial suspensions were diluted 1:200 in Bradford reagent (Roti-Quant, Carl ROTH, Karlsruhe, Germany); diluted 2:7.5). Absorbance was measured at 590 nm with a microplate reader (TECAN Infinite M200, Tecan Group Ltd.). Mitochondrial protein concentration was assessed using a KHE-diluted BSA standard.

Respirometry of isolated mitochondria

Mitochondrial respiration was assessed by the XF96 Extracellular Flux Analyzer (Seahorse Bioscience, Billerica, MA). Sensor cartridges were hydrated overnight in the XF Prep Station at 37°C (Seahorse Bioscience) using the XF96 Calibrant solution (200 μL per well). Isolated mitochondria were seeded in collagen-coated XF96-PS cell culture plates (5 μg per well in 20 μL KHE containing either 5mM succinate/2μM rotenone or 5mM pyruvate/5mM malate or 40μM palmitoyl-L-carnitine/5mM malate). By centrifugation at 2000× *g* for 20 minutes at 4°C mitochondria were attached to the plate bottom. Prewarmed (37°C) buffer containing substrate (180 μL per well, for substrates see above) were added after mitochondria were acclimatized for 5 minutes at RT. Finally, mitochondria were incubated for 30 minutes in the XF Prep Station at 37°C before the measurement of mitochondrial respiration was started.

Oxygen consumption was calculated by plotting oxygen concentration (nmol O_2) vs time (min). Mitochondrial respiration was measured in the presence of ADP and substrate (state 3), then 2.5 μg/μL oligomycin was injected to inhibit ATP synthase (state 4o). Nonbiological background was assessed by addition of an-

timycin A (4μM) and Rotenone (2μM) and subtracted from values of the other conditions. RCRs were calculated by dividing oxygen consumption during state 3 by oxygen consumption during state 4o respiration.

Measurement of mitochondrial membrane potential

Membrane potential (Ψ_m) of isolated mitochondria was measured by safranin O fluorescence (S884, Sigma-Aldrich, St. Louis, MO). Measurements were conducted in a 96-well microplate (FLUOTRACTM 200, Greiner Bio-One, Frickenhausen, Germany) with 20 μg mitochondrial protein/well diluted in assay medium (KHE, 8μM safranin O). Fluorescence signal intensity was recorded at an excitation of 495 nm and an emission wavelength of 586 nm at 37°C in a microplate reader (TECAN Infinite M200, Tecan Group Ltd.). 15 kinetic cycles (à 1 min) were measured before state 4 respiration was induced by either succinate/rotenone (5mM/2μM) or pyruvate/malate (5mM). 10 further kinetic cycles were recorded until FCCP was injected to induce state 3u respiration. Measured fluorescence intensity was expressed as percentage of maximal fluorescence during state 3u (100%). $\Delta\Psi_m$ from state 4 to state 3u respiration was judged as ability of mitochondria to build up Ψ_m.

Immunoblotting

Immunoblots were performed with adipocyte protein lysates and isolated mitochondria, respectively. Proteins (adipocyte lysate: 37.5 μg; isolated mitochondria: 25 μg) were separated in a 12.5% SDS-PAGE and transferred to a nitrocellulose membrane (LI-COR Biosciences, Lincoln, NE; 60 min, 100V). Antibodies were targeted against citrate synthase (CS, 1:1000; Abcam, ab96600), cytochrome c oxidase subunit 4 (COX IV) (1:5000; Cell signaling, 4844), heat shock protein 60 (HSP60; 1:2000; Santa Cruz, sc-1052), histone H3 (1:2000; Cell signaling, 4499), oxidative phosphorylation (OXPHOS; 1:250, Mitosciences, MS604, just NADH dehydrogenase [ubiquinone] 1 beta subcomplex subunit 8 (NDUFB8) and complex II- subunit 30 kDa were analyzable), superoxide dismutase 2 (SOD2; 1:10 000; Abcam, ab16956) and voltage-dependent anion channel (VDAC; 1:900; Calbiochem, PC548). Infrared dye-conjugated secondary antibodies (IRDye 680, IRDye 800, LI-COR) were incubated at a dilution of 1:20 000. The Odyssey software (LI-COR, Bad Homburg, Germany) was applied to quantify band fluorescence intensities.

Measurement of mitochondrial superoxide

Superoxide release from isolated mitochondria was assessed indirectly as H_2O_2 using Amplex Red fluorescence. Measurements were performed in a 96-well microplate (FLUOTRACTM 200, Greiner Bio-One) with 20 μg mitochondrial protein/well diluted in assay medium (4 U/mL superoxide dismutase, 2 U/mL horseradish peroxidase, 100μM Amplex Red). Signal intensity was recorded at an excitation of 560 nm and an emission wavelength of 590 nm at 37°C in a microplate reader (TECAN Infinite M200; Tecan Group Ltd.). Ten kinetic cycles (à 1 min) were measured before state 4 respiration was induced by 6mM succinate/4μM rotenone or 5mM pyruvate/5mM malate. Twenty additional kinetic cycles were measured. Superoxide production was also assessed during state 3 respiration (ADP). Absolute mitochondrial superoxide production translated in pmol H_2O_2/(min*mg mitochondrial protein) was calculated using an H_2O_2 standard.

Statistical analyses

All data are presented as mean values ± SD. For statistical comparison, two-way ANOVA followed by post-hoc Bonferroni testing, two-way repeated-measures ANOVA followed by post-hoc Bonferroni testing or two-tailed Student *t* test were performed (SigmaPlot 12.5, Systat Software, Inc., San Jose, CA; GraphPad Prism4, GraphPad Software, Inc., La Jolla, CA). $P < .05$ were considered statistically significant.

Results

Subcutaneous adipocytes display a higher respiratory capacity than visceral adipocytes

We compared the epididymal and the inguinal adipose tissue depots as representatives for murine visceral and sc fat. The total mass of these two anatomically distinct depots, and thus their relative contribution to total body fat mass, was comparable (inguinal fat: 0.312 ± 0.061 g vs epididymal fat: 0.291 ± 0.080 g, n = 89–90, $P < .001$). Cell size analysis revealed that adipocytes of inguinal origin are smaller than adipocytes of epididymal origin, as indicated by a smaller mean, median, and 95th percentile diameter (Supplemental Figure 1). In random histological sections, mean and median diameter seriously underestimate the real average cell size in both fat depots. Therefore, we chose the 95th percentile as the most realistic representation of cell diameter in the larger fraction of adipocytes (inguinal, 42.9 μm; epididymal, 56.4 μm).

We first assessed mitochondrial bioenergetics of intact white adipocytes to detect possible differences in oxidative function depending on anatomical localization. Respiration profiles were recorded by chamber-based high-resolution respirometry (Oxygraph-2k, OROBOROS). Basal, leak, and maximal cellular respiration rates were lower in epididymal when compared with inguinal adipocytes with the most significant difference for maximal respiration rate (Figure 1A). Thus, the capacity for substrate oxidation is higher in inguinal adipocytes. We used absolute oxygen consumption rates to calculate key parameters of cellular respiratory control (30). Spare respiratory capacity (Figure 1B) was higher in inguinal adipocytes, supporting a higher oxidative capacity of inguinal compared with epididymal adipocytes. Thus, inguinal adipocytes are able to increase substrate oxidation to a higher extent in the case of a sudden increase in ATP demand.

To assess ADP-dependent maximal oxidative phosphorylation (OXPHOS) capacity, we conducted chamber-based high-resolution respirometry of digitonin-permeabilized inguinal vs epididymal adipocytes (Figure 2A).

doi: 10.1210/en.2014-1689

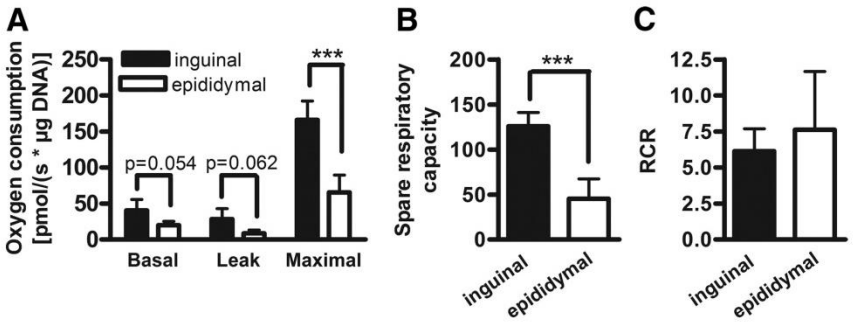

Figure 1. Cellular respiration of intact inguinal and epididymal adipocytes obtained by respiration analysis using the Oxygraph-2k. A, Higher respiratory capacity in inguinal adipocytes. After determination of basal respiration using pyruvate as substrate, we employed the ATP synthase inhibitor oligomycin to identify the proportion of basal respiration that contributes to either ATP turnover or proton leak, respectively. We added FCCP to determine the maximal cellular respiratory capacity. Finally, nonmitochondrial background was assessed by addition of complex III inhibitor antimycin A and subtracted from all other respiratory states. Oxygen consumption rates are expressed per μg DNA. ***, $P < .001$. B, Higher spare respiratory capacity in inguinal adipocytes. Spare respiratory capacity was calculated by subtracting basal from maximal oxygen consumption rates. ***, $P < .001$. C, No difference in mitochondrial integrity of inguinal and epididymal adipocytes. As indicator for mitochondrial integrity cRCR was calculated as quotient of maximal to leak oxygen consumption. All data are presented as means ± SD of eight independent experiments.

There was no difference in respiratory states determined by the proton leak (state 4 and state 4o) between both types of adipocytes. State 3 and state 3u respiration rates of inguinal adipocytes exceeded those from epididymal adipocytes, again showing a higher oxidative and respiratory capacity.

Notably, respiratory control ratios of inguinal and epididymal adipocytes were of comparable magnitude, revealing tightly coupled mitochondria in adipocytes of both fat depots (Figures 1C and 2B).

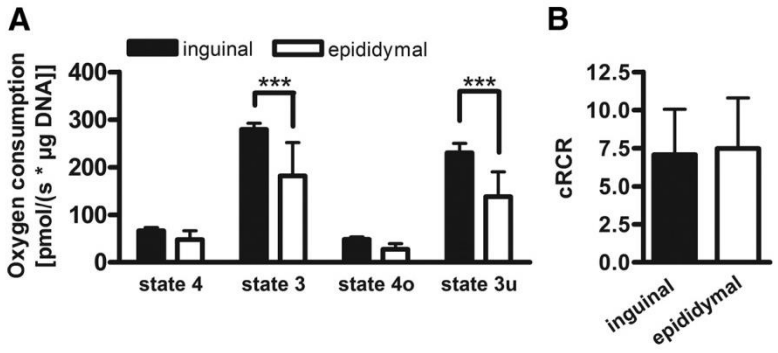

Figure 2. Oxygen consumption of permeabilized inguinal and epididymal adipocytes obtained by respiration analysis using the Oxygraph-2k. A, Higher oxidative and respiratory capacity in inguinal adipocytes. First, plasma membranes of adipocytes were permeabilized by digitonin and state 4 oxygen consumption was determined in the presence of succinate/rotenone before state 3 respiration was measured succeeded by addition of ADP. ATP-synthase was inhibited and state 4o respiration measured by addition of oligomycin. Next, state 3u was induced by addition of the uncoupler FCCP. Finally, injection of antimycin A led to blockade of electron flow and nonmitochondrial background was subtracted from other respiratory states. Oxygen consumption rates are expressed per μg DNA. ***, $P < .001$. B, No difference in mitochondrial integrity of permeabilized inguinal and epididymal adipocytes. As indicator for mitochondrial integrity, mitochondrial respiratory control ratio (RCR) was calculated as ratio of state 3 to state 4o oxygen consumption. All data are presented as means ± SD of eight independent experiments.

Taken together, inguinal adipocytes featured a markedly higher capacity for substrate turnover, reflected by both absolute respiration rates and spare respiratory capacity. Nonetheless, epididymal adipocytes were not dysfunctional per se as reflected by a high cRCR and RCR, respectively, which were both comparable to that of inguinal adipocytes.

Higher capacity for oxidative phosphorylation of inguinal adipocytes is attributable to higher mitochondrial capacity, not abundance.

Principally, the observed difference in maximal respiratory capacity can be explained either by a different abundance of mitochondria in a cell or by a different capacity of the mitochondria themselves. To discriminate between these possibilities, we quantified several markers for mitochondrial abundance. Each of them, mtDNA content (Figure 3A), citrate synthase activity level (Figure 3B), and protein level of mitochondrial matrix proteins (CS, Figure 3C; SOD2, Figure 3D; HSP60, Figure 3E) were comparable between adipocytes of both fat depots analyzed. Therefore, the differences observed in respirometry were not caused by differences in mitochondrial abundance per cell.

To detect a possible difference in mitochondrial characteristics, we isolated mitochondria from inguinal and epididymal adipocytes and subjected them to plate-based respirometry. Because inguinal adipocytes are smaller when compared with epididymal adipocytes (Supplemental Figure 1) but contain equal amounts of mitochondria, isolation of mitochondria resulted in a higher yield per gram fat mass in inguinal vs epididymal fat cells (Figure 3F). Respiring on all three different substrates succinate, pyruvate, and palmitate, we consistently observed a higher capacity for oxidative phosphorylation (state 3) in mitochondria isolated from inguinal when compared with epididymal white adipocytes (Figure 3G). Interestingly, we observed no differences in state 4o (pro-

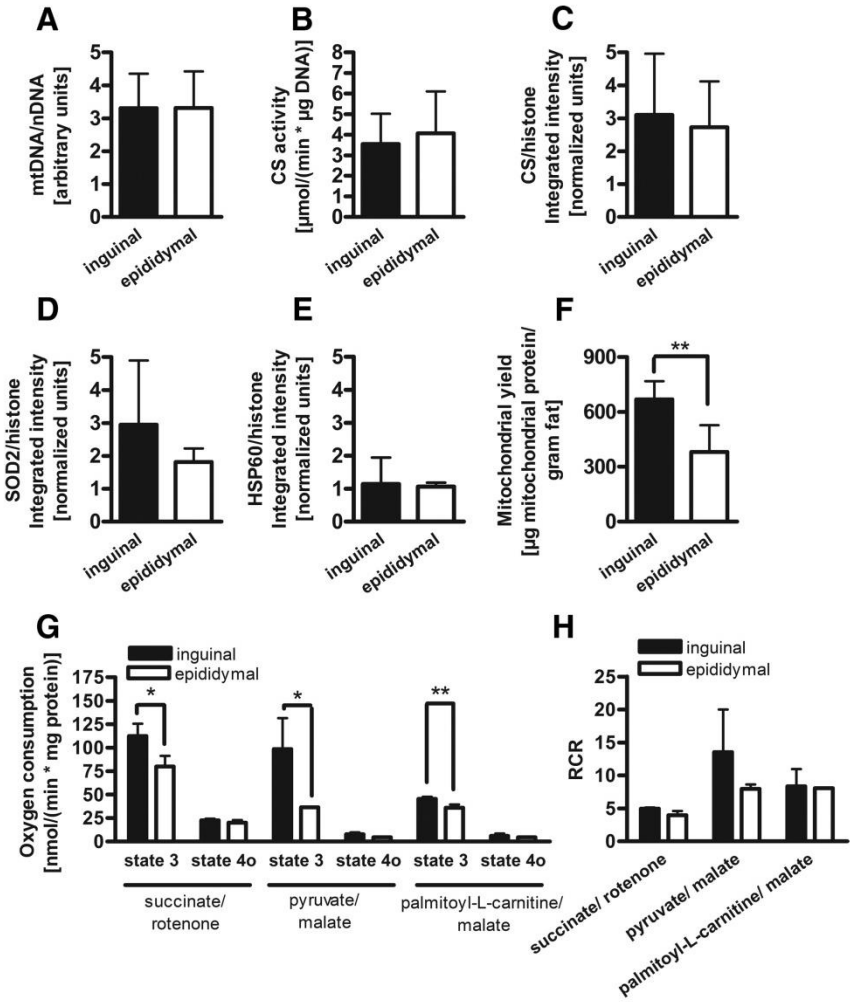

Figure 3. Higher capacity for oxidative phosphorylation of inguinal adipocytes is attributable to higher mitochondrial capacity, not abundance. A, Abundance of mtDNA in adipocytes, relative to nDNA. Data are presented as means ± SD (n = 5). B, CS activity in adipocyte samples used for respiration analysis and normalized to the respective DNA content. Data are presented as means ± SD (n = 8). C–E, Protein levels of mitochondrial CS, SOD2, HSP60 determined by immunoblot analysis, normalized to histone H3. Data are presented as means ± SD (n = 3–4). F, Mitochondrial yield from inguinal and epididymal white adipocytes. Data are presented as means ± SD (n = 6), **, $P < .01$. G, Bioenergetics of isolated white adipocyte mitochondria were measured using three different substrate combinations. First, phosphorylating state 3 respiration was assessed in the presence of ATP and substrate (succinate/rotenone, pyruvate/malate, palmitoyl-L-carnitine/malate). Then, ATP synthesis was inhibited and state 4o respiration was induced by oligomycin. Nonbiological background was determined by blockade of electron flow at complex III with antimycin A and subtracted from the other respiratory rates. Data are presented as mean values ± SD of 3 independent mitochondrial preparations. Two-way repeated-measures ANOVA with Bonferroni posttest was performed for every substrate individually. *, $P < .05$; **, $P < .01$. H, No difference in mitochondrial integrity of mitochondria isolated from inguinal and epididymal adipocytes. Because indicator for mitochondrial integrity RCR was calculated as ratio of state 3 to state 4o oxygen consumption. Data are presented as mean values ± SD of three independent mitochondrial preparations. Student *t* test was performed for every substrate individually.

ton leak dependent respiration) or respiratory control ratios indicating well-coupled mitochondria in both types of adipocytes (Figure 3H). Thus, the higher respiratory capacity of intact and permeabilized inguinal adipocytes is clearly attributable to a higher mitochondrial capability itself and does not result from a higher mitochondrial abundance.

Furthermore, the capability of mitochondria to build up membrane potential (Ψ_m) was assessed using the membrane-permeant fluorescent dye safranin O. Independent of the substrate used (succinate/rotenone, Figure 4A; pyruvate/malate, Figure 4B), we observed a higher Ψ_m in inguinal when compared with epididymal adipocytes.

Higher mitochondrial respiratory capacity of inguinal adipocytes coincides with higher content in respiratory chain complexes

We further investigated the difference observed in oxidative phosphorylation of mitochondria isolated from inguinal and epididymal adipocytes by quantifying the protein amount of OXPHOS enzymes. We observed higher protein levels of complex I subunit NDUFB8, complex II-30 kDa subunit and COX IV in mitochondria from inguinal vs epididymal adipocytes (Figure 5A), independent of normalization to either mitochondrial outer membrane protein voltage-dependent anion channel (VDAC; depot effect $P < .01$) or matrix protein SOD2 (depot effect $P < .001$; Figure 5B). No difference was observed relating VDAC to SOD2. Thus, the higher mitochondrial oxidative capacity of inguinal vs epididymal adipocytes can be ascribed to a more abundant respiratory chain per mitochondrion.

Taken together, all evidence supports a difference in maximal respiratory capacity specifically in the mitochondria of white inguinal and epididymal adipose tissue.

Higher superoxide production in relation to OXPHOS capacity in epididymal adipocytes

A high mitochondrial membrane potential can be associated with excessive production of reactive oxygen species (ROS) (31). We therefore determined ROS production in mitochondria isolated from both depots. In detail, we

doi: 10.1210/en.2014-1689

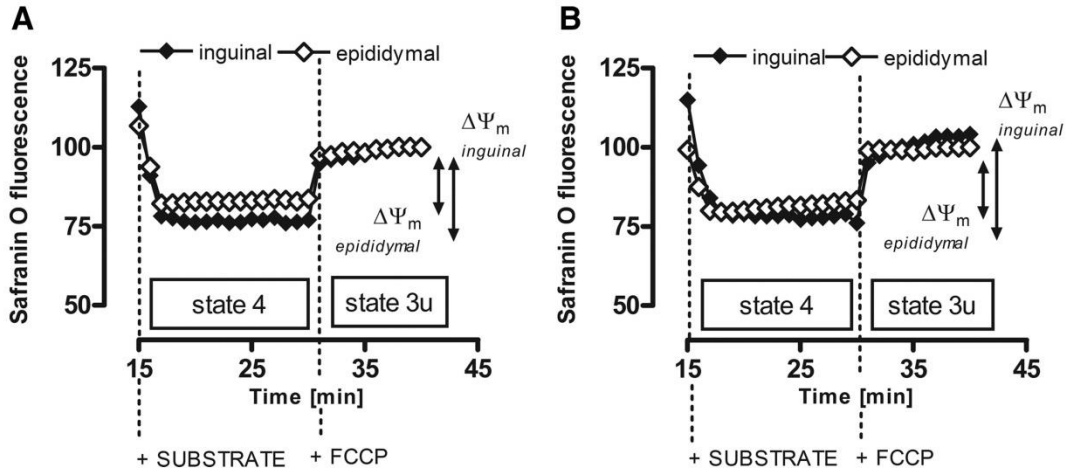

Figure 4. Isolated mitochondria from inguinal adipocytes show a higher potential (Ψ_m) across the mitochondrial inner membrane. Ψ_m was assessed by measuring safranin O fluorescence over 45 cycles (à 1 minute). The higher the potential across the mitochondrial inner membrane, the lower is the recorded fluorescence signal intensity. Fifteen minutes after starting the experiment, state 4 respiration was induced by injection of (A) succinate/rotenone, or (B) pyruvate/malate. Finally, after 10 further minutes state 3u was induced by injection of the uncoupling agent FCCP. $\Delta\Psi_m$, from state 4 to state 3u respiration was judged as ability of mitochondria to build up Ψ_m. Data are presented as means of 3 independent experiments.

investigated whether mitochondria from inguinal and epididymal adipocytes differ in terms of superoxide radical anion ($O_2^{\bullet-}$) formation, the primary ROS generated by mitochondria. $O_2^{\bullet-}$ is converted by SOD2 to membrane-permeable H_2O_2 (32–34). For all tested conditions (state 3 and state 4 respiration of isolated mitochondria energized with succinate and pyruvate, respectively) H_2O_2 release of mitochondria from inguinal and epididymal adipocytes was comparable (Table 1). Importantly, for pyruvate, the relative generation of $O_2^{\bullet-}$ per nmol O_2 consumed at maximal OXPHOS performance was more than twice as high in mitochondria from epididymal vs inguinal adipocytes.

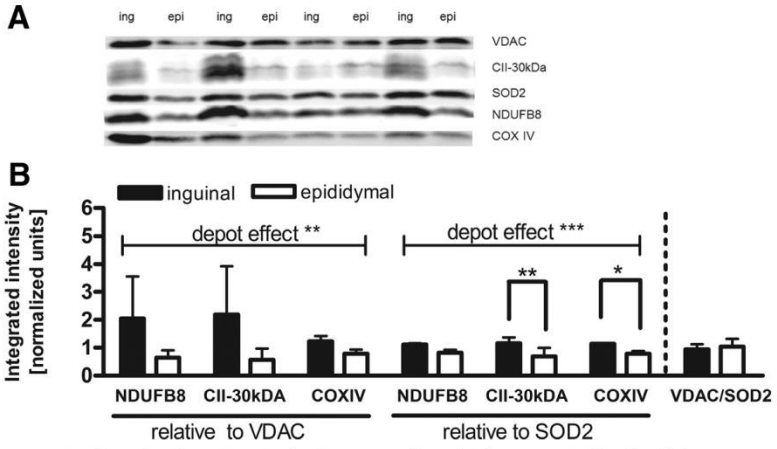

Figure 5. Mitochondria from inguinal adipocytes show higher protein levels of electron transport chain enzymes. A, Immunoblot of mitochondrial fractions isolated from inguinal (ing) and epididymal (epi) adipocytes against complex I subunit NDUFB, complex II-30 kDa subunit, COX IV, outer membrane protein VDAC, and the matrix enzyme SOD2. B, NDUFB8, CII-30 kDa, and COX IV abundance in mitochondria normalized to VDAC and SOD2 and relation between matrix and outer membrane marker. Data are presented as means ± SD of four independent mitochondrial preparations. *, $P < .05$; **, $P < .01$; ***, $P < .001$. Two-way ANOVA with Bonferroni posttest was performed for VDAC and SOD2 individually.

Short-time high-fat feeding impairs mitochondrial capacity mainly in epididymal adipocytes and affects body glucose homeostasis

To scrutinize whether the limitation in oxidative and respiratory capacity in epididymal vs inguinal adipocytes could account for the metabolic risk associated with visceral fat we exposed our mice to a metabolic challenge by feeding a high-fat diet (HFD) for 1 week. This experiment addressed the following hypotheses: 1) the deficit in mitochondrial oxidative capacity of epididymal adipocytes could deteriorate during fat mass gain caused by HFD feeding and, 2) if white adipocyte mitochondrial dysfunction, particularly in visceral fat, is causally involved in the development of insulin resistance it must occur prior to or at least instantaneously with the emergence of impaired glucose metabolism.

In this feeding trial we determined the effect of a short-time HFD exposure on glucose metabolism and white adipocyte mitochondrial functionality comparing the two anatomically distinct fat depots. HFD feeding resulted in a slight but not significant increase in body weight and body fat content (Figure 6, A and B) as well as inguinal and epididymal fat pad mass (data not shown). Of note, HFD-fed mice stood out by impaired glucose tolerance as indicated by a lower glucose clearance rate and a higher area under the curve (AUC; Figure 6, C and D).

Table 1. Comparable H_2O_2 Release Rates in Isolated Mitochondria from Inguinal and Epididymal Adipocytes

H_2O_2 Release, pmol/(min*mg protein)	Succinate/Rotenone		Pyruvate/Malate	
	State 3	State 4	State 3	State 4
Inguinal	271 ± 97	349 ± 177	201 ± 77	218 ± 42
Epididymal	200 ± 92	310 ± 150	158 ± 112	216 ± 56

H_2O_2 release was assessed in succinate (+ rotenone) or pyruvate/malate energized mitochondria isolated from inguinal and epididymal white adipocytes using Amplex Red fluorescence. Measurements were conducted during state 3 and state 4 respiration. Data are presented as means ± SD of 5–6 independent experiments.

Respirometry of intact adipocytes revealed markedly lowered maximal oxygen consumption in inguinal and epididymal adipocytes of the HFD group. No differences in basal and leak respiration were detected (Figure 7, A and E). Accordingly, spare respiratory capacity as the difference between maximal and basal respiration was lower in both types of adipocytes of HFD-fed mice (Figure 7, B and F). From a comparable basal level, these adipocytes are unable to increase substrate oxidation in case of an increase in ATP demand to the same degree as adipocytes from CD-fed mice do. CS activity as marker for mitochondrial abundance was lower in inguinal adipocytes of HFD-fed mice but comparable in epididymal adipocytes (Figure 7, C and G). Cellular RCR was markedly lowered in epididymal but not inguinal adipocytes (Figure 7, D and H). Therefore, the difference in maximal respiratory capacity in inguinal adipocytes is most likely ascribable to a lowered mitochondrial abundance. Limited maximal cellular respiration and restricted spare respiratory capacity in epididymal adipocytes, however, was only ascribable to lowered mitochondrial capacity as indicated by comparable mitochondrial abundance but lowered cRCR.

Altogether, we revealed here that short-time HFD feeding affects mitochondrial capacity in white adipocytes. This functional limitation is much more pronounced in visceral-epididymal vs sc-inguinal adipocytes. Because white adipocyte mitochondrial dysfunction—mainly in epididymal adipocytes—was paralleled by glucose intolerance, a causal relationship is possible.

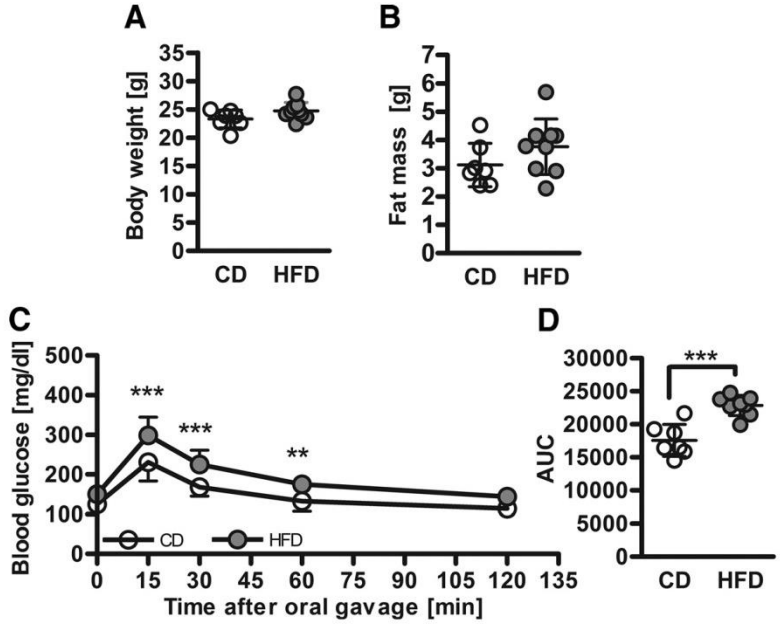

Figure 6. One-week high-fat diet feeding causes impaired glucose tolerance. At the age of 8 weeks mice were matched by body weight into an HFD and a CD group. Diets were fed for one week. All parameters were measured at the end of the feeding period. (A) Body weight, (B) Fat mass, (C) Oral glucose tolerance test, (D) Total AUC calculated from panel C as measure for glucose tolerance. Data are presented as means ± SD (n = 7–9). **, $P < .01$; ***, $P < .001$.

Discussion

Alterations or differences in white adipocyte mitochondrial bioenergetics have repeatedly been implicated in the pathogenesis of insulin resistance and type 2 diabetes (35, 36). In addition, the mass of anatomically distinct fat depots exerts a divergent metabolic risk (1, 4–6). In this study, we investigated whether this difference in risk coincides with a difference in mitochondrial function of white adipocytes.

We characterized mitochondrial bioenergetics of peripheral-inguinal and visceral-epididymal white adipocytes of lean and healthy, male C57Bl/6N mice by analyzing a comprehensive set of respiration parameters in cellular and organellar models. First, we isolated mature white adipocytes from inguinal and epididymal fat depots as the most physiological approach to assess cellular bioenergetics. Mitochondria are maintained in their undisturbed cellular environment and interactions with other cellular organelles or signaling molecules are preserved (30). Second, we determined maximal OXPHOS capacity by respirometry of digitonin-permeabilized adipocytes. Plasma membrane permeabilization still allows interaction of mitochondria with intracellular proteins, the cytoskeleton and intracellular membranes (37), hence conserving many aspects of normal cell physiology (30, 37). Notably, this approach bypasses the disadvantage of the permeability barrier given by the plasma membrane allowing ADP passage to

doi: 10.1210/en.2014-1689

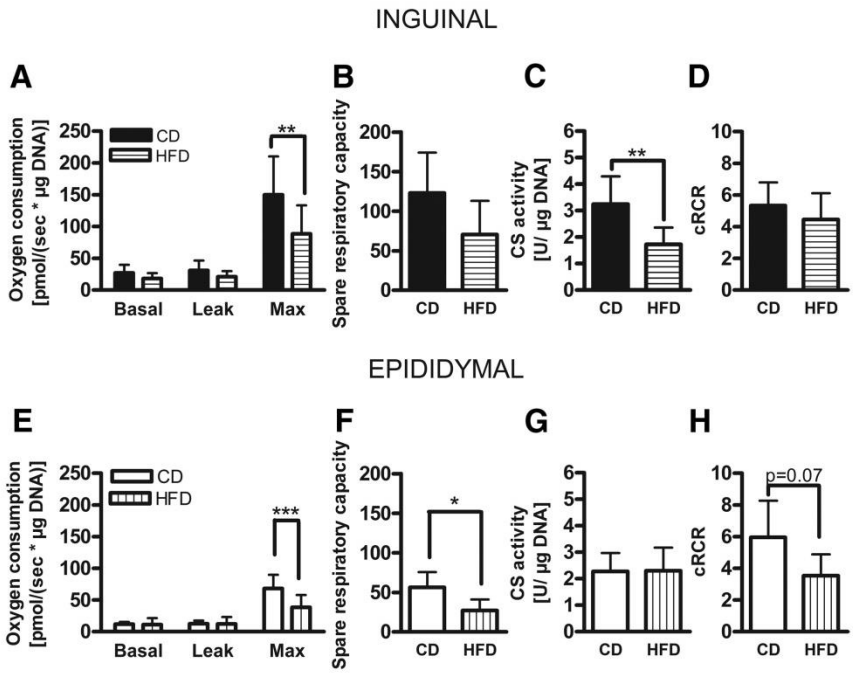

Figure 7. Cellular respiration of adipocytes from mice fed HFD or CD for 1 week obtained by respiration analysis using the Oxygraph-2k: HFD feeding results in limited maximal respiratory capacity in epididymal adipocytes. A and E, After determination of basal respiration using pyruvate as substrate, we employed the ATP synthase inhibitor oligomycin to identify the proportion of basal respiration that contributes to either ATP turnover or proton leak, respectively. We added FCCP to determine the maximal cellular respiratory capacity. Finally, nonmitochondrial background was assessed by addition of complex III inhibitor antimycin A and subtracted from all other respiratory states. Oxygen consumption rates are expressed per μg DNA. B and F, Lower spare respiratory capacity in epiddymal adipocytes from HFD fed mice. Spare respiratory capacity = max − basal. C and G Lower mitochondrial abundance in inguinal adipocytes from HFD-fed mice. CS activity was measured as marker for mitochondrial abundance and expressed as CS activity per μg DNA. D and H, Lower cRCR (quotient of maximal-to-leak oxygen consumption) in epididymal adipocytes of HFD-fed mice. Data are presented as means ± SD (n = 6–8). *, $P < .05$; **, $P < .01$; ***, $P < .001$.

induce maximal phosphorylating respiration. Third, we conducted respirometry of isolated white adipocyte mitochondria to analyze mitochondrial bioenergetics free from the influence of cellular factors and undisturbed by differences in mitochondrial abundance (38).

Adipocytes of inguinal white fat were characterized by a higher maximal respiratory capacity compared with epididymal adipocytes. Leak (state 4o for isolated and permeabilized mitochondria) respiration rate was comparable between the two fat depots in all experimental setups. However, when mitochondria were brought to maximal oxygen consumption, either by chemical uncoupling or by addition of ADP, respiration of both epididymal adipocytes and their isolated mitochondria were consistently lower compared with adipocytes and mitochondria of inguinal origin. This finding is in line with the lower abundance of respiratory complex I, II, and IV in mitochondria of epididymal adipocytes. Given that there is no difference detectable in states of low oxygen consumption, obviously epididymal adipocytes are more likely to attain at their bioenergetic limit in situations of high ATP demand.

In comparison, a higher mitochondrial abundance has been reported to cause a higher respiration of epididymal compared with inguinal adipocytes in rats (39). Conversely, and in line with our findings, in obese humans sc adipose tissue displayed higher respiratory rates per cell and per mtDNA than visceral fat (40). Nonetheless, given that entire tissue biopsies were analyzed in that study, the contribution of the stromal vascular fraction to respiratory capacity remains elusive. Thus, to the best of our knowledge, the present study is the first demonstrating a higher metabolic capacity of sc adipocytes compared with visceral adipocytes due to higher mitochondrial performance.

Adipocyte heterogeneity in white adipose tissue depots may contribute to the observed differences in mitochondrial function. Brown-adipocyte-like cells, known as beige or brite adipocytes, are inducible in sc fat, but are scarce in visceral fat (41, 42). In the induced state, these *brite* adipocytes contain more mitochondria than classical white adipocytes and express the thermogenic uncoupling protein 1 (43). In our study, however, the contribution of brite adipocytes seems negligible as adult C57Bl/6N mice housed at room temperature exhibit very low numbers of brites in white adipose tissue (44, 45). On the functional level, respiratory control ratios of mitochondria from inguinal and epididymal adipocytes were similar.

The main function of white adipose tissue is storage and mobilization of lipids. Lipogenesis, triglyceride synthesis, and lipolysis are regulated dependent on organismic energy demand. In addition, white adipocytes exert various other functions including the synthesis and secretion of endocrine-, paracrine-, and autocrine-acting molecules known as adipokines, which in concert contribute to the regulation of whole-body metabolism (46). Each of these functions require functional, intact mitochondria with the ability to flexibly alter OXPHOS performance according to variable cellular ATP demand. Weight gain and obesity

are metabolically challenging states for adipocytes, as for instance, triglyceride synthesis must be increased due to the excessive fuel supply. Because epididymal adipocytes are operating closer to their bioenergetic limit, they might fail to satisfy cellular ATP demands during this metabolic challenge before sc adipocytes do. Simultaneously, mitochondria from epididymal adipocytes generate higher levels of superoxide during maximal OXPHOS activity. This could interfere with cellular insulin signaling (47) or adipokine secretion (48, 49). In summary, a lower OXPHOS capacity combined with an increased ROS release in epididymal adipocytes can be regarded as metabolic inflexibility, which further deteriorates during adipocyte hypertrophy. Possibly, this incapacity causes elevated oxidative damage, increased free fatty acid levels and an altered adipokine secretion pattern, thereby contributing to the tremendous consequences of obesity for whole-body energy and glucose homeostasis. Concordantly, visceral mass gain is a well-known risk factor for insulin resistance and type 2 diabetes (1, 4–6) while expansion of sc adipose tissue even prevents the development of insulin resistance associated with obesity in laboratory mice (50). This is in line with our observation that HFD exposure for 1 week lowered white adipocyte mitochondrial capacity in adipocytes from visceral fat much more than in cells from inguinal fat, accompanied by the emergence of body glucose intolerance. A causal relationship between these two phenomena is possible.

Taken together, we analyzed a suite of mitochondrial functions in intact and permeabilized cells and native organelles to reveal differences in mitochondrial bioenergetics of white adipocytes from anatomically distinct fat depots. The design of our study can serve as a starting point for further investigations focusing on comprehensive characterization of white adipocyte bioenergetics in the context of various metabolic diseases, dietary and genetic manipulations of body weight, pharmacological treatments, aging, and others.

Subcutaneous inguinal adipocytes displayed a markedly higher respiratory capacity and flexibility when compared with mitochondria from epididymal fat. The divergent oxidative capacity was intrinsic to mitochondria and did not result from higher mitochondrial abundance or other intracellular structures and signals influencing mitochondrial function. Feeding a HFD for 1 week affected white adipocyte mitochondrial capacity, with much stronger deficits in epididymal when compared with inguinal adipocytes, paralleled by impaired whole-body glucose homeostasis. The extent to which regional differences of adipose tissue depots in the vulnerability of their OXPHOS system accounts for the divergent metabolic risk of sc and visceral fat must be clarified in future studies.

Acknowledgments

Address all correspondence and requests for reprints to: Dr Martin Klingenspor, Professor for Molecular Nutritional Medicine, Technische Universität München, Gregor-Mendel-Strasse 2, D-85356 Freising-Weihenstephan, Germany. E-mail: mk@tum.de.

Financial Support: The Chair of Molecular Nutritional Medicine received financial support from the Else Kröner-Fresenius Foundation (2007–2014). This study was partly funded by the Federal Ministry of Education and Research, Germany (BMBF AZ 0315674).

Disclosure Summary: The authors have nothing to disclose.

References

1. **Bjørndal B, Burri L, Staalesen V, Skorve J, Berge RK.** Different adipose depots: their role in the development of metabolic syndrome and mitochondrial response to hypolipidemic agents. 2011;2011:490650.
2. **Kopelman PG.** Obesity as a medical problem. *Nature*. 2000;404(6778):635–643.
3. **Kaur J.** A Comprehensive review on metabolic syndrome. *Cardiol Res Pract*. 2014;2014:943162.
4. **Vague J.** The degree of masculine differentiation of obesities: A factor determining predisposition to diabetes, atherosclerosis, gout, and uric calculous disease. *Am J Clin Nutr*. 1956;4(1):20–34.
5. **Tran TT, Yamamoto Y, Gesta S, Kahn CR.** Beneficial effects of subcutaneous fat transplantation on metabolism. *Cell Metab*. 2008;7(5):410–420.
6. **Hocking SL, Chisholm DJ, James DE.** Studies of regional adipose transplantation reveal a unique and beneficial interaction between subcutaneous adipose tissue and the intra-abdominal compartment. *Diabetologia*. 2008;51(5):900–902.
7. **Fox CS, Massaro JM, Hoffmann U, et al.** Abdominal visceral and subcutaneous adipose tissue compartments: Association with metabolic risk factors in the Framingham Heart Study. *Circulation*. 2007;116(1):39–48.
8. **Lefebvre AM, Laville M, Vega N, et al.** Depot-specific differences in adipose tissue gene expression in lean and obese subjects. *Diabetes*. 1998;47(1):98–103.
9. **Macotela Y, Emanuelli B, Mori MA, et al.** Intrinsic differences in adipocyte precursor cells from different white fat depots. *Diabetes*. 2012;61(7):1691–1699.
10. **Sackmann-Sala L, Berryman DE, Munn RD, Lubbers ER, Kopchick JJ.** Heterogeneity among white adipose tissue depots in male C57BL/6J mice. *Obesity*. 2012;20(1):101–111.
11. **Vohl MC, Sladek R, Robitaille J, et al.** A survey of genes differentially expressed in subcutaneous and visceral adipose tissue in men. *Obes Res*. 2004;12(8):1217–1222.
12. **O'Rourke RW, Metcalf MD, White AE, et al.** Depot-specific differences in inflammatory mediators and a role for NK cells and IFN-gamma in inflammation in human adipose tissue. *International J Obes*. 2009;33(9):978–990.
13. **Montague CT, O'Rahilly S.** The perils of portliness: Causes and consequences of visceral adiposity. *Diabetes*. 2000;49(6):883–888.
14. **Hellmér J, Marcus C, Sonnenfeld T, Arner P.** Mechanisms for differences in lipolysis between human subcutaneous and omental fat cells. *J Clin Endocrinol Metab*. 1992;75(1):15–20.
15. **Richelsen B, Pedersen SB, Moller-Pedersen T, Bak JF.** Regional differences in triglyceride breakdown in human adipose tissue: Effects of catecholamines, insulin, and prostaglandin E2. *Metabolism*. 1991;40(9):990–996.
16. **Alessi MC, Peiretti F, Morange P, Henry M, Nalbone G, Juhan-**

Vague I. Production of plasminogen activator inhibitor 1 by human adipose tissue: Possible link between visceral fat accumulation and vascular disease. *Diabetes*. 1997;46(5):860–867.
17. **Fried SK, Bunkin DA, Greenberg AS.** Omental and subcutaneous adipose tissues of obese subjects release interleukin-6: Depot difference and regulation by glucocorticoid. *J Clin Endocrinol Metab*. 1998;83(3):847–850.
18. **Montague CT, Prins JB, Sanders L, Digby JE, O'Rahilly S.** Depot- and sex-specific differences in human leptin mRNA expression: Implications for the control of regional fat distribution. *Diabetes*. 1997;46(3):342–347.
19. **Chau YY, Bandiera R, Serrels A, et al.** Visceral and subcutaneous fat have different origins and evidence supports a mesothelial source. *Nat Cell Biol*. 2014;16(4):367–375.
20. **Giordano A, Smorlesi A, Frontini A, Barbatelli G, Cinti S.** White, brown and pink adipocytes: The extraordinary plasticity of the adipose organ. *Eur J Endocrinol*. 2014;170(5):R159–R171.
21. **Cinti S.** The adipose organ. *Prostaglandins Leukot Essent Fatty Acids*. 2005;73(1):9–15.
22. **Frontini A, Cinti S.** Distribution and development of brown adipocytes in the murine and human adipose organ. *Cell Metab*. 2010; 11(4):253–256.
23. **Rong JX, Qiu Y, Hansen MK, et al.** Adipose mitochondrial biogenesis is suppressed in db/db and high-fat diet-fed mice and improved by rosiglitazone. *Diabetes*. 2007;56(7):1751–1760.
24. **Wang PW, Kuo HM, Huang HT, et al.** Biphasic response of mitochondrial biogenesis to oxidative stress in visceral fat of diet-induced obesity mice. *Antioxid Redox Signal*. 2014;20(16):2572–2588.
25. **Dahlman I, Forsgren M, Sjögren A, et al.** Downregulation of electron transport chain genes in visceral adipose tissue in type 2 diabetes independent of obesity and possibly involving tumor necrosis factor-alpha. *Diabetes*. 2006;55(6):1792–1799.
26. **Choo HJ, Kim JH, Kwon OB, et al.** Mitochondria are impaired in the adipocytes of type 2 diabetic mice. *Diabetologia*. 2006;49(4): 784–791.
27. **Bogacka I, Xie H, Bray GA, Smith SR.** Pioglitazone induces mitochondrial biogenesis in human subcutaneous adipose tissue in vivo. *Diabetes*. 2005;54(5):1392–1399.
28. **Lindinger A, Peterli R, Peters T, et al.** Mitochondrial DNA content in human omental adipose tissue. *Obes Surg*. 2010;20(1):84–92.
29. **Even PC, Nadkarni NA.** Indirect calorimetry in laboratory mice and rats: Principles, practical considerations, interpretation and perspectives. *Am J Physiol Regul Integr Comp Physiol*. 2012;303(5): R459–R476.
30. **Brand MD, Nicholls DG.** Assessing mitochondrial dysfunction in cells. *Biochem J*. 2011;435(2):297–312.
31. **Korshunov SS, Skulachev VP, Starkov AA.** High protonic potential actuates a mechanism of production of reactive oxygen species in mitochondria. *FEBS Lett*. 1997;416(1):15–18.
32. **Loschen G, Azzi A.** On the formation of hydrogen peroxide and oxygen radicals in heart mitochondria. *Recent Adv Stud Cardiac Struct Metab*. 1975;7:3–12.
33. **Loschen G, Azzi A, Richter C, Flohé L.** Superoxide radicals as precursors of mitochondrial hydrogen peroxide. *FEBS Lett*. 1974; 42(1):68–72.
34. **Boveris A, Cadenas E.** Mitochondrial production of superoxide anions and its relationship to the antimycin insensitive respiration. *FEBS Lett*. 1975;54(3):311–314.
35. **Kusminski CM, Holland WL, Sun K, et al.** MitoNEET-driven alterations in adipocyte mitochondrial activity reveal a crucial adaptive process that preserves insulin sensitivity in obesity. *Nat Med*. 2012;18(10):1539–1549.
36. **Vernochet C, Mourier A, Bezy O, et al.** Adipose-specific deletion of TFAM increases mitochondrial oxidation and protects mice against obesity and insulin resistance. *Cell Metab*. 2012;16(6):765–776.
37. **Appaix F, Kuznetsov AV, Usson Y, et al.** Possible role of cytoskeleton in intracellular arrangement and regulation of mitochondria. *Experimental physiology*. 2003;88(1):175–190.
38. **Perry CG, Kane DA, Lanza IR, Neufer PD.** Methods for assessing mitochondrial function in diabetes. *Diabetes*. 2013;62(4):1041–1053.
39. **Deveaud C, Beauvoit B, Salin B, Schaeffer J, Rigoulet M.** Regional differences in oxidative capacity of rat white adipose tissue are linked to the mitochondrial content of mature adipocytes. *Mol Cell Biochem*. 2004;267(1–2):157–166.
40. **Kraunsøe R, Boushel R, Hansen CN, et al.** Mitochondrial respiration in subcutaneous and visceral adipose tissue from patients with morbid obesity. *J Physiol*. 2010;588(Pt 12):2023–2032.
41. **Barbatelli G, Murano I, Madsen L, et al.** The emergence of cold-induced brown adipocytes in mouse white fat depots is determined predominantly by white to brown adipocyte transdifferentiation. *Am J Physiol Endocrinol Metab*. 2010;298(6):E1244–E1253.
42. **Guerra C, Koza RA, Yamashita H, Walsh K, Kozak LP.** Emergence of brown adipocytes in white fat in mice is under genetic control. Effects on body weight and adiposity. *J Clin Invest*. 1998;102(2): 412–420.
43. **Li Y, Lasar D, Fromme T, Klingenspor M.** White, brite, and brown adipocytes: The evolution and function of a heater organ in mammals. *Can J Zool*. 2014;92:615–626.
44. **Xue B, Coulter A, Rim JS, Koza RA, Kozak LP.** Transcriptional synergy and the regulation of Ucp1 during brown adipocyte induction in white fat depots. *Mol Cell Biol*. 2005;25(18):8311–8322.
45. **Okamatsu-Ogura Y, Fukano K, Tsubota A, et al.** Thermogenic ability of uncoupling protein 1 in beige adipocytes in mice. *PloS One*. 2013;8(12):e84229.
46. **Lago F, Dieguez C, Gómez-Reino J, Gualillo O.** Adipokines as emerging mediators of immune response and inflammation. *Nat Clin Pract Rheumatol*. 2007;3(12):716–724.
47. **Lin Y, Berg AH, Iyengar P, et al.** The hyperglycemia-induced inflammatory response in adipocytes: The role of reactive oxygen species. *J Biol Chem*. 2005;280(6):4617–4626.
48. **Soares AF, Guichardant M, Cozzone D, et al.** Effects of oxidative stress on adiponectin secretion and lactate production in 3T3–L1 adipocytes. *Free Radic Biol Med*. 2005;38(7):882–889.
49. **Furukawa S, Fujita T, Shimabukuro M, et al.** Increased oxidative stress in obesity and its impact on metabolic syndrome. *J Clin Invest*. 2004;114(12):1752–1761.
50. **Kim JY, van de Wall E, Laplante M, et al.** Obesity-associated improvements in metabolic profile through expansion of adipose tissue. *J Clin Invest*. 2007;117(9):2621–2637.

Supplemental material

Figure S1

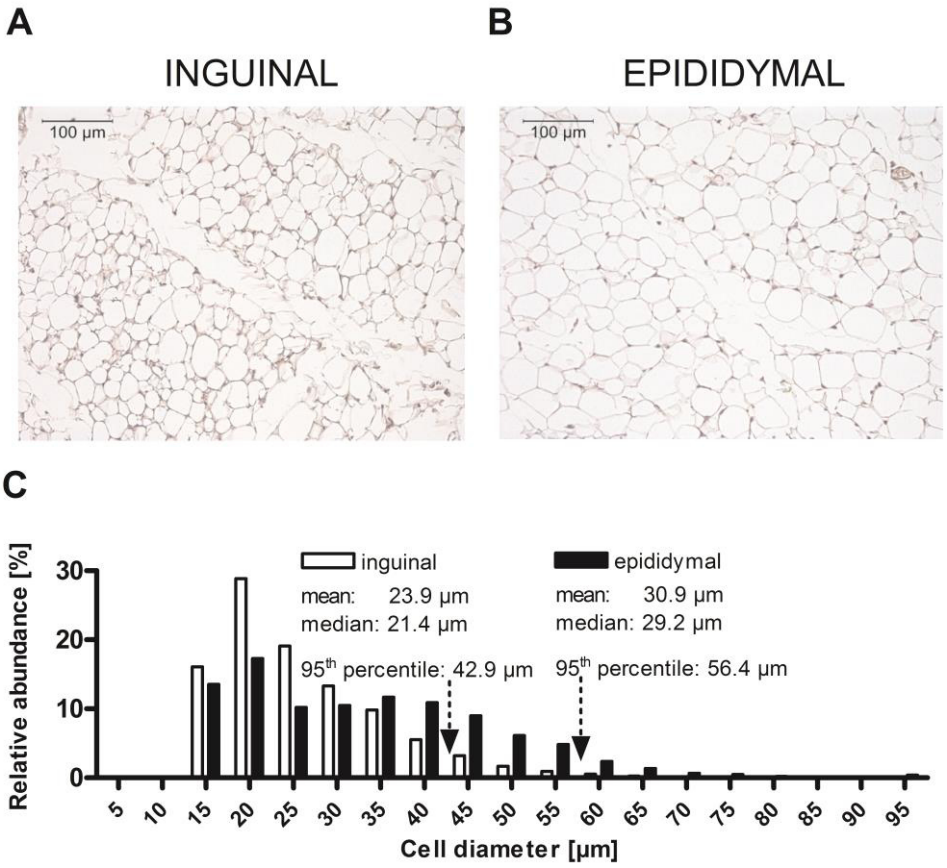

Figure S1. Adipocyte sizes of inguinal versus epididymal adipocytes. Representative images of histological sections of **(A)** inguinal and **(B)** epididymal white adipose tissue. Scale bar = 100 µm. **(C)** Histograms show relative size distributions. Cell diameters were analyzed in fat depots of six mice (n=6) each with five independent histological sections (N=5).

CHAPTER II

"OBESITY MEDIATED ALTERATIONS IN WHITE ADIPOCYTE MITOCHONDRIAL BIOENERGETICS AND THEIR RELATION TO SYSTEMIC GLUCOSE HOMEOSTASIS"

MOLECULAR METABOLISM, 2015 JUL 21 [EPUB AHEAD OF PRINT]

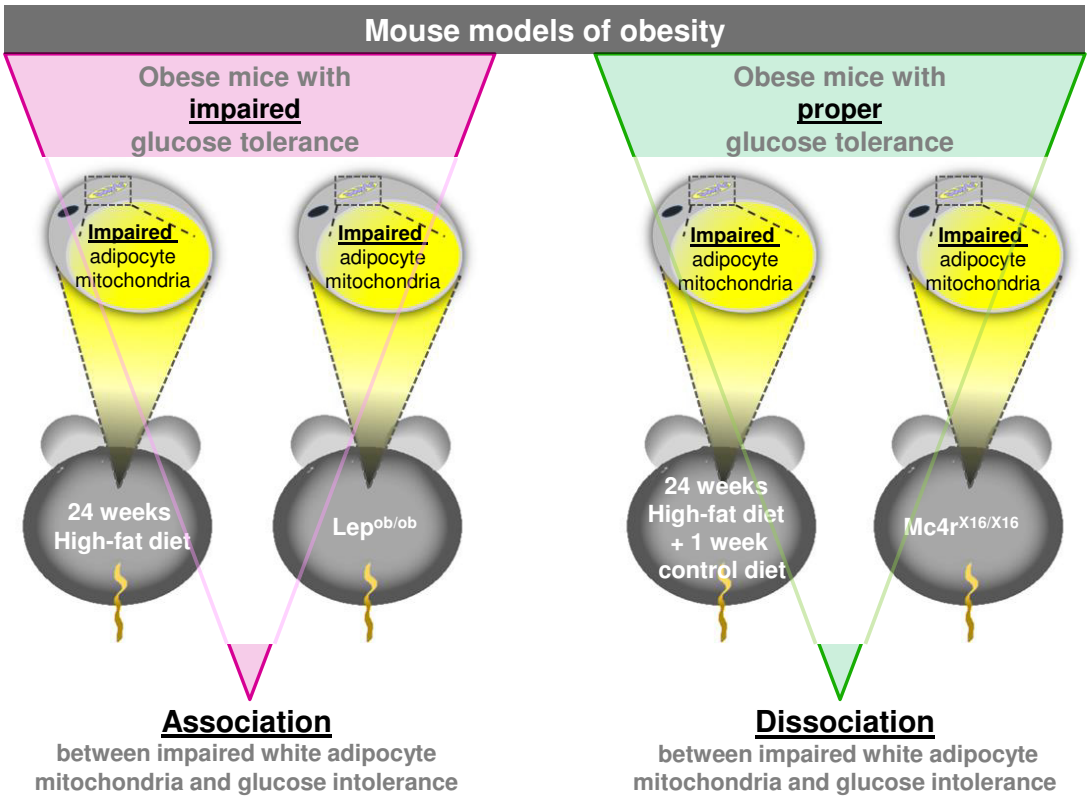

Original article

MOLECULAR METABOLISM

Limited OXPHOS capacity in white adipocytes is a hallmark of obesity in laboratory mice irrespective of the glucose tolerance status

Theresa Schöttl, Lisa Kappler, Tobias Fromme, Martin Klingenspor*

ABSTRACT

Objective: Several human and rodent obesity studies speculate on a causal link between altered white adipocyte mitochondria in the obese state and changes in glucose homeostasis. We here aimed to dissect whether alterations in white adipocyte mitochondrial respiratory function are a specific phenomenon of obesity or impaired glucose tolerance or both.
Methods: Mature white adipocytes were purified from posterior subcutaneous and intraabdominal epididymal fat of four murine obesity models characterized by either impaired or normal oral glucose tolerance. Bioenergetic profiles, including basal, leak, and maximal respiration, were generated using high-resolution respirometry. Cell respiratory control ratios were calculated to evaluate mitochondrial respiratory function.
Results: Maximal respiration capacity and cell respiratory control ratios were diminished in white adipocytes of each of the four murine obesity models, both in the absence and the presence of impaired glucose tolerance. Limitation was more pronounced in adipocytes of intraabdominal versus subcutaneous fat.
Conclusion: Reduced mitochondrial respiratory capacity in white adipocytes is a hallmark of murine obesity irrespective of the glucose tolerance status. Impaired respiratory capacity in white adipocytes solely is not sufficient for the development of systemic glucose intolerance.

Keywords Obesity; Glucose tolerance; White adipocyte metabolism; Mitochondria

1. INTRODUCTION

Mass-specific resting metabolic rate of white adipose tissue (WAT) is low and may appear negligible compared to the high metabolic rate of organs such as brain, kidneys, heart or liver [1,2]. Statistical modeling of whole body energy expenditure, however, reveals an unexpectedly large contribution of adipose tissue mass to the intra-individual variation in resting metabolic rate. This is not caused by the metabolic cost of the adipose organ itself but rather by the influence on metabolism of other organs including liver and skeletal muscle, most likely involving the well-established endocrine function of adipocytes in body energy and glucose homeostasis regulation [3]. Thus, the impact of adipocyte function on whole body energy and glucose metabolism is much larger than expected from their intrinsic metabolic rate.

Mitochondria are the major site of energy turnover in cells consuming oxygen for ATP synthesis by oxidative phosphorylation (OXPHOS). Furthermore, they play a central role in the metabolism of reactive oxygen species (ROS), the regulation of apoptosis and the regulation of calcium levels in both cytoplasm and matrix, in addition to many other functions [4,5]. In adipocytes, proper mitochondrial function is essential for differentiation, lipogenesis and lipolysis [6], as well as the production and secretion of adipokines [7]. Thus, alterations in white adipocyte mitochondrial function can be expected to affect adipocyte physiology with tremendous secondary effects on whole body energy and glucose homeostasis.

Several human and rodent studies highlighted the simultaneous appearance of deranged white adipocyte mitochondria and impaired glucose homeostasis. Mitochondrial biogenesis and abundance, the expression of genes and proteins involved in OXPHOS, and mitochondrial oxygen consumption, as a key parameter for mitochondrial function, are reduced in WAT or isolated adipocytes of obese and/or type 2 diabetic rodent models and humans [8–13]. Moreover, we recently uncovered reduced mitochondrial OXPHOS functionality in white adipocytes, which emerges in parallel with impaired glucose tolerance after one week of high-fat diet feeding [14]. The fact that obesity is often accompanied by impaired glucose tolerance and reduced adipocyte mitochondrial function, however, does not prove causality between these phenomena. The ultimate challenge is to clarify the relationship between obesity, white adipocyte mitochondrial function, and glucose intolerance.

In the present study, we determined glucose tolerance and white adipocyte OXPHOS, as a parameter for mitochondrial function, in anatomically distinct fat depots of several murine obesity models. We first comprehensively analyzed mitochondrial respiration of isolated adipocytes from both posterior subcutaneous and intraabdominal epididymal fat of diet-induced obese mice with pronounced glucose

Molecular Nutritional Medicine, Technische Universität München, Else Kröner Fresenius Center for Nutritional Medicine, Freising, Germany

*Corresponding author. Molecular Nutritional Medicine, Technische Universität München, Gregor-Mendel-Str. 2, D-85356 Freising-Weihenstephan, Germany. Tel.: +49 8161 71 2386; fax: +49 8161 71 2366. E-mail: mk@tum.de (M. Klingenspor).

Received June 16, 2015 • Revision received July 3, 2015 • Accepted July 7, 2015 • Available online xxx

http://dx.doi.org/10.1016/j.molmet.2015.07.001

Original article

Abbreviations

AUC	area under the curve
BSA	bovine serum albumin
CD	control diet
cRCR	cell respiratory control ratio
CS	citrate synthase
ETC	electron transport chain
eWAT	epididymal white adipose tissue
HFD	high-fat diet
psWAT	posterior subcutaneous white adipose tissue
Mc4R	melanocortin-4-receptor
OXPHOS	oxidative phosphorylation
RCR	respiratory control ratio
ROS	reactive oxygen species
T2DM	type 2 diabetes mellitus
WAT	white adipose tissue

intolerance, describing the extent of functional mitochondrial alterations associated with obesity and/or glucose intolerance. Second, we demonstrated mitochondrial OXPHOS capacity to be limited in any state of elevated body fat content by experimenting with diet-induced obese mice with recovered glucose tolerance in response to energy restriction and two monogenetic models of obesity.

2. MATERIALS AND METHODS

2.1. Mice

All experiments were conducted on male mice. Before and throughout the whole experiment, mice were housed in groups in a specific pathogen-free environment on a 12:12 h light–dark photocycle at 22 °C with ad libitum access to water and food.

The study was performed with permission of the government of Upper Bavaria (Regierung von Oberbayern, reference number Az. 55.2.1.54-2532-148-13).

2.1.1. Diet induced obesity models

At the age of 7 weeks, wildtype C57BL/6N mice were switched from chow (type M-Z, Ssniff, Soest, Germany) to a purified research control diet (CD, 12 kJ% fat, SS745-E702, Ssniff). After an acclimatization phase of one week, mice were matched by body weight into a CD and a high-fat diet group (HFD, 48% kJ% fat SS745-E712; Ssniff). Feeding was conducted for 24 weeks. Mice of the HF-recovery cohort received CD for one week subsequent to HFD feeding for 24 weeks. Mice were killed and dissected at the end of the respective feeding period.

2.1.2. Genetic obesity

$Lep^{ob/ob}$ mice and mice with melanocortin-4-receptor (Mc4R) deficiency, including $Mc4R^{X16/X16}$, are well established models for monogenetic obesity characterized by enormous weight and fat mass gain on a regular diet [15,16].

$Mc4r^{X16/X16}$ – Generation of $Mc4r^{X16/X16}$ knock-in mice has been described in detail before [16]. At the age of 7 weeks $Mc4r^{X16/X16}$ mice and $Mc4r^{wt/wt}$ littermates were switched from normal chow to CD diet until dissection at the age of 32 weeks.

$Lep^{ob/ob}$ – $Lep^{ob/ob}$ mice and wildtype $Lep^{+/+}$ littermates received normal chow diet until dissection at the age of 14 weeks.

2.1.3. Body weight and body composition

Body weight and body composition (analyzed with nuclear magnetic resonance spectroscopy -The Minispec mq 7.5 POY Live mice analyzer, Bruker, Billerica, MA, USA) of all mice were measured at the end of experimental duration (HFD versus CD: after 24 weeks feeding, $Mc4R^{X16/X16}$ versus $Mc4R^{wt/wt}$: at the age of 32 weeks, $Lep^{ob/ob}$ versus $Lep^{+/+}$: at the age of 14 weeks, HF-recovery mice and controls: after 24 weeks HFD/CD feeding when HFD was replaced by CD as well as after one week CD refeeding).

2.1.4. Oral glucose tolerance

After a fasting period of six hours, mice received 2.66 mg glucose per [(lean mass + 0.2 fat mass) g] by single oral gavage, referring to [17]. Blood glucose was monitored before and 15, 30, 60 and 90 min after gavage. Total area-under-the-curve (AUC) was calculated as measure for glucose tolerance.

2.1.5. Plasma insulin levels

For plasma preparation, cardiac blood was sampled from CO_2 anesthetized mice in heparin-coated tubes and centrifuged for 2 min at 2000 *g*. Plasma concentration of insulin was ascertained using a commercial Kit system (Ultra Sensitive Mouse Insulin ELISA Kit, 90080 Christyl Chem, Downers Grove, IL, USA).

2.2. Tissue dissection and isolation of adipocytes

Mice were killed by carbon dioxide exposure and exsanguination. Posterior subcutaneous and intraabdominal epididymal fat depots were dissected and weighed. For assessment of adipocyte bioenergetics on the cellular level, fat depots of individual mice were used. Due to the low yield of mitochondria per ml adipocyte suspension at mitochondrial isolation, fat depots of 8–12 mice were combined for experiments on isolated mitochondria. Therefore, fat pools were generated for posterior subcutaneous and intraabdominal epididymal fat separately, and they were analyzed individually throughout our study. Mature adipocytes were separated from other cell types by collagenase-digestion as described in detail previously [14] (collagenase type A, Roche Applied Science; Penzberg, Germany; 1 g/l in Hank's Balanced Salt Solution [HBSS 14025-092, Gibco®, live technologies, Carlsbad, CA, USA] containing 4% BSA). Isolated mature adipocytes were washed with STE-buffer containing 4% BSA-fatty acid free (250 mM sucrose, 5 mM Tris, 2 mM EGTA, pH = 7.4 at 4 °C).

2.3. Characterization of isolated mature adipocytes

2.3.1. Bioenergetics

Oxygen consumption of adipocytes was measured with high-resolution respirometry (Oxygraph-2k, OROBOROS INSTRUMENTS, Innsbruck, Austria) as described previously [14]. Briefly, 100 µl of adipocyte suspension was pipetted into 2 ml MIR05 buffer (110 mM sucrose, 60 mM potassium lactobionate, 0.5 mM EGTA, 3 mM $MgCl_2$*$6H_2O$, 20 mM taurine, 10 mM KH_2PO_4, 20 mM Hepes, 1 g/l BSA-fatty acid free, 5 mM malate, pH 7.1 at 37 °C, as described by OROBOROS INSTRUMENTS). First, pyruvate (5 mM) was added, and basal cellular respiration was recorded. Respiration determined by proton leak was assessed by addition of complex V inhibitor oligomycin (2.5 µg/ml). Titration of FCCP (0.5 µM steps) was performed to measure maximal cellular respiration rates. Non-mitochondrial oxygen consumption was determined by addition of complex III inhibitor antimycin A (2.5 µM) and subtracted from the other respiratory states. Spare respiratory capacity was calculated by subtracting basal from maximal oxygen consumption. For mitochondrial integrity control cell respiratory control

MOLECULAR METABOLISM

ratio (cRCR) was calculated as ratio of maximal to leak oxygen consumption.

2.3.2. Cellular DNA quantification

DNA content of adipocyte suspensions was assessed by quantitative PCR targeting a unique region of genomic DNA (promotor resistin) as described previously (primers: fw 5′-ACCTCTCTTGGGGTCAGATGT-3′, rev 5′-CTGGGTATTAGCTCCTGTCCC-3′) [14].

2.3.3. Citrate synthase activity

Citrate synthase activity was measured as a surrogate for mitochondrial content in adipocyte suspensions. Adipocyte suspensions were homogenized and diluted 1:25 in reaction buffer (100 mM Tris, 1 mM $MgCl_2$, 1 mM EGTA, 0.1 mM DTNB, 3.6 mM Acetyl-CoA, pH 8.2). Absorption was measured at 30 °C and 412 nm with a microplate reader (TECAN Infinite® M200, Tecan Group Ltd.; Männedorf, Switzerland) before and after oxaloacetate (0.5 mM) was injected. Enzyme activity [μmol/min*mg protein] was calculated on the basis of the absorption change before and after injection of oxaloacetate with respect to dilution factor, extinction coefficient of DTNB and path length of the plate.

2.4. Characterization of isolated mitochondria

2.4.1. Isolation of mitochondria

Mitochondrial isolation from adipocytes was performed as already described [14]. Briefly, mature adipocytes were transferred into a glass-teflon homogenizer (15 ml), filled with STE to 15 ml and disrupted by 5 rotating strokes. Mitochondria were isolated from the homogenate via differential centrifugation (10 min at 800 *g*, 10 min at 10,000 *g*). Pellets were resuspended in KHE-buffer (120 mM KCL, 5 mM KH_2PO_4, 3 mM HEPES, 1 mM EGTA, 0.5% BSA-fatty acid free, pH = 7.2). Protein concentration determination of mitochondrial suspensions by Bradford protein assay was performed as described previously [14].

2.4.2. Bioenergetics

Oxygen consumption of isolated mitochondria was measured using microplate respirometry (XF96 Extracellular Flux Analyzer, Seahorse Bioscience, Billerica, MA, USA). Isolated mitochondria diluted in 20 μl KHE-buffer were seeded in collagen coated XF96-PS cell culture plates (Seahorse Bioscience, 5 μg per well). Mitochondrial respiration was measured in the presence of substrate only (complex I linked substrates: pyruvate and palmitoyl-L-carnitine; complex II substrate: succinate, state 4). ADP (6 mM) was injected to induce phosphorylating respiration (state 3). Next, 2.5 μg/ml oligomycin was injected to inhibit ATP-synthase and measure leak respiration (state 4o). The chemical uncoupler carbonyl cyanide 4-(trifluoromethoxy) phenylhydrazone FCCP (4 μM) was added for measuring maximal uncoupled respiration rates (state 3u). Finally, non-OXPHOS oxygen consumption was assessed by the addition of antimycin A (4 μM) and rotenone (2 μM) and subtracted from values of the other conditions. Terminology of respiratory states refers to [4]. Oxygen consumption was calculated automatically by plotting oxygen concentration (nmoles O_2) versus time (min), using the original (gain) fixed algorithm of the XF Software. Respiratory control ratios were ascertained by dividing oxygen consumption during state 3 respiration by oxygen consumption during state 4o respiration.

2.4.3. Measurement of mitochondrial ROS

Mitochondrial H_2O_2 efflux was assessed using Amplex® Red fluorescence. Measurements and analysis were performed as described before [14]. Substrates: 5 mM pyruvate/5 mM malate, 40 μM palmitoyl-L-carnitine, 5 mM malate.

2.5. Immunoblotting

Mitochondrial protein (25 μg) was resolved on a 7.5% SDS-PAGE, transferred to a nitrocellulose membrane (LI-COR Biosciences, Lincoln, NE, USA; 60 min, 100 V) and probed with an antibody cocktail targeting one representative subunit of each of the five ETC complexes (MitoProfile® total OXPHOS Rodent WB Antibody Cocktail, 1:250, ab110413, complex I subunit NDUFB8, complex II-30kDa, complex III-Core protein 2, complex IV subunit I, complex V alpha subunit) and rabbit anti-protein voltage-dependent anion channel (VDAC) antibody (1:900, Calbiochem, PC548). Infrared dye conjugated secondary antibodies (IRDye® 680, IRDye® 800, LI-COR Biosciences) were incubated at a dilution of 1:20,000. The Odyssey software (LI-COR Biosciences) was applied to quantify band fluorescence intensities.

2.6. Statistical analyses

Data are presented as single or mean values ± standard deviation. For statistical comparison, Two-Way and Two-Way Repeated-Measures ANOVA followed by post-hoc Bonferroni testing, One-Way ANOVA followed by Tukey's multicomparison test or two-tailed Student's t-test were performed (SigmaPlot 12.5, Systat Software, Inc., San Jose, CA, USA; GraphPad Prism4, GraphPad Software, Inc., La Jolla, CA, USA). p Values < 0.05 were considered statistically significant.

3. RESULTS

3.1. Diet induced obesity is associated with glucose intolerance and limited mitochondrial OXPHOS capacity in white adipocytes

We analyzed the impact of obesity on glucose tolerance and white adipocyte mitochondrial oxidative phosphorylation (OXPHOS) with special attention to a) a possible association between both phenomena and b) differences in anatomically distinct fat depots.

As a first step, we determined glucose tolerance and white adipocyte mitochondrial OXPHOS functionality in subcutaneous and intra-abdominal fat of diet-induced obese mice. At the end of a 24 weeks feeding period, high-fat diet (HFD) fed mice were massively obese as indicated by a higher body and fat mass at a comparable lean mass (Figure 1A–C). Posterior subcutaneous and intraabdominal epididymal fat depots were significantly larger in HFD vs. CD fed mice, reflecting their contribution to whole body adiposity (posterior subcutaneous: HFD 2.836 g ± 0.636 g vs. CD 0.704 g ± 0.255 g; epididymal: HFD 1.714 g ± 0.441 g vs. CD 0.710 g ± 0.311 g, both $n = 38–41$, $p < 0.001$). Diet-induced obesity was accompanied by hyperinsulinemia and impaired oral glucose tolerance, reflected by lower glucose clearance and higher area under the curve (AUC, Table 1, Figure 1D,E).

We prepared mitochondria from adipocytes of both fat depots to study organelle respiratory function free of other cellular influences and undisturbed by differences in mitochondrial abundance [4]. Leak respiration (substrate only = state 4, and state 4o) of mitochondria from both fat depots of the HFD group tended to be lower irrespective of the substrate applied (succinate, pyruvate or palmitate), but this diet effect did not reach significance. In contrast, mitochondria from the HFD group consistently stood out by a marked reduction of phosphorylating (state 3) and maximal respiratory capacity (state 3u) (Figure 2A).

Respiratory control ratio (RCR, state 3/state4o) is a quality index for mitochondrial respiratory function reflecting the ability to generally run at idle but efficiently respond to ADP supply by high ATP production

Original article

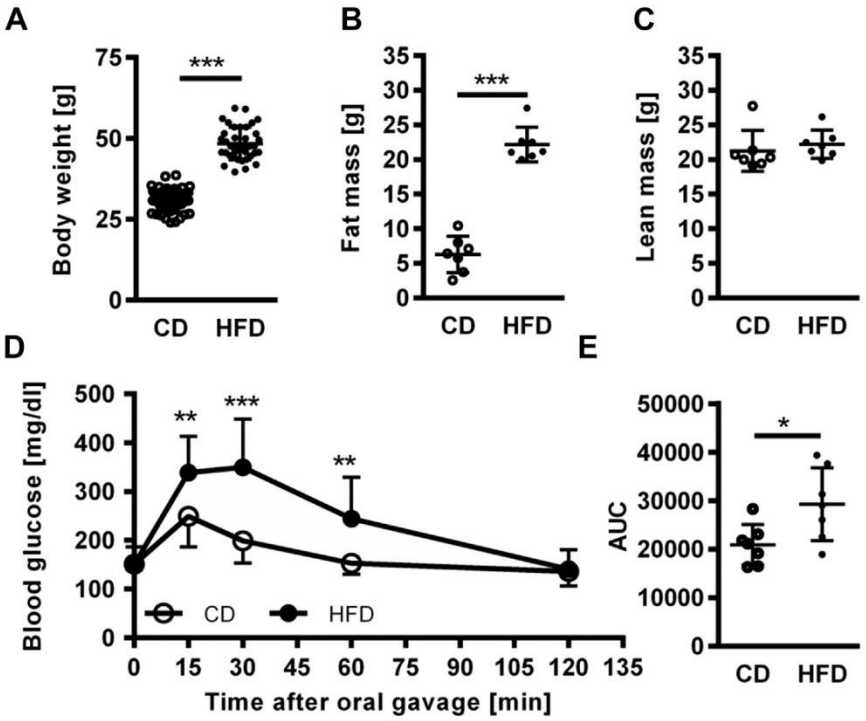

Figure 1: 24 weeks HFD feeding causes massive obesity and impaired glucose tolerance. At the age of eight weeks, mice were matched by body weight into HFD and CD groups. Diets were fed for 24 weeks. All parameters were measured at the end of the feeding period. (A) Body weight (n = 38–41), (B) Fat mass (n = 7), (C) Lean mass (n = 7), (D) Oral glucose tolerance test (n = 7), (E) Total area-under-the-curve (AUC) calculated from D as measure for glucose tolerance (n = 7). A, B, C, E was analyzed by Student's t-test. D was analyzed by two way repeated measures ANOVA. Data are presented as means ± SD. * = $p < 0.05$, ** = $p < 0.01$, *** = $p < 0.001$.

rates [4]. For mitochondria respiring on pyruvate or palmitate, but not succinate, we observed decreased RCRs in the HFD group (Figure 2B). Thus, HFD induced obesity caused a limitation in white adipocyte mitochondrial OXPHOS in posterior subcutaneous and epididymal adipocytes in states when maximal substrate oxidation capacity limits respiration (state 3, state 3u). Notably, the degree of impairment depended on the entry point of electrons into the respiratory chain: deficits were more pronounced in mitochondria respiring on complex I vs. complex II substrates, indicated by lower RCRs for pyruvate and palmitate but not succinate.

Lower abundance of respiratory chain complexes has been associated with lower OXPHOS capacity in mitochondria [18]. Thus, we quantified protein amount of representative subunits of each of the five OXPHOS complexes in relation to a surrogate marker of total mitochondrial abundance, the outer membrane channel porin/VDAC. Diet-group comparison revealed a significant reduction of the five enzyme complexes in both posterior subcutaneous ($p < 0.001$) and epididymal adipocyte mitochondria ($p < 0.01$) of HFD fed mice (Figure 3). Together, the lower absolute respiration capacity of isolated white adipocyte mitochondria of the HFD group may be explained by a decreased abundance in electron transport chain complexes per mitochondrion.

Elevated levels of reactive oxygen species (ROS) in adipocytes have been associated with obesity dependent impaired glucose tolerance and insulin resistance [19]. We determined whether mitochondria from posterior subcutaneous and epididymal adipocytes of HFD vs. control diet (CD) fed mice differ in terms of H_2O_2 efflux, as a result of superoxide radical anion formation. Superoxide, the main ROS produced by the electron transport chain, is converted by superoxide dismutase 2 (SOD2) to membrane permeable H_2O_2 [20,21] which is either

Table 1 — Plasma levels of insulin (non-fasted) and glucose (fasted and non-fasted) of different mouse models of obesity.

	Insulin [ng/ml]	Glucose [mg/dl] fasted	Glucose [mg/dl] non-fasted	n
CD	1.32 ± 0.93	150.90 ± 17.53	156.10 ± 14.93	5–7
HFD	11.66 ± 3.71***, a	149.20 ± 39.94	163.00 ± 38.47	6–7
CD (recovery model)	1.53 ± 0.63	140.70 ± 12.34	157.40 ± 12.90	6–7
HF-recovery	2.42 ± 0.68, b	136.10 ± 19.64	153.10 ± 15.83	6–7
$Lep^{+/+}$	1.43 ± 0.39	188.00 ± 37.11	154.30 ± 23.68	4–6
$Lep^{ob/ob}$	38.30 ± 15.25***, c	228.00 ± 52.26	158.60 ± 18.60	4–6
$Mc4R^{wt/wt}$	1.32 ± 0.52	169.30 ± 27.83	Not analyzed	6–8
$Mc4R^{X16/X16}$	7.22 ± 1.65***, a	147.30 ± 31.32	Not analyzed	6–8

Values are means ± SD. Data were analyzed by two-way ANOVA.
*$p < 0.05$, **$p < 0.01$, ***$p < 0.001$, significant differences compared to respective lean controls. Letters indicate significant group differences between obesity models.

MOLECULAR METABOLISM

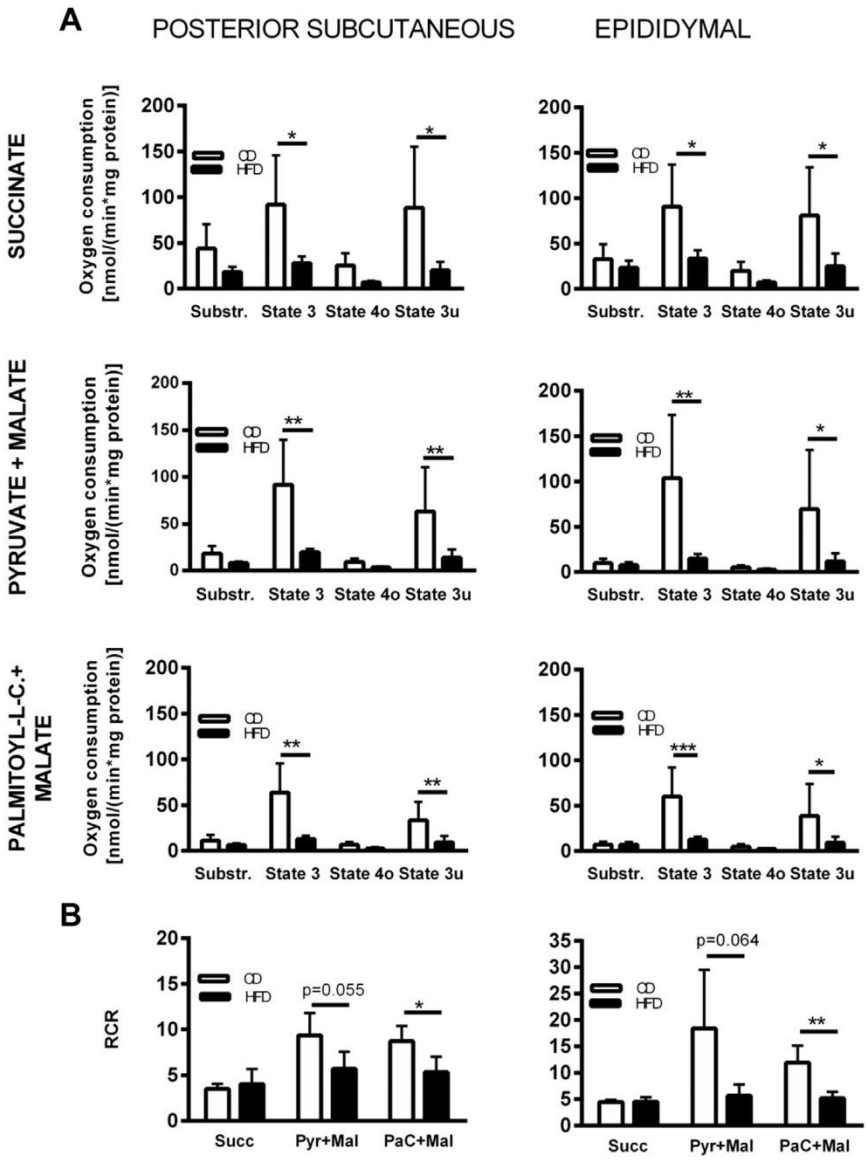

Figure 2: Bioenergetic characterization of isolated mitochondria from posterior subcutaneous and epididymal white adipocytes of mice fed either HFD or CD for 24 weeks: Obesity causes limited oxidative and respiratory capacity. (A) Bioenergetics of isolated white adipocyte mitochondria were measured using three different substrates (complex II linked substrate succinate and complex I linked substrates pyruvate or palmitate). First, respiration was assessed in presence of substrate only (state 4). Phosphorylating state 3 respiration was measured in the presence of ADP and substrate. ATP synthesis was inhibited and state 4o respiration was induced by oligomycin. Addition of the chemical uncoupler FCCP resulted in maximal uncoupled respiration (state 3u). Finally, non-biological background was determined by blockade of electron flow at complex III with antimycin A and subtracted from the other respiratory rates. Data were analyzed by Two-way repeated measures ANOVA (Bonferroni correction). (B) Mitochondrial respiratory control ratio (RCR) was calculated as indicator for mitochondrial integrity. It is defined as the ratio of state 3 to state 4o oxygen consumption (Succ = succinate, Pyr = pyruvate, Mal = malate, PaC = palmitoyl-L-carnitine). Data were analyzed by Student's t-test. Data are presented as means ± SD of 3–4 experiments.*$p = 0.05$, ** = $p < 0.01$, *** = $p < 0.001$.

released from the mitochondria or degraded by matrix antioxidant processes [22]. Mitochondrial H_2O_2 efflux, as a surrogate measure for ROS metabolism, was comparable in the two feeding groups of this study. We found no evidence for elevated ROS release from isolated white adipocyte mitochondria, which could be associated with impaired glucose tolerance observed in HFD fed mice. If anything, we detected a minor reduction of ROS release in mitochondria of the HFD group (Figure 4). This finding does not support the view that excessive mitochondrial ROS release in adipocytes from HFD fed mice contributes to the development of impaired glucose metabolism.

As oxygen consumption, but not ROS release, of isolated mitochondria was markedly affected in HFD fed mice, we further focused on respirometry. Studying intact cells prevents possible artifacts caused by the mitochondrial isolation procedure and is the most physiological approach to investigate cellular bioenergetics [4]. Therefore, we assessed whether the functional impairment observed in isolated mitochondria holds true for intact adipocytes. We observed no differences concerning basal and leak respiration but maximal cellular respiration rates in adipocytes (both fat depots) of the HFD group were markedly lower compared to the control group (Figure 5A,B).

Original article

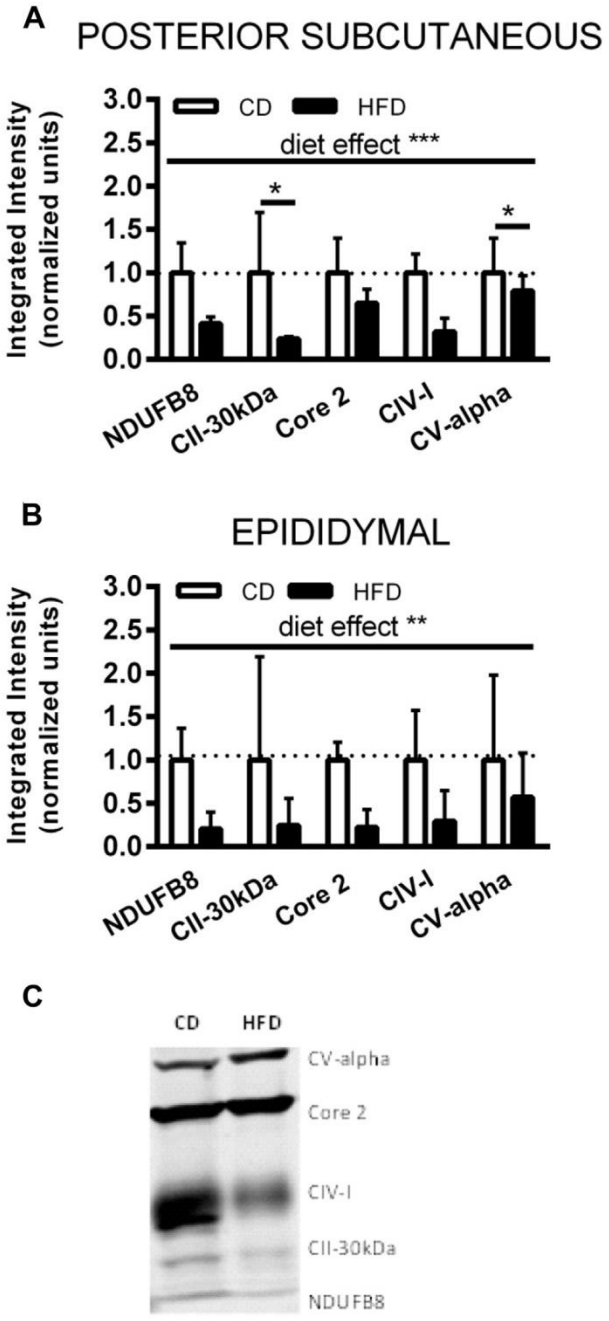

Figure 3: Reduced oxidative and respiratory capacity in white adipocyte mitochondria of HFD fed mice can be explained by lower enzymatic equipment of the respiratory chain. (A, B) Protein levels of representative subunits of each of the five OXPHOS complexes determined by immunoblot analysis of isolated mitochondria. MitoProfile® total OXPHOS antibody cocktail is targeted against complex I subunit NDUFB8, complex II-30kDa, complex III-Core protein 2, complex IV subunit I, and complex V alpha subunit. Bands were normalized to the outer membrane protein voltage-dependent anion channel (VDAC). Values of the HFD group are expressed as part of the CD group (=1). Data were analyzed by Two-way repeated measures ANOVA (Bonferroni correction) and presented as means ± SD of 3–4 experiments.*$p = 0.05$, ** $= p < 0.01$, *** $= p < 0.001$. (C) Representative OXPHOS immunoblot of isolated mitochondria from posterior subcutaneous adipocytes.

Accordingly, spare respiratory capacity — calculated as the difference in maximal and basal respiration — was lower in HFD adipocytes (Figure 5C,D). Thus, from a comparable basal level, adipocytes of HFD mice are unable to increase substrate oxidation in case of increased ATP demand to the same extent as adipocytes from control mice.

Differences in maximal respiratory capacity can be caused either by a different mitochondrial abundance per adipocyte, by a different functionality of mitochondria themselves, or by a combination of both. We quantified citrate synthase (CS) activity as a surrogate marker for mitochondrial abundance and observed lower mitochondrial mass in adipocytes of HFD fed versus CD fed mice, which only reached statistical significance for cells from posterior subcutaneous fat (Figure 5E,F). We calculated cell RCR (cRCR, maximal/leak respiration) as a measure for mitochondrial dysfunction, analogous to RCR of isolated mitochondria [4]. We observed reduced cRCRs for adipocytes of HFD fed mice in both fat depots analyzed but this reduction reached statistical significance only in epididymal fat (Figure 5G,H). Limited respiratory capacity in adipocytes of HFD fed mice can thus be explained by a combination of lower mitochondrial abundance per cell and insufficient mitochondrial OXPHOS capacity. The contribution of the latter is more prominent in adipocytes of epididymal fat.

We conclude that obesity caused by 24-weeks exposure to HFD results in glucose intolerance and a limitation in white adipocyte respiratory function. The latter is caused by both lower mitochondrial abundance per cell and impaired mitochondrial function as reflected by down-regulation of electron transport chain enzymes and reduced cRCRs/RCRs. Effects are more evident in adipocytes of epididymal as compared to posterior subcutaneous fat. We demonstrate simultaneous occurrence of reduced white adipocyte mitochondrial OXPHOS function and impaired glucose tolerance in the obese state.

3.2. Energy restriction rapidly recovers glucose tolerance, but not mitochondrial function

In a previous study, we found glucose tolerance of HFD fed mice to recover shortly after HFD is replaced by CD [23]. In detail, glucose tolerance of 12 weeks HFD fed mice of the strains AKR/J, SWR/J, and C57BL/6J was normalized after one week of CD refeeding. Of note, this phenomenon clearly occurred well in advance of a major decline in diet-induced body fat mass (unpublished data). This model should allow the dissection of a possible causality between white adipocyte mitochondrial function and glucose (in-)tolerance. Thus, we transferred the experimental design of our previous work to the present study and, in a second trial, refed mice with CD for one week after 24 weeks of HFD feeding (HF-recovery). During this period, HF-recovery mice markedly lost weight (HF-recovery -5.081 g $\pm$ 1.823 g vs. CD -0.064 g $\pm$ 1.640 g, $n = 7$, $p < 0.001$) but were still obese as indicated by final body weight and fat mass higher than that of controls (Figure 6A–B). Lean mass was comparable between the feeding groups (Figure 6C). Posterior subcutaneous and epididymal fat pads were significantly larger in HF-recovery compared to control mice, reflecting their contribution to whole body adiposity (posterior subcutaneous: HF-recovery 2.085 g $\pm$ 0.376 g vs. CD 0.732 g $\pm$ 0.280 g; epididymal: HF-recovery 1.540 g $\pm$ 0.156 g vs. CD 0.824 g $\pm$ 0.230 g, both $n = 7$, $p < 0.001$). Notably, HF-recovery mice displayed improved glucose tolerance which tended to be even better than that of controls (Figure 6D,E). To assess whether compensatory hyperinsulinemia masks peripheral insulin resistance, we analyzed plasma insulin levels. Compared to HFD fed mice HF-recovery mice stood out by significantly lower insulin concentrations which were similar to those of the control group (Table 1).

MOLECULAR METABOLISM

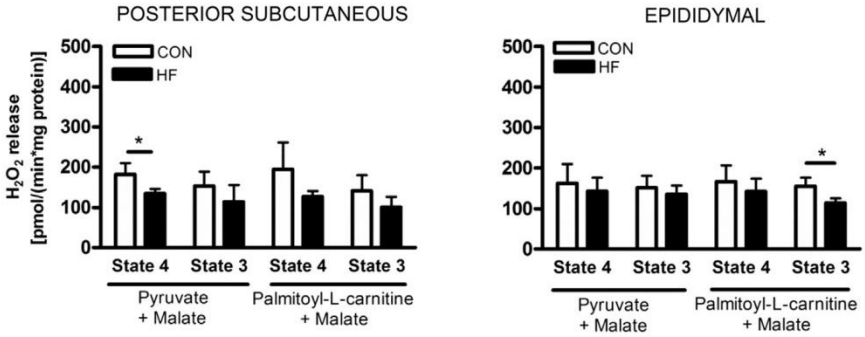

Figure 4: H_2O_2 release of isolated mitochondria from adipocytes of 24 weeks HFD versus CD fed mice. H_2O_2 release was assessed in pyruvate or palmitate energized mitochondria using Amplex® Red fluorescence. Measurements were conducted during state 4 (substrate only) and state 3 (substrate + ADP) respiration. Data are presented as means ± SD of 4 experiments. * = $p < 0.05$.

Respirometry of intact adipocytes revealed no difference between the CD und the HF-recovery group in basal and leak respiration. Maximal oxygen consumption of both types of adipocytes, however, was lower in the HF-recovery group (Figure 7A,B). Concordantly, spare respiratory capacity was reduced in adipocytes of HF-recovery mice (Figure 7C,D). Thus, adipocytes of HF-recovery mice displayed a lower ability to increase substrate oxidation compared to CD mice. Mitochondrial abundance, based on CS activity per cell, was reduced in adipocytes of HF-recovery mice (Figure 7E,F). Cellular RCR was comparable in posterior subcutaneous but markedly decreased in epididymal adipocytes (Figure 7G,H). Thus, limited maximal cellular respiration in epididymal adipocytes is clearly ascribable to both lower mitochondrial

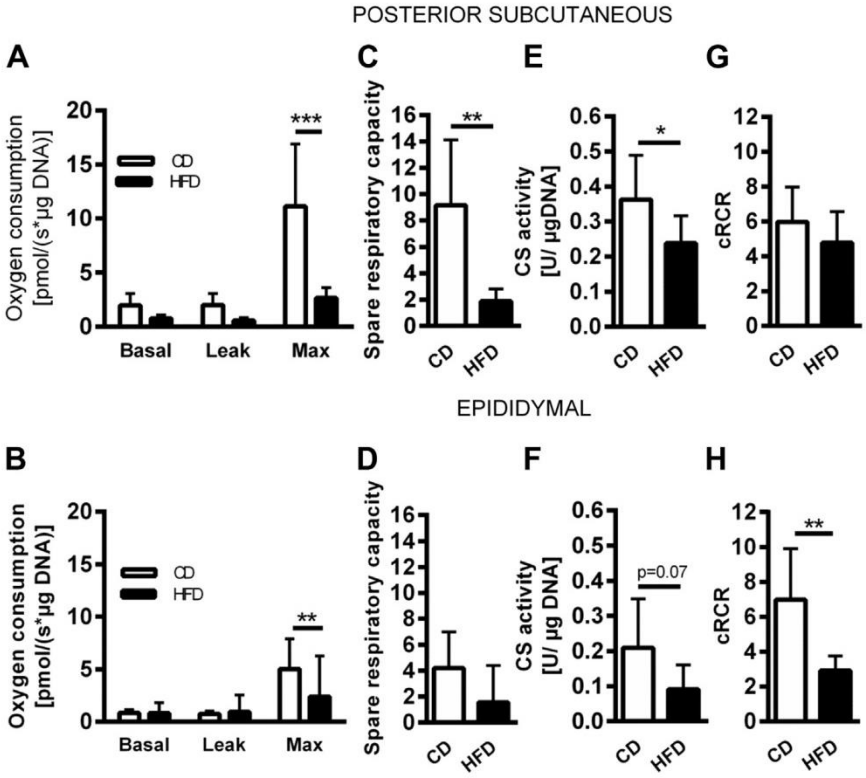

Figure 5: Cellular respiration of adipocytes from mice either fed HFD or CD for 24 weeks: HFD feeding results in limited maximal cellular respiratory capacity and reduced mitochondrial integrity. (A, B) First, basal respiration using pyruvate as substrate was assessed. ATP synthase inhibitor oligomycin was added to define the proportion of basal respiration contributing to either ATP turnover or proton leak, respectively. Next, FCCP was added to determine the maximal cellular respiratory capacity. Lastly, non-mitochondrial background was determined by addition of complex III inhibitor antimycin A and subtracted from the other respiratory states. Oxygen consumption rates are expressed per µg DNA. (C, D) Higher spare respiratory capacity in adipocytes from CD fed mice. Spare respiratory capacity = max − basal. (E, F) Citrate synthase activity was measured as a marker for mitochondrial abundance and expressed as CS activity per µg DNA (G, H). As an index for mitochondrial integrity, cell respiratory control ratio (cRCR) was calculated (quotient of maximal to leak oxygen consumption). A–B was analyzed by Two-way repeated measures ANOVA (Bonferroni correction. C-H was analyzed by Student's t-test. Data are presented as means ± SD of 7 experiments. $p < 0.05$, ** = $p < 0.01$, *** = $p < 0.001$.

abundance and lower mitochondrial capacity. In posterior subcutaneous adipocytes, mitochondrial abundance alone explains the diminished cellular respiratory capacity.

Taken together, obese HF-recovery mice exhibited limited mitochondrial OXPHOS capacity in white adipocytes, with stronger effects in epididymal vs. subcutaneous fat, i.e. in a similar pattern as observed in adipocytes of obese HFD fed mice. Notably, these mice displayed a normal, undisturbed glucose tolerance. As euglycemia was maintained by normal insulin levels, pancreatic overcompensation as a reason for normalized glucose tolerance is highly unlikely. In this model, we thus observed a clear dissociation of reduced white adipocyte mitochondrial OXPHOS capacity from impaired glucose tolerance.

3.3. Monogenetic models of obesity: different glucose tolerance but similar white adipocyte mitochondrial OXPHOS capacity

In a mouse model of diet induced obesity we observed an association between white adipocyte mitochondrial function and glucose tolerance in the obese state but a dissociation during remission. To rule out direct effects of diet or catabolism, we extended our study to monogenetic models of obesity. $Lep^{ob/ob}$ mice and mice with melanocortin-4-receptor (Mc4R) deficiency, including $Mc4R^{X16/X16}$, are well established models of monogenetic obesity characterized by enormous weight and fat mass gain on a regular diet [15,16].

Mutant mice of both models were heavily obese (Figure 8A,B; Table 2). Accordingly, posterior subcutaneous and epididymal fat pads were larger compared to wildtype mice (Table 2). Oral glucose tolerance tests revealed impaired glucose tolerance in $Lep^{ob/ob}$ mice as indicated by lower glucose clearance and higher total AUC (Figure 8A). In contrast, oral glucose tolerance of $Mc4R^{X16/X16}$ and $Mc4R^{wt/wt}$ mice was comparable (Figure 8B). At the same time, plasma insulin of $Lep^{ob/ob}$ was more than 5 times higher than plasma insulin of $Mc4R^{X16/X16}$ mice, indicating better peripheral insulin sensitivity rather than pancreatic compensation as a reason for normalized glucose tolerance in the $Mc4R^{X16/X16}$ mice (Table 1). Notably, mitochondrial OXPHOS capacity of both mutants, reflected by cRCR, tended to be lower in posterior subcutaneous adipocytes and was massively decreased in epididymal adipocytes (Figure 8A,B).

In summary, we observed simultaneous occurrence of impaired glucose tolerance and white adipocyte mitochondrial OXPHOS function in $Lep^{ob/ob}$ mice. $Mc4R^{X16/X16}$ mice, however, showed impaired OXPHOS capacity paralleled by normal glucose tolerance.

Reduced white adipocyte OXPHOS capacity seems to be a hallmark of obesity, especially in adipocytes of intraabdominal origin. It is not, however, necessarily accompanied by whole body glucose intolerance. This conclusion holds true for both the catabolic state (HF-recovery mice) and the anabolic state ($Mc4R^{X16/X16}$).

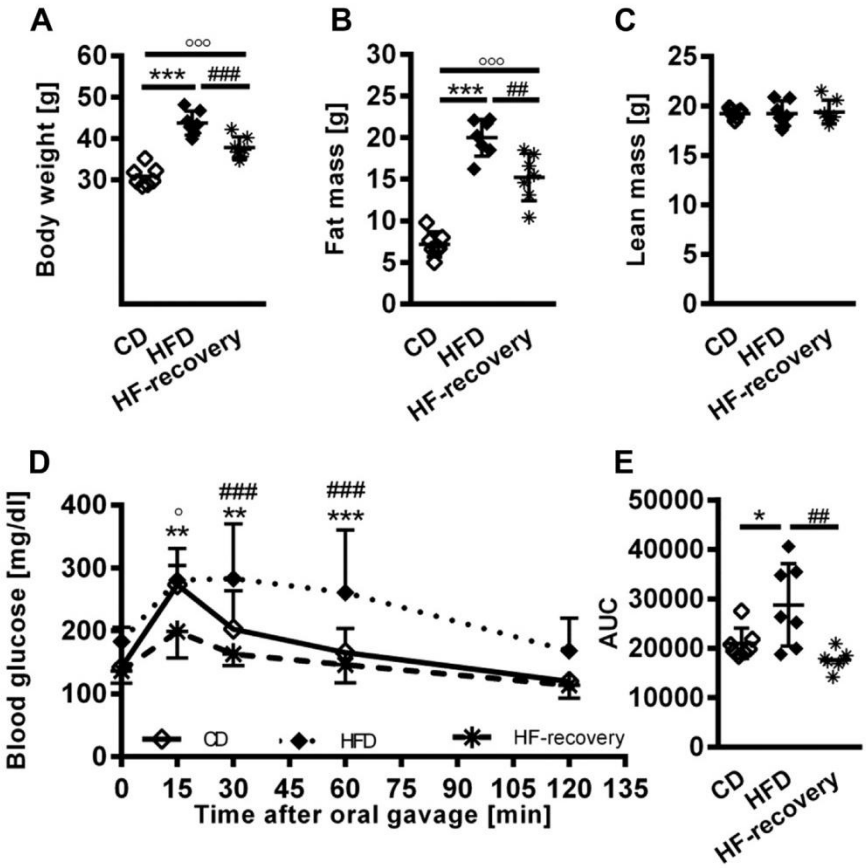

Figure 6: One week refeeding CD following 24 weeks HFD (HF-recovery) is sufficient to restore glucose tolerance. At the age of eight weeks, mice were matched by body weight into HFD and CD groups. The respective diet was fed for 24 weeks then HFD fed mice received CD for one week. (A) Body weight, (B) Fat mass, (C) Lean mass, (D) Oral glucose tolerance test, (E) Total area-under-the-curve (AUC) calculated from D as measure for glucose tolerance. Values of the HF-recovery group are shown both before and after one week CD refeeding. A-E were analyzed by one-way ANOVA. D was analyzed by two way repeated measures ANOVA, * corresponds to comparison between CD and HFD, ° corresponds to comparison between CD and HF-recovery, # corresponds to comparison between HFD and HF-recovery, $n = 7$, */#/° = $p < 0.05$, **/##/°° = $p < 0.01$, ***/###/°°° = $p < 0.001$.

MOLECULAR METABOLISM

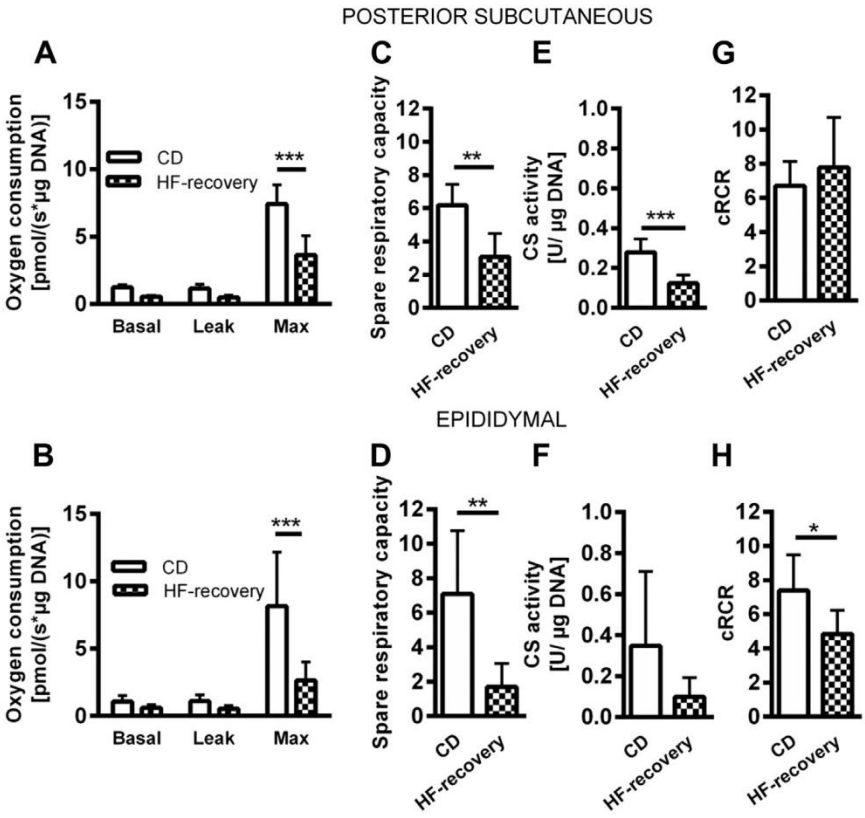

Figure 7: Cellular respiration of adipocytes from HF-recovery and CD mice. Recovery intervention does not restore limited maximal respiratory capacity and reduced mitochondrial integrity. (A, B) First, basal respiration was assessed using pyruvate as a substrate. ATP synthase inhibitor oligomycin was added to define the proportion of basal respiration contributing to either ATP turnover or proton leak, respectively. Next, FCCP was added to determine the maximal cellular respiratory capacity. Lastly, non-mitochondrial background was determined by addition of complex III inhibitor antimycin A and subtracted from the other respiratory states. Oxygen consumption rates are expressed per µg DNA. (C, D) Spare respiratory capacity = max − basal. (E, F) Citrate synthase activity was measured as marker for mitochondrial abundance and expressed as CS activity per µg DNA. (G, H) Cell respiratory control ratio (cRCR) was calculated as an index for mitochondrial integrity (quotient of maximal to leak oxygen consumption). A-B was analyzed by Two-way repeated measures ANOVA (Bonferroni correction. C-H was analyzed by Student's t-test. Data are presented as means ± SD of 5–7 experiments. $p < 0.05$, ** = $p < 0.01$, *** = $p < 0.001$.

4. DISCUSSION

It has been repeatedly proposed that altered mitochondrial metabolism of adipocytes in WAT plays a key role in the development of obesity associated impaired glucose homeostasis [14,24–27]. Clarifying the relation between white adipocyte mitochondrial alterations and impaired glucose homeostasis in obesity is thus of enormous interest. The goal of the present study was to elucidate whether alterations in white adipocyte mitochondrial respiratory function are a phenomenon of obesity, of impaired glucose tolerance, or of both, with the latter allowing further speculations about a potential causal link. We phenotyped four common murine obesity models for the status of glucose tolerance and white adipocyte mitochondrial oxidative phosphorylation (OXPHOS) function in subcutaneous as well as intraabdominal fat.

In all our model systems, obesity was generally associated with reduced white adipocyte mitochondrial OXPHOS capacity as detected by decreased cell respiratory control ratio (cRCR) in adipocytes of obese mice, particularly in cells of intraabdominal origin. As a ratio of maximal to leak respiration, cRCR is both sensitive to changes in maximal substrate oxidation capacity and proton leak [4]. The low cRCRs found in adipocytes of obese mice can thus be caused by either high proton leak, low maximal substrate oxidation capacity, or a combination of both. In this study, limitations in cRCR of adipocyte mitochondria from obese mice were mainly caused by diminished maximal substrate oxidation capacity and not by increased proton leak (Figure S1). Strikingly, impaired OXPHOS capacity was not necessarily accompanied by impaired whole body glucose tolerance. HF-recovery and $Mc4R^{X16/X16}$ mice where characterized by normal glucose tolerance despite impaired mitochondrial OXPHOS capacity, mainly in epididymal white adipocytes. Of note, normalized glucose tolerance seemed not to be caused by pancreatic overcompensation but rather by improved peripheral insulin sensitivity as plasma insulin levels appeared quite low.

We conclude that glucose intolerance occurs independently of OXPHOS impairment in white adipocytes, thus excluding the latter as a proximate trigger for impaired glucose homeostasis in obesity. Alternatively, in a scenario of complex systemic regulation, additional permissive factors unknown so far may link reduced white adipocyte mitochondrial OXPHOS to impaired glucose metabolism. In other words, impaired respiratory capacity in white adipocytes solely is not sufficient for the development of systemic glucose intolerance.

Mechanistically, reduced OXPHOS could represent an adaptive mechanism to energy overload, adipocyte hypertrophy, and massive adipose tissue expansion. First, there is evidence for relative hypoxia in

Original article

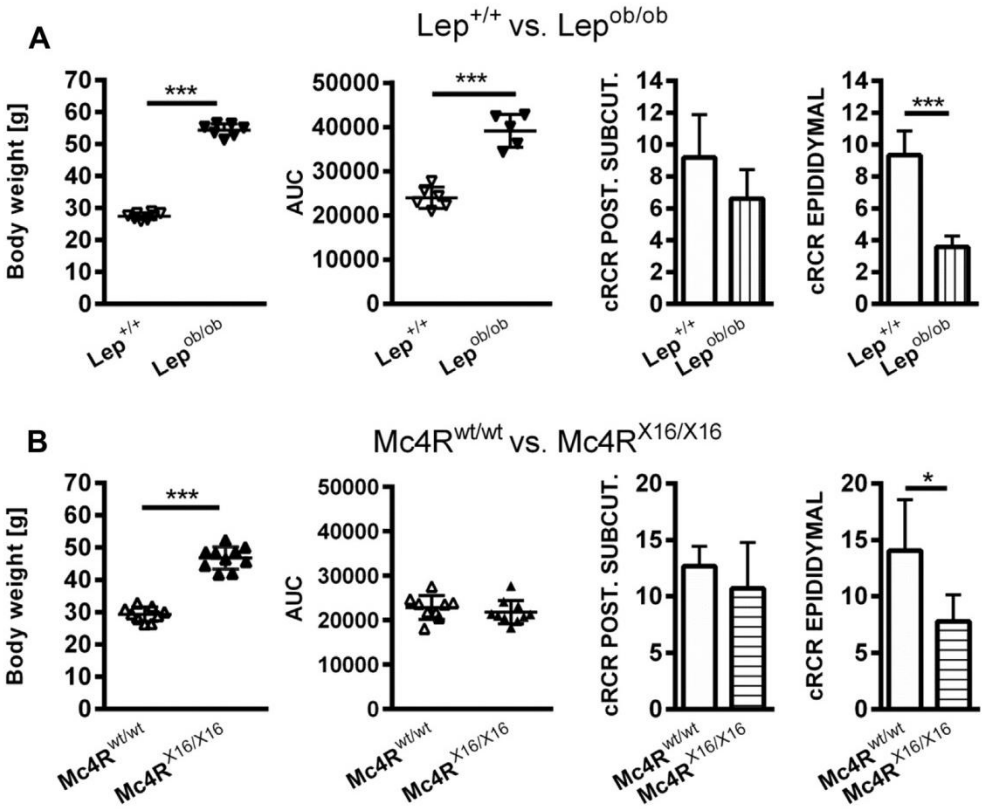

Figure 8: Monogenetic models of obesity: Differences in glucose tolerance but similarities in white adipocyte mitochondrial OXPHOS capacity. (A) **Comparison of Lep$^{ob/ob}$ mice and Lep$^{+/+}$ littermates**. Lep$^{ob/ob}$ mice show massive obesity and impaired glucose tolerance measured by total area-under-the-curve (AUC) (n = 5–8). (B) **Comparison of Mc4R$^{X16/X16}$ and Mc4R$^{wt/wt}$ littermates**. Mc4R$^{X16/X16}$ mice show massive obesity but normal glucose tolerance measured by total area-under-the-curve (AUC) (n = 5–9). (A) and (B) Mitochondrial integrity in epididymal white adipocytes is affected in both models as indicated by lowered cell respiratory capacity (cRCR). All data were analyzed by Student's t-test. Bars are presented as means ± SD. $p < 0.05$, *** = $p < 0.001$.

WAT of obese rodents. In Lep$^{ob/ob}$ and diet-induced obese mice, oxygen partial pressure is reduced 2- to 3-fold in WAT compared to lean controls [28,29]. In hypoxic WAT there may be no need for a high mitochondrial capacity since adipocytes switch from aerobic OXPHOS to anaerobic glycolysis to compensate for diminished aerobic oxidation [30–34]. Consequently, this could trigger a reduction of mitochondrial power determined by loss of mitochondrial mass, substrate oxidation capacity of the electron transport chain, and coupling efficiency. Reduced OXPHOS capacity, however, does not necessarily result in ATP-depletion, energetic stress, or adipocyte dysfunction; cellular ATP homeostasis obviously can be maintained by glycolytic ATP production as transgenic manipulation of adipocyte mitochondria and subsequent OXPHOS impairment does not change ATP levels in WAT [24].

Table 2 – Body composition and fat pad weights of Lep$^{+/+}$ vs. Lep$^{ob/ob}$ and Mc4R$^{wt/wt}$ vs. Mc4R$^{X16/X16}$ mice.

Lep$^{+/+}$ vs. Lep$^{ob/ob}$			
	Lep$^{+/+}$	Lep$^{ob/ob}$	n
Fat mass [g]	3.50 ± 0.61	32.80 ± 1.61***	5
Lean mass [g]	19.61 ± 0.40	16.28 ± 0.70***	5
psWAT mass [mg]	275.3 ± 63.5	2828 ± 388.7***	7–8
eWAT mass [mg]	339.1 ± 83.1	3571 ± 182.6***	7–8
Mc4R$^{wt/wt}$ vs. Mc4R$^{X16/X16}$			
	Mc4R$^{wt/wt}$	Mc4R$^{X16/X16}$	n
Fat mass [g]	4.26 ± 1.20	18.78 ± 3.02***	9–10
Lean mass [g]	20.84 ± 1.11	23.02 ± 0.94***	9–10
psWAT mass [mg]	432.8 ± 112.8	2421 ± 315.4***	9
eWAT mass [mg]	435.5 ± 170.5	2103 ± 465.9***	9

Values are means ± SD. Data were analyzed by Student's t-test.
*** = $p < 0.001$, significant differences compared to respective lean controls (Lep$^{+/+}$ or Mc4R$^{wt/wt}$).

Second, studies in mice, rats, and humans revealed downregulation of *de novo* lipogenesis in adipose tissue in obesity [35–37], which has been suggested as an adaptive process to limit an ongoing increase of fat mass [37]. Cellular ATP demand for lipogenic enzyme activity, and the resulting requirement for mitochondrial OXPHOS activity for this process, would therefore be reduced. Accordingly, expression of acetyl-CoA carboxylase, the rate-limiting lipogenic enzyme catalyzing the ATP-dependent first step of fatty acid synthesis, is reduced in obesity [36,37]. Of note, hypoxia inhibits lipogenesis and may thus act synergistically in this context [38]. In our study, decreased white adipocyte mitochondrial abundance and respiratory capacity were always accompanied by a body energy surplus and increased fat pad weight. It is therefore plausible that reduced mitochondrial OXPHOS capacity represents an adaptive, non-pathological mechanism of adipocytes coping with hypoxia in WAT and/or reduced cellular ATP demand.

Impaired mitochondria have earlier been observed in obesity and/or states of altered glucose homeostasis [8–13,39]. Very recently, network-based integration of enriched biological processes, respective regulators and related physiological changes revealed changes of

MOLECULAR METABOLISM

mitochondrial function in murine epididymal fat that notably continuously deteriorate during prolonged HF-diet feeding [40]. To date, however, these alterations have not been studied in detail on the functional level, i.e. by precise respirometry of both mitochondria and cells in differently energized states and with different substrates. Thus, we here comprehensively analyzed mitochondrial OXPHOS of obese and glucose intolerant versus lean and healthy mice applying state-of-the-art respirometry technologies and additional biochemical techniques. OXPHOS capacity in both adipocytes of 24-weeks high-fat diet (HFD) fed mice and their isolated mitochondria were reduced in states where maximal substrate oxidation capacity determines oxygen consumption (state 3, state 3u, max). On the level of isolated mitochondria this can be explained by limited enzymatic equipment of the respiratory chain. On the cellular level, this deficit is amplified by reduced white adipocyte mitochondrial abundance. Importantly, integrity of mitochondria from adipocytes of both fat depots, indicated by RCRs, is affected when mitochondria are energized with complex I (pyruvate, palmitate) but not complex II (succinate) linked substrates. Thus, our comprehensive analysis on isolated white adipocyte mitochondria of HFD vs. CD fed mice revealed differences in RCR depending on electron entry site into the respiratory chain. The molecular mechanisms determining this difference have to be addressed in future studies.

In summary, we analyzed the impact of obesity on white adipocyte mitochondrial respiratory function in anatomically distinct fat depots and whole body glucose metabolism with a focus on a possible association between both phenomena. We utilized four models of diet-induced or genetic obesity characterized by either impaired or normal oral glucose tolerance. We identified reduced mitochondrial OXPHOS in white adipocytes to be a general hallmark of obesity, but to be independent of glucose tolerance status.

DISCLOSURE

The authors have nothing to disclose.

ACKNOWLEDGMENTS

The Chair of Molecular Nutritional Medicine received financial support from the Else Kröner-Fresenius Foundation (2007–2014). This study was partly funded by the Federal Ministry of Education and Research, Germany (BMBF AZ 0315674) and was supported by the Technische Universität München within the funding program Open Access Publishing.

CONFLICT OF INTEREST

None declared.

APPENDIX A. SUPPLEMENTARY DATA

Supplementary data related to this article can be found at http://dx.doi.org/10.1016/j.molmet.2015.07.001.

REFERENCES

[1] Elia, M., 1992. Organ and tissue contribution to metabolic rate. In: Kinney, J., Tucker, H. (Eds.), Energy metabolism: tissue determinants and cellular corollaries. New York: Raven Press. p. 61–80.

[2] Wang, Z., Ying, Z., Bosy-Westphal, A., Zhang, J., Schautz, B., Later, W., et al., 2010. Specific metabolic rates of major organs and tissues across adulthood: evaluation by mechanistic model of resting energy expenditure. American Journal of Clinical Nutrition 92(6):1369–1377.

[3] Kaiyala, K.J., Morton, G.J., Leroux, B.G., Ogimoto, K., Wisse, B., Schwartz, M.W., 2010. Identification of body fat mass as a major determinant of metabolic rate in mice. Diabetes 59(7):1657–1666.

[4] Brand, M.D., Nicholls, D.G., 2011. Assessing mitochondrial dysfunction in cells. Biochemical Journal 435(2):297–312.

[5] Stehling, O., Wilbrecht, C., Lill, R., 2014. Mitochondrial iron-sulfur protein biogenesis and human disease. Biochimie 100:61–77.

[6] De Pauw, A., Tejerina, S., Raes, M., Keijer, J., Arnould, T., 2009. Mitochondrial (dys)function in adipocyte (de)differentiation and systemic metabolic alterations. American Journal of Pathology 175(3):927–939.

[7] Koh, E.H., Park, J.Y., Park, H.S., Jeon, M.J., Ryu, J.W., Kim, M., et al., 2007. Essential role of mitochondrial function in adiponectin synthesis in adipocytes. Diabetes 56(12):2973–2981.

[8] Hallgren, P., Sjostrom, L., Hedlund, H., Lundell, L., Olbe, L., 1989. Influence of age, fat cell weight, and obesity on O_2 consumption of human adipose tissue. American Journal of Physiology 256(4 Pt 1):E467–E474.

[9] Choo, H.J., Kim, J.H., Kwon, O.B., Lee, C.S., Mun, J.Y., Han, S.S., et al., 2006. Mitochondria are impaired in the adipocytes of type 2 diabetic mice. Diabetologia 49(4):784–791.

[10] Rong, J.X., Qiu, Y., Hansen, M.K., Zhu, L., Zhang, V., Xie, M., et al., 2007. Adipose mitochondrial biogenesis is suppressed in db/db and high-fat diet-fed mice and improved by rosiglitazone. Diabetes 56(7):1751–1760.

[11] Valerio, A., Cardile, A., Cozzi, V., Bracale, R., Tedesco, L., Pisconti, A., et al., 2006. TNF-alpha downregulates eNOS expression and mitochondrial biogenesis in fat and muscle of obese rodents. Journal of Clinical Investigation 116(10):2791–2798.

[12] Wilson-Fritch, L., Nicoloro, S., Chouinard, M., Lazar, M.A., Chui, P.C., Leszyk, J., et al., 2004. Mitochondrial remodeling in adipose tissue associated with obesity and treatment with rosiglitazone. Journal of Clinical Investigation 114(9):1281–1289.

[13] Dahlman, I., Forsgren, M., Sjogren, A., Nordstrom, E.A., Kaaman, M., Naslund, E., et al., 2006. Downregulation of electron transport chain genes in visceral adipose tissue in type 2 diabetes independent of obesity and possibly involving tumor necrosis factor-alpha. Diabetes 55(6):1792–1799.

[14] Schottl, T., Kappler, L., Braun, K., Fromme, T., Klingenspor, M., 2014. Limited mitochondrial capacity of visceral versus subcutaneous white adipocytes in male C57BL/6N mice. Endocrinology en20141689.

[15] Fellmann, L., Nascimento, A.R., Tibirica, E., Bousquet, P., 2013. Murine models for pharmacological studies of the metabolic syndrome. Pharmacology & Therapeutics 137(3):331–340.

[16] Bolze, F., Rink, N., Brumm, H., Kuhn, R., Mocek, S., Schwarz, A.E., et al., 2013. Characterization of the melanocortin-4-receptor nonsense mutation W16X in vitro and in vivo. Pharmacogenomics Journal 13(1):80–93.

[17] Even, P.C., Nadkarni, N.A., 2012. Indirect calorimetry in laboratory mice and rats: principles, practical considerations, interpretation and perspectives. American Journal of Physiology. Regulatory, Integrative and Comparative Physiology 303(5):R459–R476.

[18] Boudina, S., Sena, S., O'Neill, B.T., Tathireddy, P., Young, M.E., Abel, E.D., 2005. Reduced mitochondrial oxidative capacity and increased mitochondrial uncoupling impair myocardial energetics in obesity. Circulation 112(17):2686–2695.

[19] Wang, P.W., Kuo, H.M., Huang, H.T., Chang, A.Y., Weng, S.W., Tai, M.H., et al., 2014. Biphasic response of mitochondrial biogenesis to oxidative stress in visceral fat of diet-induced obesity mice. Antioxidants & Redox Signaling.

[20] Loschen, G., Azzi, A., Richter, C., Flohe, L., 1974. Superoxide radicals as precursors of mitochondrial hydrogen peroxide. FEBS Letters 42(1):68–72.

[21] Loschen, G., Azzi, A., 1975. On the formation of hydrogen peroxide and oxygen radicals in heart mitochondria. Recent Advances in Studies on Cardiac Structure and Metabolism 7:3–12.

[22] Treberg, J.R., Quinlan, C.L., Brand, M.D., 2010. Hydrogen peroxide efflux from muscle mitochondria underestimates matrix superoxide production – a correction using glutathione depletion. FEBS Journal 277(13):2766–2778.

[23] Kless, C., Klingenspor, M., 2013. Metabolic status of adipocytes triggers rapid adjustments of systemic glucose tolerance. FASEB Journal 27 (1071.2).

[24] Ryu, M.J., Kim, S.J., Kim, Y.K., Choi, M.J., Tadi, S., Lee, M.H., et al., 2013. Crif1 deficiency reduces adipose OXPHOS capacity and triggers inflammation and insulin resistance in mice. PLoS Genetics 9(3):e1003356.

[25] Keuper, M., Jastroch, M., Yi, C.X., Fischer-Posovszky, P., Wabitsch, M., Tschop, M.H., et al., 2014. Spare mitochondrial respiratory capacity permits human adipocytes to maintain ATP homeostasis under hypoglycemic conditions. FASEB Journal 28(2):761–770.

[26] Kusminski, C.M., Scherer, P.E., 2012. Mitochondrial dysfunction in white adipose tissue. Trends in Endocrinology Metabolism 23(9):435–443.

[27] Lee, Y.S., Kim, J.W., Osborne, O., Oh da, Y., Sasik, R., Schenk, S., et al., 2014. Increased adipocyte O_2 consumption triggers HIF-1alpha, causing inflammation and insulin resistance in obesity. Cell 157(6):1339–1352.

[28] Ye, J., Gao, Z., Yin, J., He, Q., 2007. Hypoxia is a potential risk factor for chronic inflammation and adiponectin reduction in adipose tissue of ob/ob and dietary obese mice. American Journal of Physiology, Endocrinology and Metabolism 293(4):E1118–E1128.

[29] Rausch, M.E., Weisberg, S., Vardhana, P., Tortoriello, D.V., 2008. Obesity in C57BL/6J mice is characterized by adipose tissue hypoxia and cytotoxic T-cell infiltration. International Journal of Obesity (London) 32(3):451–463.

[30] Choi, S., Cho, K., Kim, J., Yea, K., Park, G., Lee, J., et al., 2009. Comparative proteome analysis using amine-reactive isobaric tagging reagents coupled with 2D LC/MS/MS in 3T3-L1 adipocytes following hypoxia or normoxia. Biochemical and Biophysical Research Communications 383(1):135–140.

[31] Perez de Heredia, F., Wood, I.S., Trayhurn, P., 2010. Hypoxia stimulates lactate release and modulates monocarboxylate transporter (MCT1, MCT2, and MCT4) expression in human adipocytes. Pflugers Archiv 459(3):509–518.

[32] Wood, I.S., Wang, B., Lorente-Cebrian, S., Trayhurn, P., 2007. Hypoxia increases expression of selective facilitative glucose transporters (GLUT) and 2-deoxy-D-glucose uptake in human adipocytes. Biochemical and Biophysical Research Communications 361(2):468–473.

[33] Trayhurn, P., Alomar, S.Y., 2015. Oxygen deprivation and the cellular response to hypoxia in adipocytes – perspectives on white and brown adipose tissues in obesity. Frontiers in Endocrinology (Lausanne) 6:19.

[34] Geiger, K., Leiherer, A., Muendlein, A., Stark, N., Geller-Rhomberg, S., Saely, C.H., et al., 2011. Identification of hypoxia-induced genes in human SGBS adipocytes by microarray analysis. PLoS One 6(10):e26465.

[35] Diraison, F., Dusserre, E., Vidal, H., Sothier, M., Beylot, M., 2002. Increased hepatic lipogenesis but decreased expression of lipogenic gene in adipose tissue in human obesity. American Journal of Physiology, Endocrinology Metabolism 282(1):E46–E51.

[36] Vida, M., Rivera, P., Gavito, A.L., Suarez, J., Pavon, F.J., Arrabal, S., et al., 2014. CB1 blockade potentiates down-regulation of lipogenic gene expression in perirenal adipose tissue in high carbohydrate diet-induced obesity. PLoS One 9(2):e90016.

[37] Ortega, F.J., Mayas, D., Moreno-Navarrete, J.M., Catalan, V., Gomez-Ambrosi, J., Esteve, E., et al., 2010. The gene expression of the main lipogenic enzymes is downregulated in visceral adipose tissue of obese subjects. Obesity (Silver Spring) 18(1):13–20.

[38] O'Rourke, R.W., Meyer, K.A., Gaston, G., White, A.E., Lumeng, C.N., Marks, D.L., 2013. Hexosamine biosynthesis is a possible mechanism underlying hypoxia's effects on lipid metabolism in human adipocytes. PLoS One 8(8):e71165.

[39] Yin, X., Lanza, I.R., Swain, J.M., Sarr, M.G., Nair, K.S., Jensen, M.D., 2013. Adipocyte mitochondrial function is reduced in human obesity independent of fat cell size. Journal of Clinical Endocrinology and Metabolism jc20133042.

[40] Derous, D., Kelder, T., van Schothorst, E.M., van Erk, M., Voigt, A., Klaus, S., et al., 2015. Network-based integration of molecular and physiological data elucidates regulatory mechanisms underlying adaptation to high-fat diet. Genes Nutrition 10(4):470.

Supplemental figures

Figure S1

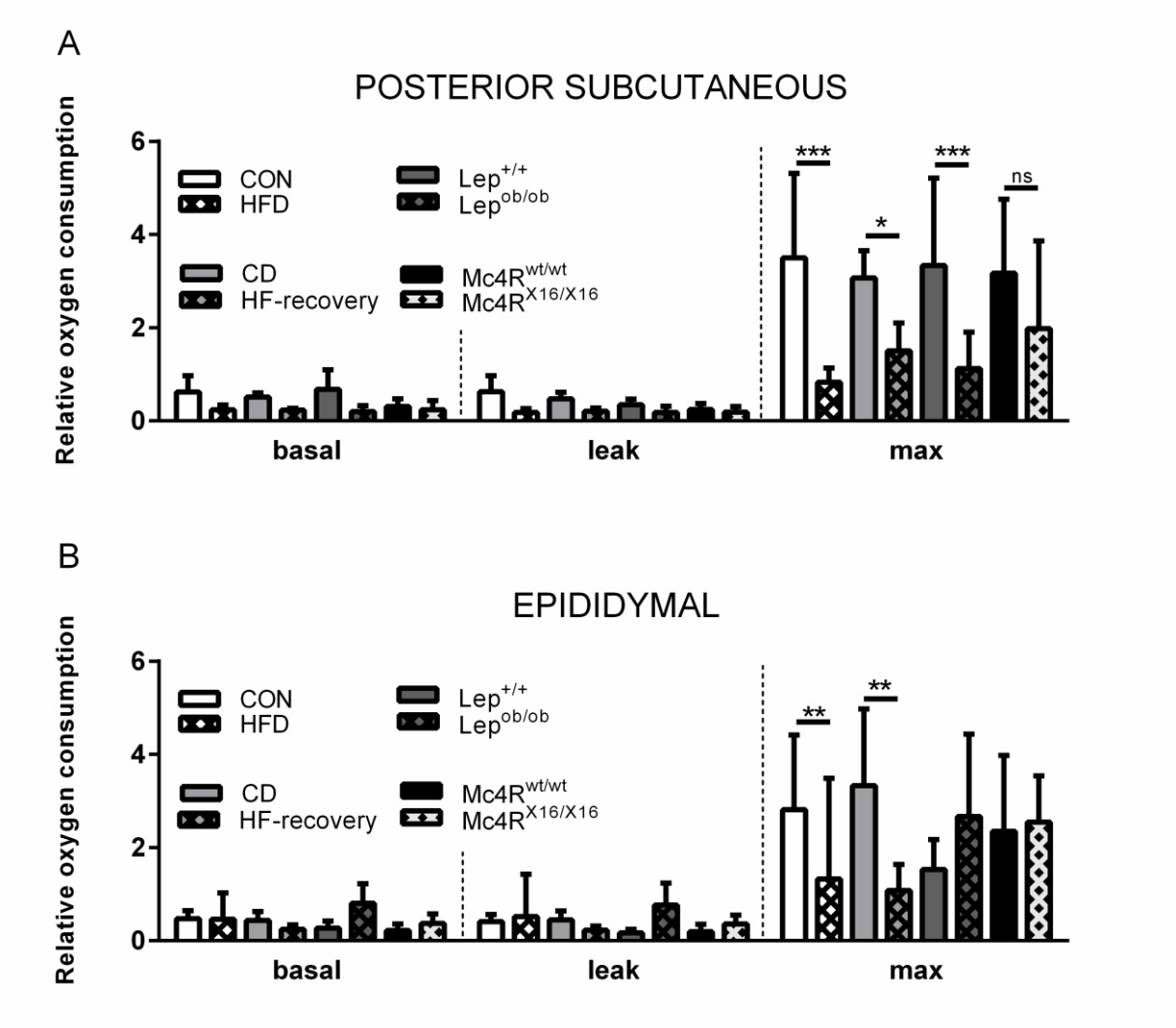

Figure S1 Integrated comparison of adipocyte respirometry data. Obese vs. lean mice of four different mouse obesity models were compared. A) posterior subcutaneous adipocytes B) epididymal adipocytes. Data obtained by respirometry analyses were intra-experiment normalized, statistically evaluated by two-way repeated measures ANOVA and presented as means ± SD. *p<0.05, ** p< 0.01, *** p<0.001, significant differences compared to respective controls.

CHAPTER III

"SYSTEMIC CONSEQUENCES OF IMPAIRED WHITE ADIPOCYTE MITOCHONDRIAL FUNCTION"

[MANUSCRIPT FOR SUBMISSION]

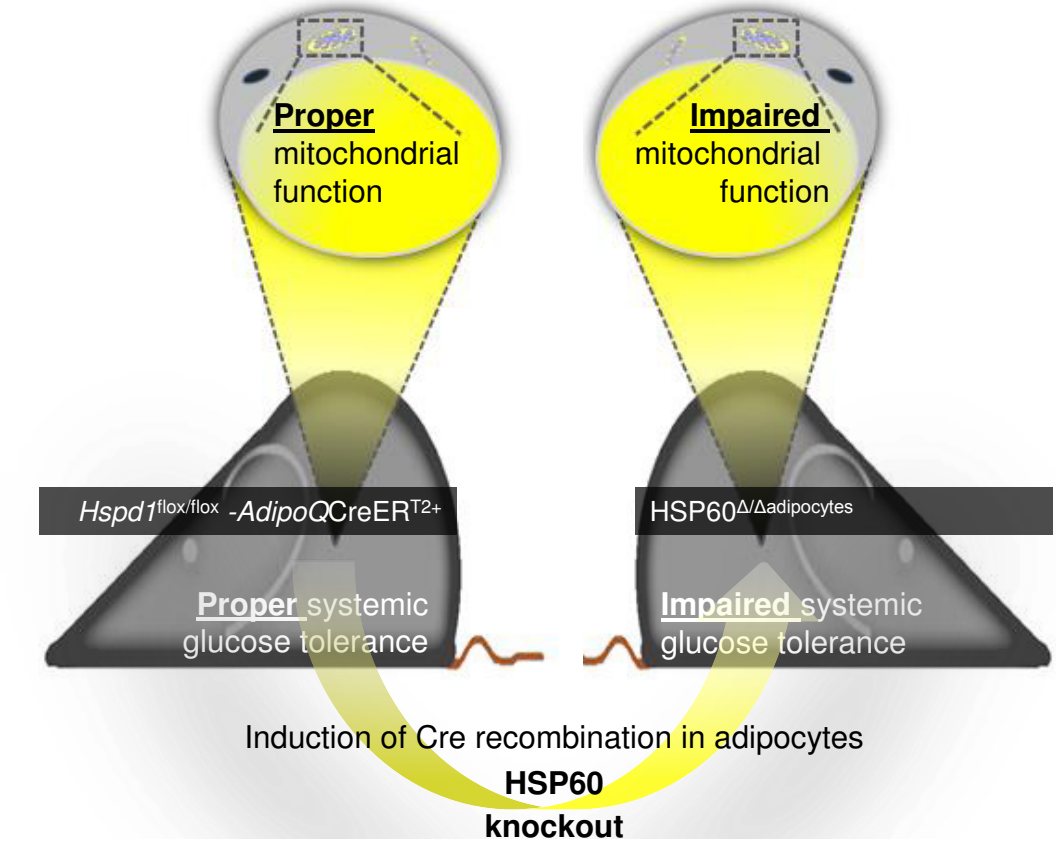

Ablation of mitochondrial heat shock protein 60 in adipocytes causes systemic glucose intolerance in laboratory mice

Theresa Schöttl[1,3,4*], Katharina Braun[1,3,4*], Emanuel Berger[2,4],Tobias Fromme[1,3,4], Dirk Haller[2,4], Martin Klingenspor[1,3,4]

[1]Molecular Nutritional Medicine, Technische Universität München, Freising, Germany
[2]Chair of Nutrition and Immunology, Technische Universität München, Freising, Germany
[3]Else Kröner Fresenius Center for Nutritional Medicine, Freising, Germany
[4]ZIEL-Research Center for Nutrition and Food Sciences, Freising, Germany

** These authors contributed equally to this work*

Manuscript for submission

Abstract

Impaired mitochondrial function in white adipose tissue is currently discussed as a causative factor for the development of obesity associated systemic glucose intolerance. We here scrutinized the possibility of a causal relationship between these phenomena. We took advantage of a novel tissue-specific and inducible knockout model to disturb mitochondrial function in white adipocytes and analyze consequences on systemic glucose homeostasis. The target gene of our investigations was heat shock protein 60 (HSP60), a mitochondrial matrix chaperonin essential for mitochondrial proteostasis. Feeding mice carrying inducible *AdipoQ*-CreER^{T2} and floxed alleles of HSP60 a tamoxifen containing diet triggered Cre-mediated HSP60 knockout in adipocytes. HSP60 knockout mice (HSP60$^{\Delta/\Delta adipocytes}$) revealed an overall 93% reduction in HSP60 protein levels in mature white adipocytes purified from posterior subcutaneous and intraabdominal epididymal white fat depots. Subsequent comprehensive bioenergetic analysis revealed markedly reduced mitochondrial respiratory capacity upon HSP60 ablation. There was no effect of white adipocyte mitochondrial impairment on body weight, body composition, fat pad mass, and plasma leptin and adiponectin levels. Most notably, however, oral glucose tolerance tests revealed significantly lower level of glucose tolerance in HSP60$^{\Delta/\Delta adipocytes}$ compared to HSP60$^{flox/flox}$ mice. Thus, our study provides *in vivo* evidence for decreased mitochondrial capacity as potential risk and trigger for the development of systemic glucose intolerance.

Abbreviations

AF adipocyte fraction, *AdipoQ* adiponectin, ap2 adipocyte protein 2, AUC area under the curve, CHOP C/EBP homologous protein, ClpP caseinolytic peptidase, Cre causes recombination, ER estrogen receptor, HSP60 heat shock protein 60, iBAT interscapular brown adipose tissue, e/psWAT epididymal/posterior subcutaneous white adipose tissue, JNK cJun-N terminal kinase, loxP locus of crossover in P1 bacteriophage, mtUPR mitochondrial unfolded protein response, OXPHOS oxidative phosphorylation, PEF phytoestrogen free chow diet, PKR double-stranded *RNA*-dependent protein kinase, SVF stromal vascular fraction, UCP1 uncoupling protein 1.

Key words

White adipocytes, mitochondrial impairment, systemic glucose intolerance

Introduction

Impaired mitochondrial function in white adipocytes is currently considered as a causative factor in the development of systemic glucose intolerance in obesity (Maassen *et al.*, 2007; Sutherland *et al.*, 2008; Kusminski & Scherer, 2012; Vernochet *et al.*, 2012; Keuper *et al.*, 2014). Speculations were initiated by a series of human und rodent studies showing co-occurrence of altered white adipocyte mitochondria and impaired glucose homeostasis in obesity. Numerous studies demonstrate that mitochondrial biogenesis and abundance, the expression of genes involved in oxidative phosphorylation (OXPHOS), and the OXPHOS capacity as a measure for mitochondrial function are reduced in adipose tissue or isolated adipocytes of obese and/ or type 2 diabetic rodents and humans (Hallgren *et al.*, 1989; Wilson-Fritch *et al.*, 2004; Choo *et al.*, 2006; Dahlman *et al.*, 2006; Valerio *et al.*, 2006; Rong *et al.*, 2007). The mere fact that altered adipocyte mitochondria and impaired glucose homoeostasis repeatedly occurred simultaneously, however, does not allow drawing conclusions about a causal relationship, especially in the light of several examples of dissociation between these parameters (Schöttl *et al.*, 2015b). Therefore, the major issue to be investigated is whether causality exists between white adipocyte mitochondrial impairment and the development of whole body glucose intolerance.

Conditional gene targeting represents an opportunity for the examination of possible cause-and-effect relationships. The Cre-*loxP* system is a sophisticated and powerful methodology for spatial control of genetic knockout. In principle, mice with *loxP* sites flanking the gene of interest are mated with mice expressing Cre recombinase under the control of a tissue or cell type specific promoter. Enzymatic Cre activity recombines the marked (“floxed”) gene resulting in gene knockout exclusively in cells with respective promotor activity (Sauer & Henderson, 1988; Gaveriaux-Ruff & Kieffer, 2007). Finally, effects of the spatial gene knockout can be assessed on organellar, cellular, tissue, and systemic level.

Heat shock protein 60 (HSP60) is a mitochondrial matrix chaperonin crucial for maintenance of mitochondrial integrity by its role in organellar protein homeostasis (Lin *et al.*, 2001). It is essential for proper folding of many mitochondrial matrix proteins synthesized in the cytosol and targeted to mitochondria (Figure 1A) (Cheng *et al.*, 1989; Ostermann *et al.*, 1989). Further, HSP60 as a chaperonin holds a key role in mitochondrial unfolded protein response (mtUPR), a mitochondrial specific stress response targeted to ensure quality of the mitochondrial proteome (Zhao *et al.*, 2002; Jovaisaite & Auwerx, 2015) (Figure 1B).

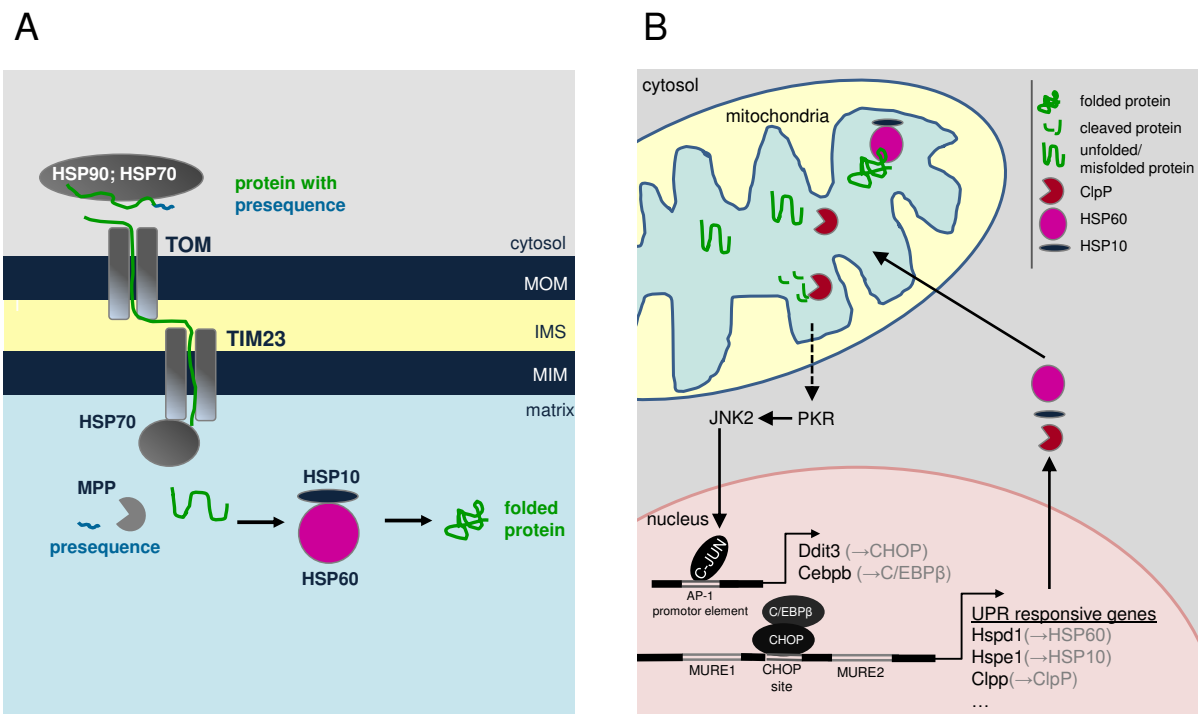

Figure 1. Role of HSP60 in mitochondrial proteostasis.
A) Schematic illustration of HSP60 mediated folding of proteins imported into mitochondria.
Supported by cytosolic chaperones, proteins with a presequence are transported to the translocase of outer membrane (TOM) complex, and then pass through TOM and the presequence translocase of the inner membrane (TIM23). TIM23 cooperates with heat shock protein 70 (HSP70) that completes the protein import into the matrix. After cleavage of the presequence from the preprotein by mitochondrial processing peptidase (MPP), a partially folded protein is delivered to heat shock protein 60 (HSP60). Final folding is processed by HSP60 in collaboration with heat shock protein 10 (HSP10) [reviewed in (Wiedemann *et al.*, 2004; Dudek *et al.*, 2013)].
(B) Suggested model for mitochondrial-nuclear signaling in mammalian mitochondrial unfolded protein response.
Protein aggregation in the mitochondrial matrix leads to caseinolytic peptidase (ClpP) activity dependent induction of double-stranded *RNA*-dependent protein kinase (PKR) (Rath *et al.*, 2012). PKR activates cJun-N terminal kinase 2 (JNK2) by phosphorylation which triggers c-Jun binding to activator protein-1 (AP-1) elements to induce transcription of C/EBP homologous protein *(*CHOP) and C/EBPβ. CHOP/C/EBPβ transcription factor dimers binds to specific unfolded protein response (UPR) promoter element (MURE) and up-regulate transcription of mitochondrial UPR target genes (Zhao et al., 2002; Aldridge *et al.*, 2007; Horibe & Hoogenraad, 2007; Rath et al., 2012; Rath & Haller, 2012; Mottis *et al.*, 2014; Jovaisaite & Auwerx, 2015).

Depletion of HSP60 impairs mitochondrial function and reduces insulin sensitivity in a hypothalamic cell line (Kleinridders *et al.*, 2013b). Moreover, HSP60 expression (mRNA and protein level) is reduced in adipose tissue of high-fat diet fed or genetically obese/diabetic rodents indicating HSP60 regulation upon weight gain and obesity, and suggesting a role of the chaperonin in obesity associated impaired glucose tolerance (Okamoto *et al.*, 2007; Rong et al., 2007; Sutherland et al., 2008). *Vice versa*, however, consequences of adipocyte-specific ablation of HSP60 on systemic glucose homeostasis were not studied *in vivo.*

We here take advantage of a new conditional tamoxifen-inducible Cre-*loxP* mouse model (*Hspd1*$^{flox/flox}$-*AdipoQ*CreER^{T2+}) characterized by temporally-controlled knockout of HSP60 in

white adipocytes. Our strategy is to disturb mitochondrial proteostasis in white adipocytes by HSP60 knockout, thereby impairing electron transport chain activity. Finally, consequences of impaired white adipocyte mitochondrial function on whole body glucose homeostasis are assessed. Using this approach, we identified adipocyte mitochondria as potential regulators of systemic glucose homeostasis.

Material and Methods

Mice

All mouse experiments were performed with permission of the government of Upper Bavaria (Regierung von Oberbayern, reference number AZ 55.2-1-54-2532-12-12).

Before and throughout the experiment mice were housed in groups in a specific pathogen-free environment on a 12:12h light-dark photocycle at 22°C with ad libitum access to water and food.

Hspd1$^{flox/flox}$ mice were crossed with *AdipoQ*CreER^{T2+} mice.

Hspd1$^{flox/flox}$ *mice*: Mice with floxed Hspd1 alleles (Hspd1 is the gene encoding for HSP60) were generated on the strain background of C57BL/6N (Berger, 2014), and kindly provided by Prof. Dr. Dirk Haller, Chair of Nutrition and Immunology, Technische Universität München.

*AdipoQ*CreER^{T2+} *mice*: *AdipoQ*CreER^{T2+} C57BL/6N mice were generated and kindly provided by Prof. Dr. Christian Wolfrum, Eidgenössische Technische Hochschule Zürich. Mice are hemizygous for the transgene Cre-ER^{T2}*;* Cre (causes recombination) recombinase is fused to a mutated human estrogen receptor binding domain (ER^{T2}). The mutated receptor is insensitive to the natural ligand 17β-estradiol at physiological concentrations but highly sensitive to 4-hydroxytamoxifen, the active metabolite of the synthetic prodrug tamoxifen (Feil *et al.*, 1997).

All experiments were conducted on male mice. At the age of 16 weeks, *Hspd1*$^{flox/flox}$*-AdipoQ*CreER^{T2+} mice and respective -CreER^{T2-} controls entered experimental feeding for 6 weeks: In week 1 and 2 mice received phytoestrogen-free chow (PEF, V1154-300) to exclude effects of phytoestrogens on the outcome of our study. In week 3 and 4 mice received tamoxifen containing chow diet (CreActive TAM400, 400 mg/ kg tamoxifen, LASvendi, phytoestrogen levels near the detection limit). In week 5 and 6 mice again received PEF, to exclude direct effects of both tamoxifen and phytoestrogens on the outcome of our study (Hesselbarth, 2015), and to provide time for the development of metabolic alterations associated with HSP60 knockout. At the end of week 6 oral glucose tolerance was assessed and mice were killed by CO_2 exposure and exsanguination.

Metabolic phenotyping

Body weight and body composition

Body weight was monitored twice a week during PEF feeding and daily during tamoxifen exposure. Body composition was assessed by using nuclear magnetic resonance spectroscopy (The Minispec mq 7.5 POY Live mice analyzer, Bruker, Billerica, MA, USA) twice a week during PEF. To avoid tamoxifen contamination of the Minispec, body composition determination was waived during TAM feeding.

Oral glucose tolerance

Oral glucose tolerance was assessed at the end of week 6 of experimental feeding. Mice were fasted for six hours. Then, they received a bolus of 2.66 mg glucose per [(lean mass + 0.2 fat mass) g] by single oral gavage, referring to (Even & Nadkarni, 2012). Blood glucose was monitored before and 15, 30, 60 and 120 minutes after gavage using a standard glucometer. Total area-under-the-curve (AUC) was calculated as measure for glucose tolerance.

Plasma leptin and adiponectin

Plasma concentrations of leptin and adiponectin were determined by using commercial Kit systems validated for murine plasma (Christal Chem, Downers Grove, IL, USA).

Tissue dissection and isolation of adipocytes

Posterior subcutaneous and intraabdominal-epididymal fat depots were dissected and weighed. Mature adipocytes were separated from other cell types by collagenase-digestion as described in detail previously (collagenase type A, Roche Applied Science; Penzberg, Germany; 1g/l in Hank's Balanced Salt Solution [HBSS 14025-092, Gibco®, Live Technologies, Carlsbad, CA, USA] containing 4% BSA) (Schöttl *et al.*, 2015a).

Characterization of isolated mature adipocytes

Bioenergetics

Oxygen consumption of permeabilized adipocytes was measured as described previously, using high resolution respirometry (Oxygraph-2k, OROBOROS INSTRUMENTS, Innsbruck, Austria) (Schöttl et al., 2015a). Briefly, 100 µl of adipocyte suspension was pipetted into 2 ml MIR05 buffer (110 mM sucrose, 60 mM potassium lactobionate, 0.5 mM EGTA, 3 mM $MgCl_2$ * $6H_2O$, 20 mM taurine, 10 mM KH_2PO_4, 20 mM Hepes, 1g/l BSA-fatty acid free, pH 7.1 at 37°C, as described by OROBOROS INSTRUMENTS). After permeabilizing plasma membrane using digitonin (2µM), state 4 respiration was measured in the presence of succinate/rotenone (5 mM/2 µM). By addition of ADP (5 mM) phosphorylating state 3 was induced. ATP synthase was inhibited by oligomycin (2 µg/ml) (state 4o). Titration of FCCP (0.5 µM steps) was performed for measuring maximal cellular respiration rates (state 3u). Non-mitochondrial oxygen consumption was determined in presence of antimycin A (2.5 µM) and subtracted from the other respiratory states. Respiratory Control Ratio (RCR) was calculated dividing state 3 by state 4o respiration.

Cellular DNA quantification

DNA content of adipocyte samples used for respirometry analysis was assessed by quantitative PCR targeting a unique region of genomic DNA (promotor resistin). Procedures were conducted as described previously (primers: fw 5'-ACCTCTCTTGGGGTCAGATGT-3', rev 5'-CTGGGTATTAGCTCCTGTCCC-3') (Schöttl et al., 2015a).

Immunoblotting

Protein extracts of isolated mature adipocytes (30 µg) were resolved on a 12.5% SDS-PAGE, transferred to a nitrocellulose membrane (LI-COR Bioscienes, Lincoln, NE, USA; 60 min, 100V) and probed with antibodies targeting HSP60 (Anti HSP60 N-20, 1:2,000, sc-1052, Santa-Cruz Biotechnology) and actin (Anti-Actin clone C4, 1:5,000, MAB1501, Millipore). Infrared dye conjugated secondary antibodies (IRDye® 800CW, IRDye® 680, LI-COR Biosciences) were incubated at a dilution of 1:20,000. The Odyssey software (LI-COR Biosciences) was used to quantify band fluorescence intensities.

Statistical Analyses

Data are presented as mean values ± standard deviation. Data were statistically analyzed by Two-Way Repeated-Measures ANOVA followed by post-hoc Bonferroni testing or two-tailed Student's t-test (SigmaPlot 12.5, Systat Software, Inc., San Jose, CA, USA; GraphPad Prism4, GraphPad Software, Inc., La Jolla, CA, USA). Significance was accepted at p-values < 0.05.

Results

*AdipoQ*CreER^{T2} generates efficient knockout of HSP60 in adipocytes

We here generated a novel mouse model characterized by adipocyte specific knockout of *Hspd1*, encoding for mitochondrial heat shock protein 60 (HSP60), to scrutinize the putative causality between white adipocyte mitochondrial impairment and systemic glucose intolerance. At first, mice with floxed *Hspd1* alleles (*Hspd1*$^{flox/flox}$) were mated with mice expressing the tamoxifen inducible transgene CreER^{T2} regulated by the adiponectin promotor (*AdipoQ*CreER^{T2+}). In a second step, feeding *Hspd1*$^{flox/flox}$-*AdipoQ*CreER^{T2+}-offspring a tamoxifen containing diet induced Cre-mediated recombination in cells with *AdipoQ* promotor activity, which predominantly is expressed in adipocytes (Ye & Scherer, 2013) (Figure 2A).

Knockout efficiency was analyzed by immunoblot analysis (Figure 2B, C). Since our previous work revealed marked differences in mitochondrial function between the posterior subcutaneous and the intraabdominal epididymal fat depot of mouse body fat (Schöttl et al., 2015a; Schöttl et al., 2015b), those fat pads were analyzed separately. In addition, as the influence of pre- and non-adipocytes on the mitochondrial environment of WAT is enormous (Vernochet et al., 2012; Müller *et al.*, 2015), we separated the stromal vascular fractions from mature white adipocytes. Compared to CreER^{T2-} controls, HSP60 was reduced by 93% in mature white adipocytes of both, posterior subcutaneous and epididymal fat in *Hspd1*$^{flox/flox}$-*AdipoQ*CreER^{T2+} mice (Figure 2B). The knockout was specific to mature adipocytes as no alterations were observed in stromal vascular fraction cells. Besides, HSP60 was reduced by 88% in interscapular brown adipose tissue (BAT) of mutant mice. HSP60 was also slightly reduced (31%) in brain, indicating adiponectin expression in murine similar to human brain regions (Psilopanagioti *et al.*, 2009). Recombination was not observed in heart, liver, kidney, and muscle (gastrocnemius). Altogether, we conclude that *AdipoQ*CreER^{T2+} generates efficient knockout of HSP60 upon induction of Cre activity by tamoxifen, in white as well as brown adipocytes. In the following, mice are termed HSP60$^{\Delta/\Delta adipocytes}$ and HSP60$^{flox/flox}$ controls.

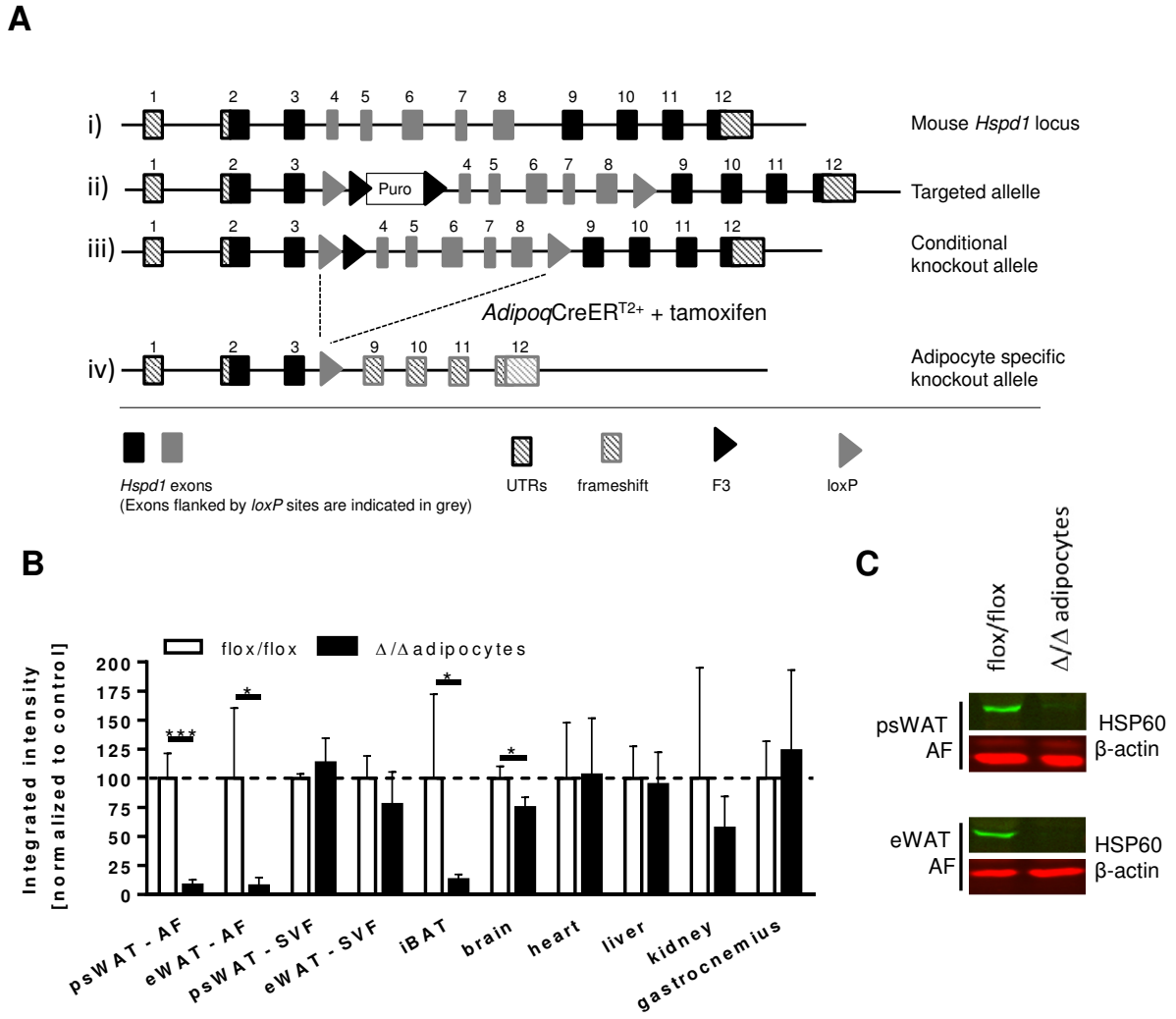

Figure 2. Generation of *HSP*60$^{\Delta/\Delta adipocytes}$ mice.
(A) Cloning and targeting strategy. i) The murine *Hspd1* gene, encoding for HSP60. Exon 2 contains the translation initiation sites. ii) Targeted allele with exons 4-8 flanked by *loxP* sites and a positive selection marker, PuroR, flanked by *F3* sites. iii) Conditional knockout allele ("flox allele") after removal of the positive selection marker (recombination of sequences between target sites *F3* by Flp) iv) Knockout allele after Cre-mediated recombination, initiated by tamoxifen-binding to the -ER^{T2} domain. Removal of exons 4-8 should result in loss of function of the *Hspd1* gene. Adapted from: (Berger, 2014).
(B) Knockout efficiency. HSP60 protein quantification in tissues/ cell fractions. Data were analyzed by Student's t-test and are presented as means ± SD. WAT AF and SVF, BAT n=7-8; non-adipose tissues n=3-4. *p<0.05, ***p<0.001.
(C) Exemplary HSP60 immunoblots of adipocyte fractions purified from posterior subcutaneous and epididymal fat, respectively. β-actin was used as housekeeping protein.
Abbreviations: psWAT/ eWAT posterior subcutaneous/ epididymal white adipose tissue, AF adipocyte fraction, SVF stromal vascular fraction, iBAT interscapular brown adipose tissue.

OXPHOS capacity is impaired in HSP60 ablated white adipocytes

As a next step, we assessed the consequences of HSP60 ablation on white adipocyte mitochondrial functionality. Generation of ATP by oxidative phosphorylation (OXPHOS) is the primary physiological function of mitochondria (Brand & Nicholls, 2011). Thus, comprehensive bioenergetic profiles of digitonin permeabilized cells from HSP60$^{\Delta/\Delta adipocytes}$ and HSP60$^{flox/flox}$ control mice, including key parameters of mitochondrial function as ATP

production, proton leak, and maximal uncoupled respiration, were assessed using chamber based high-resolution respirometry (Oxygraph-2k, OROBOROS). Substrate driven respiration (state 4) of posterior subcutaneous white adipocytes was comparable between the two genotypes (Figure 3A). Phosphorylating respiration (state 3), and also maximal uncoupled respiration (state 3u), were markedly lower in adipocytes of HSP60$^{\Delta/\Delta adipocytes}$ when compared to control mice. *Vice versa*, proton leak respiration (state 4o) was slightly elevated in HSP60$^{\Delta/\Delta adipocytes}$ mice. A similar pattern was obtained for adipocytes of epididymal fat, showing massively lower state 3 and state 3u oxygen consumption in HSP60$^{\Delta/\Delta adipocytes}$ vs. controls, but comparable state 4 and state 4o respiration (Figure 3B).

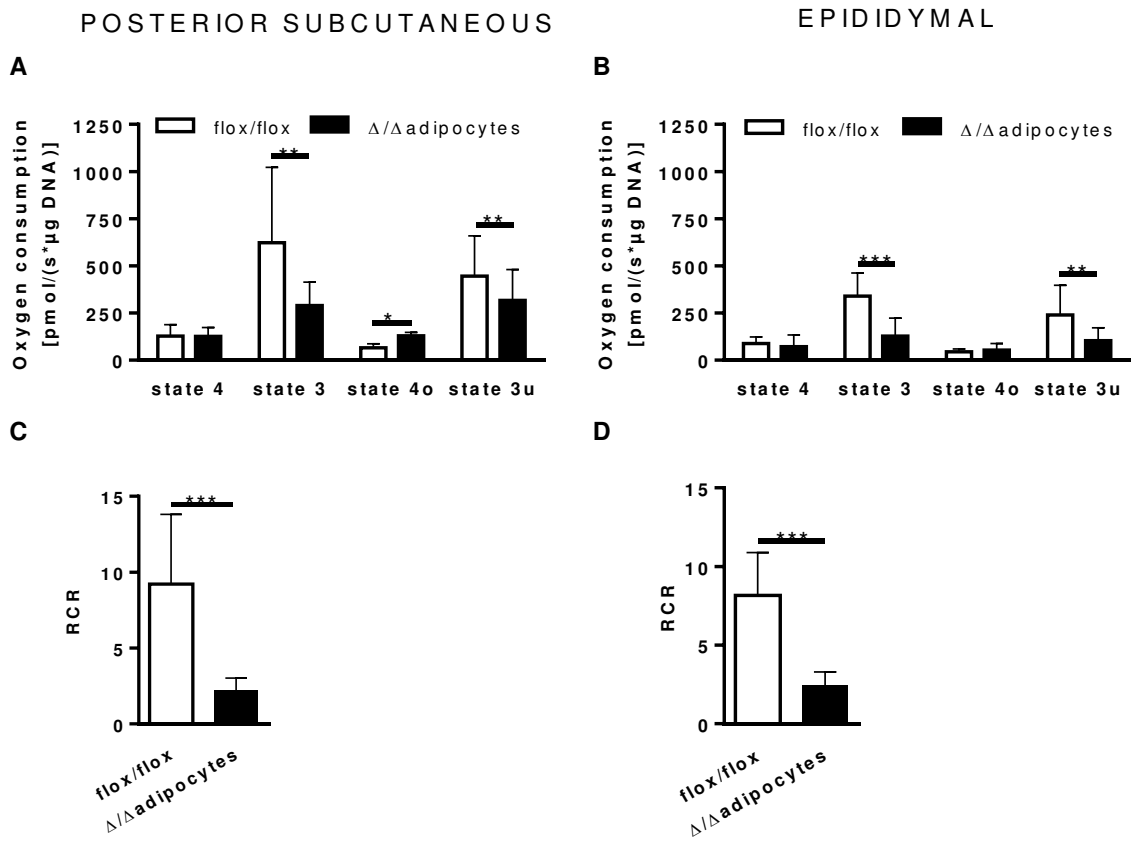

Figure 3. Respiratory/ phosphorylating capacity is limited in white adipocytes of HSP60$^{\Delta/\Delta adipocytes}$ mice. Mitochondrial respiration was assessed in digitonin permeabilized **(A)** posterior subcutaneous and **(B)** epididymal adipocytes using the Oxygraph-2k. State 4 oxygen consumption was determined in the presence of succinate/rotenone before state 3 respiration was measured by adding ADP. ATP-synthase was inhibited and state 4o respiration measured by addition of oligomycin. Next, state 3u was induced by addition of the uncoupler FCCP. Finally, non-mitochondrial oxygen consumption determined by injection of antimycin A was measured and subtracted from other respiratory states. Oxygen consumption rates are expressed per µg DNA. **(C)** and **(D)** Respiratory control ratio (RCR) was calculated as ratio of state 3 to state 4o oxygen consumption. A-B Data were analyzed by two-way repeated measures ANOVA. C-D Data were analyzed by Student's t-test. n=7-9. Data are presented as means ± SD. *= p<0.05, **=p<0.01, *** = p<0.001.

Thus, adipocytes lacking HSP60 were unable to increase substrate oxidation in case of an increase in ATP demand to the same degree as adipocytes with unaffected HSP60 levels do.

This limitation in maximal respiration capacity is also reflected in significantly diminished respiratory control ratios in both types of adipocytes (Figure 3C and D).
We conclude that HSP60 ablation markedly impairs mitochondrial respiratory capacity and integrity in white adipocytes of both subcutaneous and intraabdominal fat. Therefore, we assessed the consequences of adipocyte mitochondrial dysfunction on whole body glucose homeostasis.

Body mass and composition is comparable in HSP60$^{\Delta/\Delta adipocytes}$ and control mice

Constitutive knockout of HSP60 results in early embryonic lethality (Christensen *et al.*, 2010). On this background, we checked our conditional knockout mouse model for gross physical abnormalities. Comparison of body weight development during experimental feeding did not reveal any difference between mice of both genotypes (Figure 4A). Additionally, we observed no differences in absolute body weight, lean and fat mass (Figure 4B-D). HSP60 ablation did not affect posterior subcutaneous and epididymal white fat depot mass, neither interscapular brown adipose tissue weight (Figure 4E). Also major non-adipose tissues or organs – heart, liver, brain, kidney, and gastrocnemius – were comparable between both genotypes (Figure 4E). Lastly, we assessed plasma levels of leptin and adiponectin as measures for adipocyte endocrine activity. We found no significant differences between HSP60$^{\Delta/\Delta adipocytes}$ and their controls (Figure 4F and G). Hence, at that point, there were no physical abnormalities that could be related to HSP60 ablation in adipocytes or the limited OXPHOS capacity associated with this mutation.

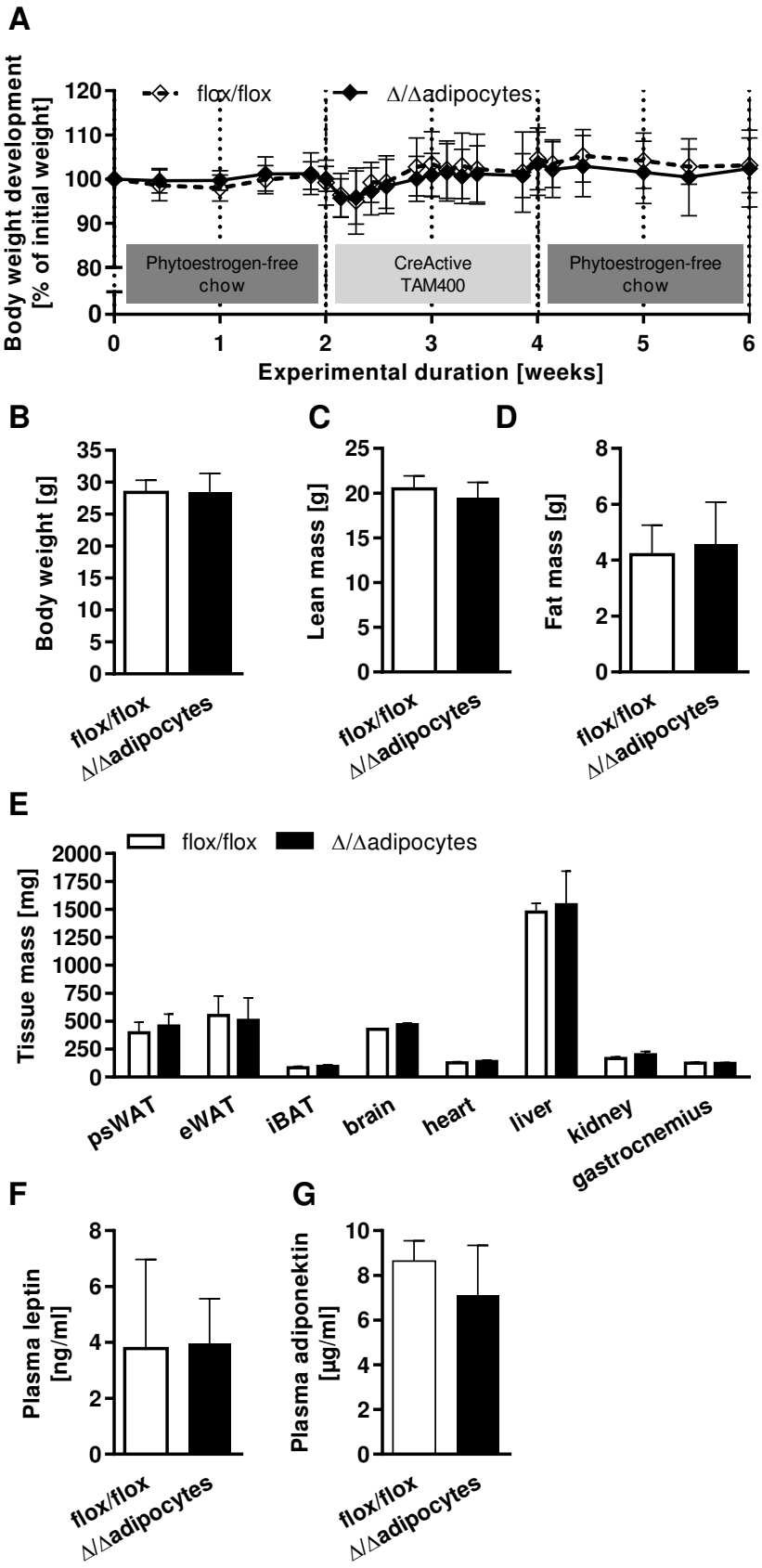

Figure 4. No gross physical differences between HSP60$^{\Delta/\Delta adipocytes}$ and HSP60$^{flox/flox}$ controls.
A) Body weight development during experimental feeding. Tamoxifen application (feeding CreActive TAM400 diet) resulted in transient body weight loss which was comparable between both genotypes. Values are shown relative to body weight at beginning of experimental feeding (=100%).
B) Body weight
C) Lean and
D) Fat mass at the end of experimental feeding.
E) Mass of posterior subcutaneous (psWAT) and epididymal (eWAT) white adipose tissue depots, interscapular brown adipose tissue
(iBAT), heart, liver, brain, kidney, gastrocnemius (skeletal muscle) at the end of experimental feeding.
F) Plasma adiponectin and
G) Plasma leptin levels, both adipokines were assessed by ELISA. Plasma was prepared from cardiac blood.
A: Data were analyzed by two-way repeated measures ANOVA. B-G: Data were analyzed by Student's t-test. All data are presented as means ± SD (n=6-9).

HSP60$^{\Delta/\Delta adipocytes}$ mice are glucose intolerant

At the end of experimental feeding (week 6, compare Figure 4A), we assessed the impact of HSP60 deficiency mediated impaired white adipocyte mitochondrial OXPHOS capacity on systemic glucose homeostasis. Basal blood glucose in the non-fasted state was comparable between HSP60$^{\Delta/\Delta adipocytes}$ and HSP60$^{flox/flox}$ controls (Figure 5A). Metabolic challenge by an oral glucose bolus, however, revealed impaired glucose tolerance in HSP60$^{\Delta/\Delta adipocytes}$ mice, indicated by lower glucose clearance rate and elevated area under the curve (Figure 5B and C). Notably, glucose intolerance was not associated with any changes in body weight, body composition, nor altered plasma leptin and adiponectin levels (compare Figure 4, S1, S2). Consequently, these factors do not mediate, or contribute to, the glucose intolerant phenotype of HSP60$^{\Delta/\Delta adipocytes}$ mice.

Using this model of temporally controlled spatial knockout of HSP60, white adipocyte mitochondria turned out as potential regulators of whole body glucose homeostasis. Limited mitochondrial (respiratory) capacity in (white) adipocytes caused impaired systemic glucose tolerance.

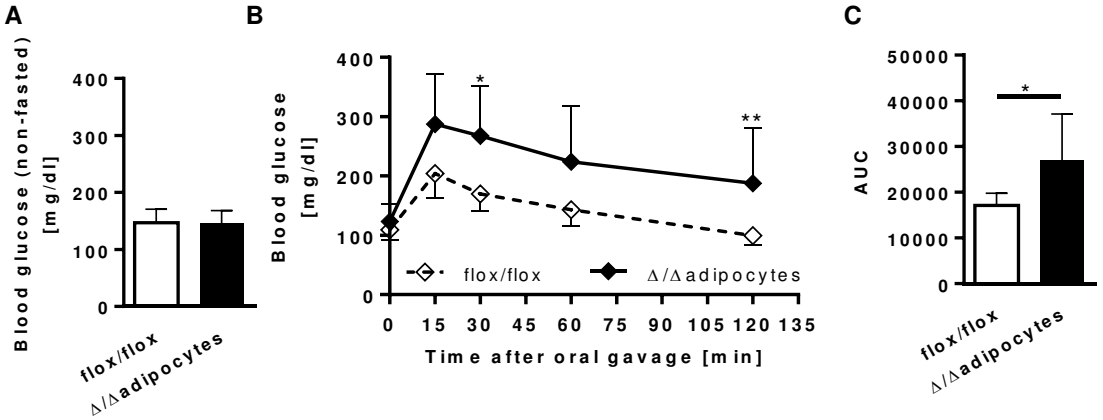

Figure 5. Oral glucose tolerance is impaired in HSP60$^{\Delta/\Delta adipocytes}$ mice. Glucose metabolism of HSP60$^{\Delta/\Delta adipocytes}$ and HSP60$^{flox/flox}$ controls was compared. **(A)** Basal non-fasted glucose. **(B)** Glucose clearance after oral glucose bolus administration. **(C)** Total area-under-the-curve (AUC) calculated from B as measure for oral glucose tolerance. A and C: Data were analyzed by Student's t-test. B: Data were analyzed by two-way repeated measures ANOVA. All data are presented as means ± SD (n=7-9). * = $p<0.05$, ** = $p<0.01$.

Discussion

We generated HSP60$^{\Delta/\Delta adipocytes}$ mice, a novel conditional knockout model, to disturb mitochondrial function in white adipocytes and assess consequences on glucose metabolism. With an important role in the maintenance of the mitochondrial proteome, and with the necessity of mitochondrial proteostasis for proper mitochondrial function (Baker *et al.*, 2012), heat shock protein 60 (HSP60) represented an excellent target for our study. We observed that ablation of the matrix chaperonin results in impaired white adipocyte oxidative phosphorylation (OXPHOS) capacity, apparent in respiratory states when maximal substrate oxidation capacity limits oxygen consumption (state 3 and state 3u, "maximal" for cultured adipocytes). Importantly, impaired OXPHOS in white adipocytes caused systemic glucose intolerance. Thus, we here describe a sophisticated tool to disturb mitochondrial OXPHOS in white adipocytes and highlight the importance of proper mitochondrial function for systemic glucose homeostasis. As a result, if the level of mitochondrial impairment observed in the present study is comparable to mitochondrial alterations in obesity, causality between impaired white adipocyte mitochondria and obesity associated impaired glucose tolerance is highly likely.

One can speculate about the mechanisms that links mitochondrial impairment triggered by HSP60 ablation to systemic glucose intolerance. Others previously reported that HSP60 depletion results in impaired insulin signaling *per se* (Kleinridders *et al.*, 2013a). The impairment in insulin signaling further leads to altered adipokine secretion patterns, which may affect insulin signaling in muscle and liver via circulation, finally resulting in whole body insulin resistance (Abel *et al.*, 2001). In our study, however, glucose intolerance was not mediated by altered adiponectin and leptin secretion as plasma levels of these adipokines were comparable between knockout and control mice. In consequence, future studies have to screen the entirety of adipocyte-derived factors to identify possible candidates.

Cre-*loxP* recombination regulated by adipocyte protein 2 (*aP2)* or *AdipoQ* gene promoters was recently used by several other groups as a tool to target different genes related to mitochondrial metabolism in white adipocytes and assess consequences of altered white adipocyte mitochondrial function on whole body (glucose) metabolism (Abel et al., 2001; Kleiner *et al.*, 2012; Kusminski *et al.*, 2012; Vernochet et al., 2012; Enguix *et al.*, 2013; Ryu *et al.*, 2013; Vernochet *et al.*, 2014; Wang *et al.*, 2015). Together, these studies do not allow drawing final conclusions about the role of altered white adipocyte mitochondria for systemic glucose tolerance - showing either improved, or worsened, or even unaffected glucose metabolism upon altered mitochondrial function in white adipocytes. These enormous

discrepancies are to some extent attributable to the different genes targeted and related functional changes, but also to the physiological adaptation to these circumstances. A major technical advance of our model is tamoxifen-dependent Cre recombinase activity- allowing not only spatial, but also temporal control of somatic mutagenesis. By tamoxifen application for two weeks in the adulthood, we eliminated potential harmful effects due to prolonged high levels of Cre activity, especially during development, as well as associated adaptations influencing the metabolic outcome (Feil *et al.*, 2009). This represents a significant improvement of our model compared to those previously used by other groups.

*AdipoQ*CreER^{T2} mediated recombination at *Hspd1* locus occurred not only in white but also in brown adipocytes, indicated by HSP60 ablation in both types of adipocytes, since brown adipocytes express adiponectin as well (Viengchareun *et al.*, 2002; Iacobellis *et al.*, 2013). Only long-term BAT dysfunction, however, is associated with the development of impaired glucose homeostasis (Thoonen, 2015), and mice of the present study were killed four weeks after knockout induction by tamoxifen, thus impaired mitochondria for a period of four weeks, it seems unlikely that there is impaired BAT mitochondrial function contributing to glucose intolerance in the present HSP60$^{\Delta/\Delta adipocytes}$ model. To exactly define the contribution of dysfunctional WAT and BAT, experiments could be repeated with HSP60$^{\Delta/\Delta adipocytes}$ mice kept at thermoneutrality or on uncoupling protein 1 (UCP1) knockout background, and *Hspd1*$^{flox/flox}$-*UCP1*CreER^{T2+} mice, respectively.

In conclusion, we here used tissue specific knockout of the mitochondrial chaperonin HSP60 as tool for time-specific manipulation of mitochondrial function in white adipocytes and to assess consequences of impaired adipocyte function on systemic glucose homeostasis. Our bioenergetic analyses revealed strikingly decreased mitochondrial OXPHOS capacity in HSP60 ablates adipocytes. This functional impairment on the organellar level was associated with reduced oral glucose tolerance in HSP60$^{\Delta/\Delta adipocytes}$ mice. Thus, we here provide *in vivo* evidence for impaired mitochondrial function in white adipocytes, indicated by reduced respiratory capacity, as possible catalyst for the development of systemic glucose intolerance. Future studies have to i) clarify whether these results can be related to obesity associated impaired glucose tolerance ii) uncover the molecular mechanisms causing this metabolic phenotype.

Supplement

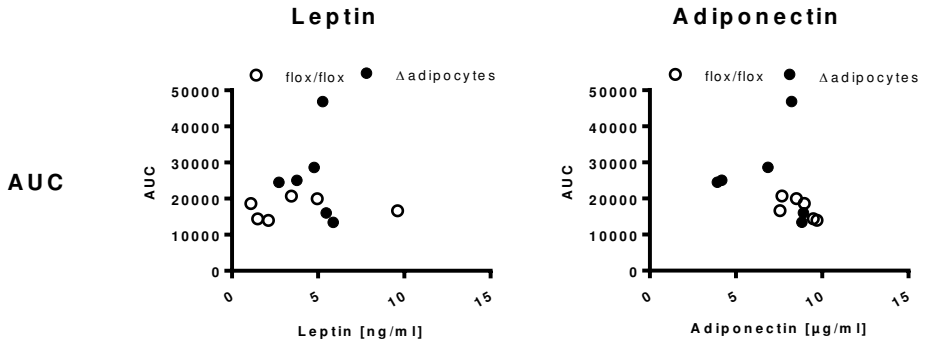

Figure S1. Regression analysis of glucose tolerance and plasma adipokines. Area under the curve calculated from oral glucose tolerance was plotted versus leptin and adiponectin plasma levels. Data are presented as single values, n=6. No significant correlation was observed.

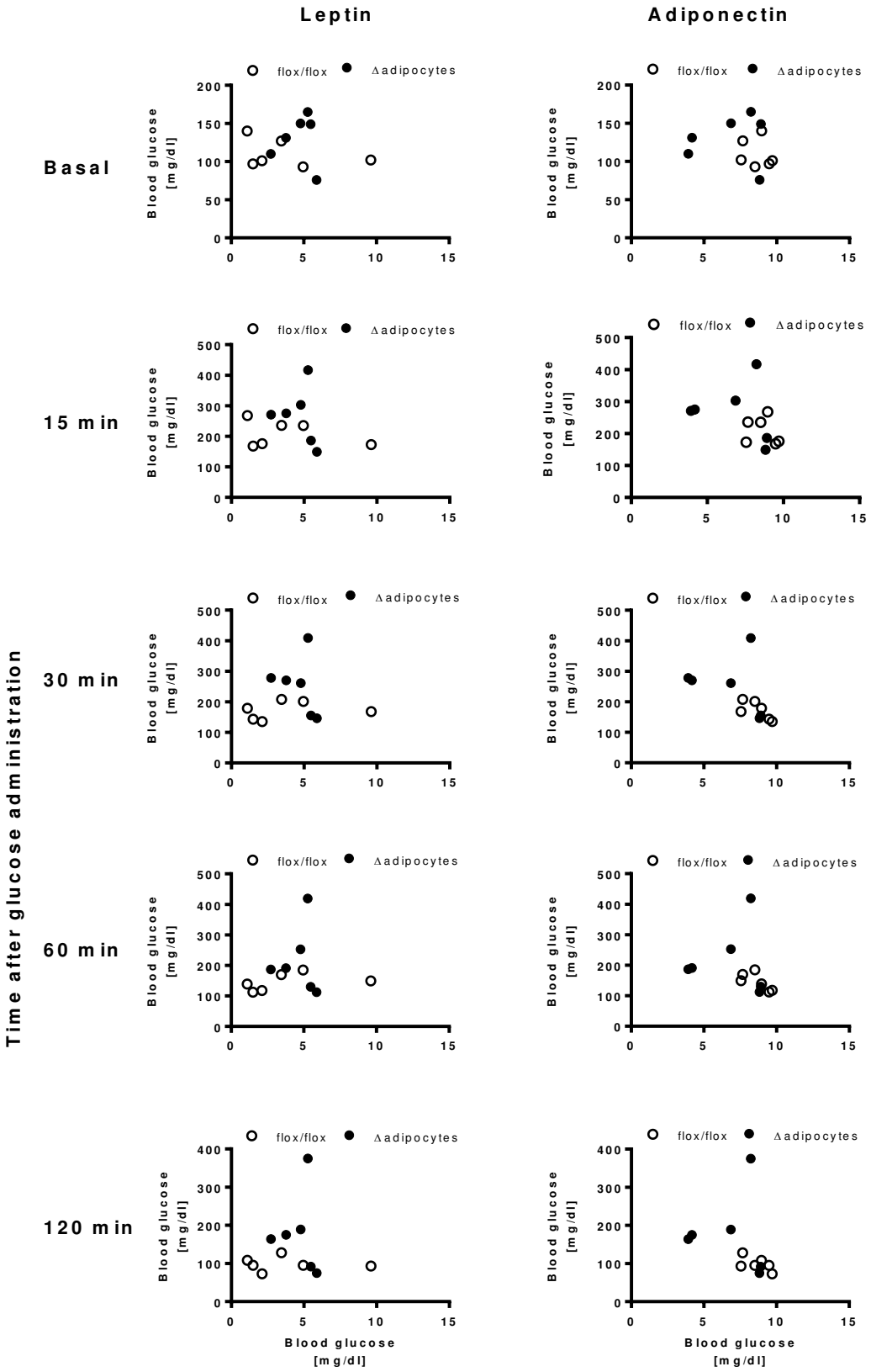

Figure S2. Regression analysis of glucose tolerance and plasma adipokines.
Glucose levels obtained during oral glucose tolerance test (before, 15, 30, 60, and 120 minutes after glucose bolus administration) were plotted versus leptin and adiponectin plasma levels. Data are presented as single values, n=6. No significant correlation was observed.

References

Abel, E. D., Peroni, O., Kim, J. K., Kim, Y. B., Boss, O., Hadro, E., Minnemann, T., Shulman, G. I. & Kahn, B. B. 2001. Adipose-selective targeting of the GLUT4 gene impairs insulin action in muscle and liver. *Nature,* 409, 729-733.

Aldridge, J. E., Horibe, T. & Hoogenraad, N. J. 2007. Discovery of genes activated by the mitochondrial unfolded protein response (mtUPR) and cognate promoter elements. *PLoS One,* 2, e874.

Baker, B. M., Nargund, A. M., Sun, T. & Haynes, C. M. 2012. Protective coupling of mitochondrial function and protein synthesis via the eIF2alpha kinase GCN-2. *PLoS Genet,* 8, e1002760.

Berger, E. 2014. Impact of unfolded protein responses on intestinal epithelial homeostasis in genetically modified mouse models. *Verlag Dr. Hut*.

Brand, M. D. & Nicholls, D. G. 2011. Assessing mitochondrial dysfunction in cells. *Biochem J,* 435, 297-312.

Cheng, M. Y., Hartl, F. U., Martin, J., Pollock, R. A., Kalousek, F., Neupert, W., Hallberg, E. M., Hallberg, R. L. & Horwich, A. L. 1989. Mitochondrial heat-shock protein hsp60 is essential for assembly of proteins imported into yeast mitochondria. *Nature,* 337, 620-625.

Choo, H. J., Kim, J. H., Kwon, O. B., Lee, C. S., Mun, J. Y., Han, S. S., Yoon, Y. S., Yoon, G., Choi, K. M. & Ko, Y. G. 2006. Mitochondria are impaired in the adipocytes of type 2 diabetic mice. *Diabetologia,* 49, 784-791.

Christensen, J. H., Nielsen, M. N., Hansen, J., Fuchtbauer, A., Fuchtbauer, E. M., West, M., Corydon, T. J., Gregersen, N. & Bross, P. 2010. Inactivation of the hereditary spastic paraplegia-associated Hspd1 gene encoding the Hsp60 chaperone results in early embryonic lethality in mice. *Cell Stress Chaperones,* 15, 851-863.

Dahlman, I., Forsgren, M., Sjogren, A., Nordstrom, E. A., Kaaman, M., Naslund, E., Attersand, A. & Arner, P. 2006. Downregulation of electron transport chain genes in visceral adipose tissue in type 2 diabetes independent of obesity and possibly involving tumor necrosis factor-alpha. *Diabetes,* 55, 1792-1799.

Dudek, J., Rehling, P. & van der Laan, M. 2013. Mitochondrial protein import: common principles and physiological networks. *Biochim Biophys Acta,* 1833, 274-285.

Enguix, N., Pardo, R., Gonzalez, A., Lopez, V. M., Simo, R., Kralli, A. & Villena, J. A. 2013. Mice lacking PGC-1beta in adipose tissues reveal a dissociation between mitochondrial dysfunction and insulin resistance. *Mol Metab,* 2, 215-226.

Even, P. C. & Nadkarni, N. A. 2012. Indirect calorimetry in laboratory mice and rats: principles, practical considerations, interpretation and perspectives. *Am J Physiol Regul Integr Comp Physiol,* 303, R459-476.

Feil, R., Wagner, J., Metzger, D. & Chambon, P. 1997. Regulation of Cre recombinase activity by mutated estrogen receptor ligand-binding domains. *Biochem Biophys Res Commun,* 237, 752-757.

Feil, S., Valtcheva, N. & Feil, R. 2009. Inducible Cre mice. *Methods Mol Biol,* 530, 343-363.

Gaveriaux-Ruff, C. & Kieffer, B. L. 2007. Conditional gene targeting in the mouse nervous system: Insights into brain function and diseases. *Pharmacol Ther,* 113, 619-634.

Hallgren, P., Sjostrom, L., Hedlund, H., Lundell, L. & Olbe, L. 1989. Influence of age, fat cell weight, and obesity on O2 consumption of human adipose tissue. *Am J Physiol,* 256, E467-474.

Hesselbarth, N. P., C; Kunath, A; Böge, E; Kern, D; Kern, M; Klöting, N 2015. Tamoxifen: how it influences adipocyte biology in vivo. *Keystone Symposia 2015,* Beige and Brown Fat: Basic Biology and Novel Therapeutics, 56.

Horibe, T. & Hoogenraad, N. J. 2007. The chop gene contains an element for the positive regulation of the mitochondrial unfolded protein response. *PLoS One,* 2, e835.

Iacobellis, G., Di Gioia, C., Petramala, L., Chiappetta, C., Serra, V., Zinnamosca, L., Marinelli, C., Ciardi, A., De Toma, G. & Letizia, C. 2013. Brown fat expresses adiponectin in humans. *Int J Endocrinol,* 2013, 126751.

Jovaisaite, V. & Auwerx, J. 2015. The mitochondrial unfolded protein response-synchronizing genomes. *Curr Opin Cell Biol,* 33, 74-81.

Keuper, M., Jastroch, M., Yi, C. X., Fischer-Posovszky, P., Wabitsch, M., Tschop, M. H. & Hofmann, S. M. 2014. Spare mitochondrial respiratory capacity permits human adipocytes to maintain ATP homeostasis under hypoglycemic conditions. *FASEB J,* 28, 761-770.

Kleiner, S., Mepani, R. J., Laznik, D., Ye, L., Jurczak, M. J., Jornayvaz, F. R., Estall, J. L., Chatterjee Bhowmick, D., Shulman, G. I. & Spiegelman, B. M. 2012. Development of insulin resistance in mice lacking PGC-1alpha in adipose tissues. *Proc Natl Acad Sci U S A,* 109, 9635-9640.

Kleinridders, A., Lauritzen, H. P., Ussar, S., Christensen, J. H., Mori, M. A., Bross, P. & Kahn, C. R. 2013a. Leptin regulation of Hsp60 impacts hypothalamic insulin signaling. *J Clin Invest,* 123, 4667-4680.

Kleinridders, A., Lauritzen, H. P., Ussar, S., Christensen, J. H., Mori, M. A., Bross, P. & Kahn, C. R. 2013b. Leptin regulation of Hsp60 impacts hypothalamic insulin signaling. *J Clin Invest*.

Kusminski, C. M., Holland, W. L., Sun, K., Park, J., Spurgin, S. B., Lin, Y., Askew, G. R., Simcox, J. A., McClain, D. A., Li, C. & Scherer, P. E. 2012. MitoNEET-driven alterations in adipocyte mitochondrial activity reveal a crucial adaptive process that preserves insulin sensitivity in obesity. *Nat Med,* 18, 1539-1549.

Kusminski, C. M. & Scherer, P. E. 2012. Mitochondrial dysfunction in white adipose tissue. *Trends Endocrinol Metab,* 23, 435-443.

Lin, K. M., Lin, B., Lian, I. Y., Mestril, R., Scheffler, I. E. & Dillmann, W. H. 2001. Combined and individual mitochondrial HSP60 and HSP10 expression in cardiac myocytes protects mitochondrial function and prevents apoptotic cell deaths induced by simulated ischemia-reoxygenation. *Circulation,* 103, 1787-1792.

Maassen, J. A., Romijn, J. A. & Heine, R. J. 2007. Fatty acid-induced mitochondrial uncoupling in adipocytes as a key protective factor against insulin resistance and beta cell dysfunction: a new concept in the pathogenesis of obesity-associated type 2 diabetes mellitus. *Diabetologia,* 50, 2036-2041.

Mottis, A., Jovaisaite, V. & Auwerx, J. 2014. The mitochondrial unfolded protein response in mammalian physiology. *Mamm Genome,* 25, 424-433.

Müller, S., Kulenkampff, E. & Wolfrum, C. 2015. Adipose Tissue Stem Cells. *Handb Exp Pharmacol*.

Okamoto, Y., Higashiyama, H., Rong, J. X., McVey, M. J., Kinoshita, M., Asano, S. & Hansen, M. K. 2007. Comparison of mitochondrial and macrophage content between subcutaneous and visceral fat in db/db mice. *Exp Mol Pathol,* 83, 73-83.

Ostermann, J., Horwich, A. L., Neupert, W. & Hartl, F. U. 1989. Protein folding in mitochondria requires complex formation with hsp60 and ATP hydrolysis. *Nature,* 341, 125-130.

Psilopanagioti, A., Papadaki, H., Kranioti, E. F., Alexandrides, T. K. & Varakis, J. N. 2009. Expression of adiponectin and adiponectin receptors in human pituitary gland and brain. *Neuroendocrinology,* 89, 38-47.

Rath, E., Berger, E., Messlik, A., Nunes, T., Liu, B., Kim, S. C., Hoogenraad, N., Sans, M., Sartor, R. B. & Haller, D. 2012. Induction of dsRNA-activated protein kinase links mitochondrial unfolded protein response to the pathogenesis of intestinal inflammation. *Gut,* 61, 1269-1278.

Rath, E. & Haller, D. 2012. Mitochondria at the interface between danger signaling and metabolism: role of unfolded protein responses in chronic inflammation. *Inflamm Bowel Dis,* 18, 1364-1377.

Rong, J. X., Qiu, Y., Hansen, M. K., Zhu, L., Zhang, V., Xie, M., Okamoto, Y., Mattie, M. D., Higashiyama, H., Asano, S., Strum, J. C. & Ryan, T. E. 2007. Adipose mitochondrial

biogenesis is suppressed in db/db and high-fat diet-fed mice and improved by rosiglitazone. *Diabetes,* 56, 1751-1760.

Ryu, M. J., Kim, S. J., Kim, Y. K., Choi, M. J., Tadi, S., Lee, M. H., Lee, S. E., Chung, H. K., Jung, S. B., Kim, H. J., Jo, Y. S., Kim, K. S., Lee, S. H., Kim, J. M., Kweon, G. R., Park, K. C., Lee, J. U., Kong, Y. Y., Lee, C. H., Chung, J. & Shong, M. 2013. Crif1 deficiency reduces adipose OXPHOS capacity and triggers inflammation and insulin resistance in mice. *PLoS Genet,* 9, e1003356.

Sauer, B. & Henderson, N. 1988. Site-specific DNA recombination in mammalian cells by the Cre recombinase of bacteriophage P1. *Proc Natl Acad Sci U S A,* 85, 5166-5170.

Schöttl, T., Kappler, L., Braun, K., Fromme, T. & Klingenspor, M. 2015a. Limited mitochondrial capacity of visceral versus subcutaneous white adipocytes in male C57BL/6N mice. *Endocrinology,* 156, 923-933.

Schöttl, T., Kappler, L., Fromme, T. & Klingenspor, M. 2015b. Limited OXPHOS capacity in white adipocytes is a hallmark of obesity in laboratory mice irrespective of the glucose tolerance status. *Molecular Metabolism,* Epub ahead of print 21-JUL-2015.

Sutherland, L. N., Capozzi, L. C., Turchinsky, N. J., Bell, R. C. & Wright, D. C. 2008. Time course of high-fat diet-induced reductions in adipose tissue mitochondrial proteins: potential mechanisms and the relationship to glucose intolerance. *Am J Physiol Endocrinol Metab,* 295, E1076-1083.

Thoonen 2015. Brown Adipocyte Dysfunction in UCP1 Knockout Mice leads to Age-Dependent Development of Type 2 Diabetes. *FASEB J,* vol. 29 no. 1 Supplement 995.13.

Valerio, A., Cardile, A., Cozzi, V., Bracale, R., Tedesco, L., Pisconti, A., Palomba, L., Cantoni, O., Clementi, E., Moncada, S., Carruba, M. O. & Nisoli, E. 2006. TNF-alpha downregulates eNOS expression and mitochondrial biogenesis in fat and muscle of obese rodents. *J Clin Invest,* 116, 2791-2798.

Vernochet, C., Damilano, F., Mourier, A., Bezy, O., Mori, M. A., Smyth, G., Rosenzweig, A., Larsson, N. G. & Kahn, C. R. 2014. Adipose tissue mitochondrial dysfunction triggers a lipodystrophic syndrome with insulin resistance, hepatosteatosis, and cardiovascular complications. *FASEB J,* 28, 4408-4419.

Vernochet, C., Mourier, A., Bezy, O., Macotela, Y., Boucher, J., Rardin, M. J., An, D., Lee, K. Y., Ilkayeva, O. R., Zingaretti, C. M., Emanuelli, B., Smyth, G., Cinti, S., Newgard, C. B., Gibson, B. W., Larsson, N. G. & Kahn, C. R. 2012. Adipose-specific deletion of TFAM increases mitochondrial oxidation and protects mice against obesity and insulin resistance. *Cell Metab,* 16, 765-776.

Viengchareun, S., Zennaro, M. C., Pascual-Le Tallec, L. & Lombes, M. 2002. Brown adipocytes are novel sites of expression and regulation of adiponectin and resistin. *FEBS Lett,* 532, 345-350.

Wang, Y., Katayama, A., Terami, T., Han, X., Nunoue, T., Zhang, D., Teshigawara, S., Eguchi, J., Nakatsuka, A., Murakami, K., Ogawa, D., Furuta, Y., Makino, H. & Wada, J. 2015. Translocase of inner mitochondrial membrane 44 alters the mitochondrial fusion and fission dynamics and protects from type 2 diabetes. *Metabolism,* 64, 677-688.

Wiedemann, N., Frazier, A. E. & Pfanner, N. 2004. The protein import machinery of mitochondria. *J Biol Chem,* 279, 14473-14476.

Wilson-Fritch, L., Nicoloro, S., Chouinard, M., Lazar, M. A., Chui, P. C., Leszyk, J., Straubhaar, J., Czech, M. P. & Corvera, S. 2004. Mitochondrial remodeling in adipose tissue associated with obesity and treatment with rosiglitazone. *J Clin Invest,* 114, 1281-1289.

Ye, R. & Scherer, P. E. 2013. Adiponectin, driver or passenger on the road to insulin sensitivity? *Mol Metab,* 2, 133-141.

Zhao, Q., Wang, J., Levichkin, I. V., Stasinopoulos, S., Ryan, M. T. & Hoogenraad, N. J. 2002. A mitochondrial specific stress response in mammalian cells. *EMBO J,* 21, 4411-4419.

PUBLICATIONS AND MANUSCRIPTS - SUMMARY OF KEY FINDINGS

This PhD-thesis aimed to provide new perspectives on the impact of white adipocyte mitochondrial bioenergetics on systemic glucose homeostasis as an indicator for metabolic health. Initially, a novel protocol for comprehensive characterization of white adipocyte mitochondrial bioenergetics was established. On this basis, the first specific research aim was to elucidate whether differences in the divergent metabolic risk associated with excessive visceral/intraabdominal versus subcutaneous white adipose tissue (WAT) are predetermined by differences in mitochondrial respiratory function between these types of white body fat. The second aim was to clarify relations between obesity, white adipocyte mitochondrial respiratory capacity, and glucose intolerance. The third aim was to analyze systemic consequences of targeted interference of white adipocyte mitochondrial functionality. Using a broad array of mouse models, ranging from lean and healthy to metabolically challenged by high-fat diet (HFD) feeding or genetic mutations affecting energy homeostasis or mitochondrial function, the present work demonstrates:

CHAPTER I - Adipocytes of subcutaneous origin have a higher respiratory capacity as compared to adipocytes of intraabdominal origin. This finding holds true on the level of intact cells, permeabilized cells, and isolated mitochondria. Further, HFD feeding for one week results in reduction of white adipocyte mitochondrial capacity. This limitation is more pronounced in intraabdominal when compared to subcutaneous adipocytes, and is, interestingly, paralleled by systemic glucose intolerance. Thus, the limited mitochondrial respiratory capacity of adipocytes from intraabdominal fat may be part of the elevated metabolic risk associated with excessive accumulation of intraabdominal body fat.

CHAPTER II - Reduced mitochondrial respiratory capacity in white adipocytes is a general hallmark of murine obesity (diet-induced and genetic), and is more prominent in intraabdominal versus subcutaneous fat. Most notably, limitations occur in both, glucose intolerant (HFD, $Lep^{ob/ob}$) and glucose tolerant (HF-recovery, $Mc4R^{X16/X16}$) obese mice, thus are irrespective of the glucose tolerance status. Therefore, reduced white adipocyte mitochondrial capacity, to the extent it occurs in obesity, solely is not sufficient for the development of systemic glucose intolerance.

CHAPTER III – Knockout of the mitochondrial matrix chaperonin heat shock protein 60 (HSP60) results in massively impaired mitochondrial function, indicated by reduced respiratory capacity in white adipocytes, and causes impaired oral glucose tolerance. Thus, HSP60-deficiency associated impairment in white adipocyte mitochondrial (respiratory) function represents a potential trigger for systemic glucose intolerance.

4 DISCUSSION

This PhD project aimed to clarify the impact of white adipocyte mitochondrial function on systemic glucose homeostasis. The studies generated detailed bioenergetic fingerprints of white adipocyte mitochondria of C57Bl/6 mice in different metabolic conditions. Altogether, this work provides new insights into functional analyzes of white adipocyte mitochondrial metabolism and its potential as regulator of systemic glucose homeostasis. The ensuing discussion illustrates the uniqueness of the experimental design, and points out the requirement of understanding the complexity of mitochondrial function(s) - beyond oxidative phosphorylation (OXPHOS).

4.1 A NOVEL GUIDELINE FOR COMPREHENSIVE ANALYSIS OF MITOCHONDRIAL BIOENERGETICS IN ADIPOCYTES

Meanwhile a plethora of studies analyzed mitochondria of WAT (or white adipocytes) in obesity and/or impaired glucose homeostasis (Hallgren *et al.*, 1989; Wilson-Fritch *et al.*, 2004; Bogacka *et al.*, 2005; Choo *et al.*, 2006; Dahlman *et al.*, 2006; Valerio *et al.*, 2006; Kaaman *et al.*, 2007; Rong *et al.*, 2007; Sutherland *et al.*, 2008; Lindinger *et al.*, 2010; Yehuda-Shnaidman *et al.*, 2010; Christe *et al.*, 2013; Wang *et al.*, 2014; Fischer *et al.*, 2015). Notably, data obtained by these investigations are mainly based on surrogate measures like mitochondrial morphology, citrate synthase activity, mitochondrial DNA abundance, or mitochondrial mRNA and protein levels. Assessment of mitochondrial respiration as the key parameter of mitochondrial function is scarce. If analyzed at all, data have not been obtained for different energetic states and the extent of functional alterations remains elusive. Often only a single fat depot is analyzed but results are extrapolated to total body fat. In conclusion, detailed analyses of mitochondrial bioenergetics in white adipocytes purified from anatomically different fat depots were urgently required. Thus, as a cornerstone of this PhD project, a set of protocols for the comprehensive characterization of white adipocyte mitochondrial bioenergetics was established. As a first highlight, adipocyte mitochondrial respiration was assessed on three levels: intact cells, permeabilized cells, and isolated mitochondria. This allowed dissecting whether mitochondrial alterations occur on organellar level, or (also) result from altered mitochondrial mass per cell or altered mitochondrial-cytoplasmic or mitochondrial-nuclear communication. As a second highlight, different key parameters of mitochondrial respiratory function, including basal proton leak, ATP turnover, and maximal substrate oxidation capacity (Brand, 1990; Brand *et al.*, 1994; Brand & Nicholls, 2011), were assessed. Thereby, extent of OXPHOS impairment could be defined. As a third highlight, posterior subcutaneous and intraabdominal white adipocytes

were analyzed separately to rule out potential differences between those types of body fat in relation to the respective metabolic risk.

Finally, we here provide a novel guideline for detailed characterization of white adipocyte mitochondrial bioenergetics, the key parameter of mitochondrial function. Our methodological approach can be applied for investigations analyzing the impact of obesity, various metabolic diseases, aging, medication, etc. on white adipocyte mitochondrial respiratory capacity.

4.2 UNFOLDING MITOCHONDRIAL FUNCTION IN WHITE ADIPOCYTES – ASPECTS BEYOND OXPHOS SEEM CRUCIAL FOR SYSTEMIC GLUCOSE HOMEOSTASIS

Using the protocols established we analyzed the interrelation between white adipocyte mitochondrial bioenergetics and systemic glucose homeostasis. Therefore, two distinct experimental strategies were developed.

The first, a descriptive approach, was based on close observation of mitochondrial function and state of glucose tolerance in different metabolic conditions: theoretically, if white adipocyte mitochondrial dysfunction triggers the development of obesity associated impaired glucose homeostasis it i) must occur prior to, or instantaneously with the emergence of impaired glucose metabolism ii) is always paralleled by impaired glucose tolerance and does never occur alone iii) disappears before or synchronously with recovery of glucose tolerance. In practice, this work demonstrates that i) white adipocyte mitochondrial dysfunction and glucose intolerance both develop after one week of high-fat diet (HFD) feeding (Schöttl *et al.*, 2015a) ii) both parameters persist during prolonged HFD feeding and massive obesity (Schöttl *et al.*, 2015b), but iii) mitochondrial impairment still exists at recovery of glucose tolerance after HFD is replaced by control diet (Schöttl et al., 2015b). Besides, genetically obese $Mc4R^{X16/X16}$ mice display normal glucose tolerance despite impaired white adipocyte mitochondrial OXPHOS capacity (Schöttl et al., 2015b). Thus, we twice demonstrate dissociation between impaired mitochondrial respiratory function in white adipocytes and impaired tolerance. Consequently, reduced white adipocyte mitochondrial respiratory function, to the extent it occurs in obesity, is not sufficient for the development systemic glucose intolerance.

In a second approach, consequences of manipulated mitochondrial function in white adipocytes on systemic glucose homeostasis were assessed. Notably, disturbing mitochondrial function in white adipocytes by silencing heat shock protein 60 (HSP60) massively affected oral glucose tolerance (publications and manuscripts - chapter III). Compared with data obtained by the descriptive approach, this state of facts at first glance may appear contradictory - it is, however, not in the least. A detailed view on the tremendous

consequences of HSP60 ablation is required to clarify this situation, and is provided in the following.

4.2.1 DIVERSE ASPECTS OF MITOCHONDRIAL FUNCTION ARE AFFECTED UPON SILENCING MITOCHONDRIAL HEAT SHOCK PROTEIN 60

More than 99% of mitochondrial proteins are encoded by the nuclear genome, synthesized in the cytosol, and imported as precursors into mitochondria, as only 13 ((Anderson *et al.*, 1981), example for human mitochondria) of a total of more than 1500 mitochondrial proteins (Lopez *et al.*, 2000) are encoded by the mitochondrial genome and synthesized in the organelle itself. Once arrived in the matrix proteins are folded by assistance of HSP60 (Cheng *et al.*, 1989; Ostermann *et al.*, 1989). Even if not all mitochondrial proteins require folding by the chaperonin (Rospert *et al.*, 1996), the number of (unfolded) proteins affected by HSP60 ablation, and resulting functional impairment, is not restricted to OXPHOS. As just one example, for the matrix enzyme citrate synthase classically folded by assistance of HSP60 (Buchner *et al.*, 1991), significantly decreased protein and activity levels were observed in HSP60 deficient cells (Kleinridders *et al.*, 2013). Thus, beyond OXPHOS, various other aspects of mitochondrial functionality (compare introduction) get impaired upon HSP60 ablation. Secondarily, this may affect mitochondrial-nuclear, mitochondrial-cytoplasmic, or intramitochondrial communication (Whelan & Zuckerbraun, 2013), essential to adapt mitochondrial functions to cellular needs. Together, one can expect that the impairment in adipocyte (mitochondrial) physiology in HSP60$^{\Delta/\Delta adipocytes}$ mice exceeds limitations in OXPHOS capacity. Impairment of any of the numerous mitochondrial functions, alone or in combination with others, may account for the glucose intolerant phenotype of HSP60$^{\Delta/\Delta adipocytes}$ mice. Respective contributions to altered adipocyte physiology and the development of systemic glucose intolerance have to be clarified.

4.2.2 INDUCTION OF MITOCHONDRIAL UNFOLDED PROTEIN RESPONSE IN ADIPOCYTES COULD ACCOUNT FOR IMPAIRED SYSTEMIC GLUCOSE HOMEOSTASIS

HSP60 is not only required for folding proteins newly imported into the mitochondrial matrix. The chaperonin holds also a major role in mitochondrial unfolded protein response (mtUPR), an emerging mitochondrial specific stress response pathway inducing transcription of nuclear-encoded mitochondrial genes to ensure protein homeostasis within the organelle (Zhao *et al.*, 2002; Haynes & Ron, 2010; Jovaisaite & Auwerx, 2015). Within this context, HSP60 refolds damaged matrix proteins (Jovaisaite & Auwerx, 2015). Upon silencing HSP60, the mitochondrial matrix protein folding machinery gets injured, impairing mitochondrial proteostasis (Kleinridders et al., 2013) and triggering mtUPR - a vicious cycle as mtUPR lacks HSP60 as one of its key players.

Induction of mtUPR also implies increased activity of c-Jun N-terminal kinase (JNK), which, by inhibition of phosphotyrosine-binding domain in insulin-receptor substrate 1 (IRS-1) via phosphorylation of serine 307, impairs insulin signal transduction, causing adipocyte insulin resistance (Aguirre *et al.*, 2002). Secondarily, insulin resistance in white adipocytes causes insulin resistance in liver and muscle. Endocrine activity of adipocytes may account for this phenomenon, as it occurs *in vivo,* but not *ex vivo* (Abel *et al.*, 2001). Thus, proper mtUPR signaling and function in adipocytes could be essential for both cellular insulin sensitivity and systemic glucose homeostasis.

In conclusion, the contrasting juxtaposition of HFD fed and genetically obese mice to HSP60$^{\Delta/\Delta adipocytes}$ mice emphasizes the necessity of mitochondrial proteostasis for adipocyte physiology and, in the end, systemic glucose metabolism. As the primary finding of this PhD project, aspects of mitochondrial function other than OXPHOS capacity and yet unexplored, including elements of mitochondrial communication, turned out crucial for the maintenance of systemic glucose homeostasis.

4.3 ALTERED MITOCHONDRIAL FUNCTION DOES NOT NECESSARILY IMPLY DYSFUNCTION

Currently, any abnormality in the various aspects of mitochondrial function is referred to as *mitochondrial dysfunction* (Brand & Nicholls, 2011). This definition, however, certainly misconceives several states as dysfunctional without having any adverse effect. Here, as an example, the extent of reduced mitochondrial OXPHOS capacity observed in obese mice rather may represent physiological adaption to adipocyte hypertrophy and hypoxia than meaning true dysfunction (Schöttl et al., 2015b). In other words, the current definition of *mitochondrial dysfunction* does not differentiate whether or not mitochondrial alterations imply dysfunction, thus failure to supply the cell with energy or other defects impairing cellular, tissue, or systemic physiology. At the same time, however, *mitochondrial dysfunction* is discussed as potential causative factor in the development of insulin resistance and type 2 diabetes mellitus (Lowell & Shulman, 2005; Sivitz & Yorek, 2010; Martin & McGee, 2014; Montgomery & Turner, 2015; Rieusset, 2015). Therefore, the term *mitochondrial dysfunction* requires redefinition.

As a suggestion, first *mitochondrial dysfunction* should be replaced by *altered mitochondrial function*. In fact, *altered mitochondrial function* implies any functional divergence from general mitochondrial physiology. Second, *mitochondrial dysfunction* should be reserved for a category within *altered mitochondrial function*, with evidence for true functional failure.

Using this terminology may avoid misinterpreting e.g. adaptive processes as pathologic states.

Here, *altered white adipocyte mitochondrial function* (limited OXPHOS capacity) was observed for HFD-fed (short-time and long-time) and genetically obese mice, as well as HSP60 mice. Only in case of the latter, however, the definition of *mitochondrial dysfunction* seems fulfilled. In the end, the level of *mitochondrial dysfunction* caused by HSP60 ablation in white adipocytes unambiguously represents a trigger for glucose intolerance.

4.4 CONCLUSION AND PERSPECTIVES

Altogether, this PhD thesis forwards the understanding of white adipocyte mitochondrial physiology and its impact on systemic glucose tolerance. Studies on HFD fed and genetically obese mice revealed that, even if white adipocyte mitochondrial OXPHOS capacity is affected by weight gain and obesity, it is not sufficient to impair systemic glucose homeostasis. HSP60$^{\Delta/\Delta adipocytes}$ mice, however, suggest additional (unknown) aspects of mitochondrial function crucial for the maintenance of glucose tolerance. Future studies now have to identify candidate pathway(s) accounting for glucose intolerance in HSP60$^{\Delta/\Delta adipocytes}$ (and possibly glucose intolerant obese) mice. As a first step, systematic identification and quantification of the complete mitochondrial proteome of these mouse models, followed by pathway analysis, will clarify the contribution of different aspects of mitochondrial function to impaired glucose homeostasis.

5 REFERENCE LIST

Abel, E. D., Peroni, O., Kim, J. K., Kim, Y. B., Boss, O., Hadro, E., Minnemann, T., Shulman, G. I. & Kahn, B. B. 2001. Adipose-selective targeting of the GLUT4 gene impairs insulin action in muscle and liver. *Nature,* 409, 729-733.

Aguirre, V., Werner, E. D., Giraud, J., Lee, Y. H., Shoelson, S. E. & White, M. F. 2002. Phosphorylation of Ser307 in insulin receptor substrate-1 blocks interactions with the insulin receptor and inhibits insulin action. *J Biol Chem,* 277, 1531-1537.

Akerman, K. E. & Wikstrom, M. K. 1976. Safranine as a probe of the mitochondrial membrane potential. *FEBS Lett,* 68, 191-197.

Alessi, M. C., Peiretti, F., Morange, P., Henry, M., Nalbone, G. & Juhan-Vague, I. 1997. Production of plasminogen activator inhibitor 1 by human adipose tissue: possible link between visceral fat accumulation and vascular disease. *Diabetes,* 46, 860-867.

Alexson, S. E. & Nedergaard, J. 1988. A novel type of short- and medium-chain acyl-CoA hydrolases in brown adipose tissue mitochondria. *J Biol Chem,* 263, 13564-13571.

Anderson, S., Bankier, A. T., Barrell, B. G., de Bruijn, M. H., Coulson, A. R., Drouin, J., Eperon, I. C., Nierlich, D. P., Roe, B. A., Sanger, F., Schreier, P. H., Smith, A. J., Staden, R. & Young, I. G. 1981. Sequence and organization of the human mitochondrial genome. *Nature,* 290, 457-465.

Bjorndal, B., Burri, L., Staalesen, V., Skorve, J. & Berge, R. K. 2011. Different adipose depots: their role in the development of metabolic syndrome and mitochondrial response to hypolipidemic agents. *J Obes,* 2011, 490650.

Blüher, M. 2012. Clinical relevance of adipokines. *Diabetes Metab J,* 36, 317-327.

Bogacka, I., Xie, H., Bray, G. A. & Smith, S. R. 2005. Pioglitazone induces mitochondrial biogenesis in human subcutaneous adipose tissue in vivo. *Diabetes,* 54, 1392-1399.

Brand, M. D. 1990. The proton leak across the mitochondrial inner membrane. *Biochim Biophys Acta,* 1018, 128-133.

Brand, M. D., Chien, L. F., Ainscow, E. K., Rolfe, D. F. & Porter, R. K. 1994. The causes and functions of mitochondrial proton leak. *Biochim Biophys Acta,* 1187, 132-139.

Brand, M. D. & Nicholls, D. G. 2011. Assessing mitochondrial dysfunction in cells. *Biochem J,* 435, 297-312.

Buchner, J., Schmidt, M., Fuchs, M., Jaenicke, R., Rudolph, R., Schmid, F. X. & Kiefhaber, T. 1991. GroE facilitates refolding of citrate synthase by suppressing aggregation. *Biochemistry,* 30, 1586-1591.

Chau, Y. Y., Bandiera, R., Serrels, A., Martinez-Estrada, O. M., Qing, W., Lee, M., Slight, J., Thornburn, A., Berry, R., McHaffie, S., Stimson, R. H., Walker, B. R., Chapuli, R. M., Schedl, A. & Hastie, N. 2014. Visceral and subcutaneous fat have different origins and evidence supports a mesothelial source. *Nat Cell Biol,* 16, 367-375.

Cheng, M. Y., Hartl, F. U., Martin, J., Pollock, R. A., Kalousek, F., Neupert, W., Hallberg, E. M., Hallberg, R. L. & Horwich, A. L. 1989. Mitochondrial heat-shock protein hsp60 is essential for assembly of proteins imported into yeast mitochondria. *Nature,* 337, 620-625.

Choo, H. J., Kim, J. H., Kwon, O. B., Lee, C. S., Mun, J. Y., Han, S. S., Yoon, Y. S., Yoon, G., Choi, K. M. & Ko, Y. G. 2006. Mitochondria are impaired in the adipocytes of type 2 diabetic mice. *Diabetologia,* 49, 784-791.

Christe, M., Hirzel, E., Lindinger, A., Kern, B., von Flue, M., Peterli, R., Peters, T., Eberle, A. N. & Lindinger, P. W. 2013. Obesity affects mitochondrial citrate synthase in human omental adipose tissue. *ISRN Obes,* 2013, 826027.

Cinti, S. 2002. Adipocyte differentiation and transdifferentiation: plasticity of the adipose organ. *J Endocrinol Invest,* 25, 823-835.

Cinti, S. 2012. The adipose organ at a glance. *Dis Model Mech,* 5, 588-594.

Dahlman, I., Forsgren, M., Sjogren, A., Nordstrom, E. A., Kaaman, M., Naslund, E., Attersand, A. & Arner, P. 2006. Downregulation of electron transport chain genes in visceral adipose tissue in type 2 diabetes independent of obesity and possibly involving tumor necrosis factor-alpha. *Diabetes,* 55, 1792-1799.

De Pauw, A., Tejerina, S., Raes, M., Keijer, J. & Arnould, T. 2009. Mitochondrial (dys)function in adipocyte (de)differentiation and systemic metabolic alterations. *Am J Pathol,* 175, 927-939.

Derous, D., Kelder, T., van Schothorst, E. M., van Erk, M., Voigt, A., Klaus, S., Keijer, J. & Radonjic, M. 2015. Network-based integration of molecular and physiological data elucidates regulatory mechanisms underlying adaptation to high-fat diet. *Genes Nutr,* 10, 470.

Eriksson, O., Fontaine, E. & Bernardi, P. 1998. Chemical modification of arginines by 2,3-butanedione and phenylglyoxal causes closure of the mitochondrial permeability transition pore. *J Biol Chem,* 273, 12669-12674.

Fasshauer, M. & Blüher, M. 2015. Adipokines in health and disease. *Trends Pharmacol Sci*.

Ferrick, D. A., Neilson, A. & Beeson, C. 2008. Advances in measuring cellular bioenergetics using extracellular flux. *Drug Discov Today,* 13, 268-274.

Fischer, B., Schottl, T., Schempp, C., Fromme, T., Hauner, H., Klingenspor, M. & Skurk, T. 2015. Inverse relationship between body mass index and mitochondrial oxidative phosphorylation capacity in human subcutaneous adipocytes. *Am J Physiol Endocrinol Metab*, ajpendo 00524 02014.

Forner, F., Kumar, C., Luber, C. A., Fromme, T., Klingenspor, M. & Mann, M. 2009. Proteome differences between brown and white fat mitochondria reveal specialized metabolic functions. *Cell Metab,* 10, 324-335.

Fox, C. S., Massaro, J. M., Hoffmann, U., Pou, K. M., Maurovich-Horvat, P., Liu, C. Y., Vasan, R. S., Murabito, J. M., Meigs, J. B., Cupples, L. A., D'Agostino, R. B., Sr. & O'Donnell, C. J. 2007. Abdominal visceral and subcutaneous adipose tissue compartments: association with metabolic risk factors in the Framingham Heart Study. *Circulation,* 116, 39-48.

Franckhauser, S., Munoz, S., Pujol, A., Casellas, A., Riu, E., Otaegui, P., Su, B. & Bosch, F. 2002. Increased fatty acid re-esterification by PEPCK overexpression in adipose tissue leads to obesity without insulin resistance. *Diabetes,* 51, 624-630.

Fried, S. K., Bunkin, D. A. & Greenberg, A. S. 1998. Omental and subcutaneous adipose tissues of obese subjects release interleukin-6: depot difference and regulation by glucocorticoid. *J Clin Endocrinol Metab,* 83, 847-850.

Frizzell, N., Rajesh, M., Jepson, M. J., Nagai, R., Carson, J. A., Thorpe, S. R. & Baynes, J. W. 2009. Succination of thiol groups in adipose tissue proteins in diabetes: succination inhibits polymerization and secretion of adiponectin. *J Biol Chem,* 284, 25772-25781.

Garthwaite, T. L., Martinson, D. R., Tseng, L. F., Hagen, T. C. & Menahan, L. A. 1980. A longitudinal hormonal profile of the genetically obese mouse. *Endocrinology,* 107, 671-676.

Hallgren, P., Sjostrom, L., Hedlund, H., Lundell, L. & Olbe, L. 1989. Influence of age, fat cell weight, and obesity on O2 consumption of human adipose tissue. *Am J Physiol,* 256, E467-474.

Haynes, C. M. & Ron, D. 2010. The mitochondrial UPR - protecting organelle protein homeostasis. *J Cell Sci,* 123, 3849-3855.

Hellmer, J., Marcus, C., Sonnenfeld, T. & Arner, P. 1992. Mechanisms for differences in lipolysis between human subcutaneous and omental fat cells. *J Clin Endocrinol Metab,* 75, 15-20.

Hocking, S. L., Chisholm, D. J. & James, D. E. 2008. Studies of regional adipose transplantation reveal a unique and beneficial interaction between subcutaneous adipose tissue and the intra-abdominal compartment. *Diabetologia,* 51, 900-902.

Hocking, S. L., Stewart, R. L., Brandon, A. E., Suryana, E., Stuart, E., Baldwin, E. M., Kolumam, G. A., Modrusan, Z., Junutula, J. R., Gunton, J. E., Medynskyj, M., Blaber, S. P., Karsten, E., Herbert, B. R., James, D. E., Cooney, G. J. & Swarbrick, M. M.

2015. Subcutaneous fat transplantation alleviates diet-induced glucose intolerance and inflammation in mice. *Diabetologia*.

Jeon, M. J., Leem, J., Ko, M. S., Jang, J. E., Park, H. S., Kim, H. S., Kim, M., Kim, E. H., Yoo, H. J., Lee, C. H., Park, I. S., Lee, K. U. & Koh, E. H. 2012. Mitochondrial dysfunction and activation of iNOS are responsible for the palmitate-induced decrease in adiponectin synthesis in 3T3L1 adipocytes. *Exp Mol Med,* 44, 562-570.

Jo, J., Gavrilova, O., Pack, S., Jou, W., Mullen, S., Sumner, A. E., Cushman, S. W. & Periwal, V. 2009. Hypertrophy and/or Hyperplasia: Dynamics of Adipose Tissue Growth. *PLoS Comput Biol,* 5, e1000324.

Jovaisaite, V. & Auwerx, J. 2015. The mitochondrial unfolded protein response-synchronizing genomes. *Curr Opin Cell Biol,* 33, 74-81.

Kaaman, M., Sparks, L. M., van Harmelen, V., Smith, S. R., Sjolin, E., Dahlman, I. & Arner, P. 2007. Strong association between mitochondrial DNA copy number and lipogenesis in human white adipose tissue. *Diabetologia,* 50, 2526-2533.

Kanneganti, T. D. & Dixit, V. D. 2012. Immunological complications of obesity. *Nat Immunol,* 13, 707-712.

Kim, J. I., Huh, J. Y., Sohn, J. H., Choe, S. S., Lee, Y. S., Lim, C. Y., Jo, A., Park, S. B., Han, W. & Kim, J. B. 2015. Lipid-overloaded enlarged adipocytes provoke insulin resistance independent of inflammation. *Mol Cell Biol,* 35, 1686-1699.

Kim, J. Y., van de Wall, E., Laplante, M., Azzara, A., Trujillo, M. E., Hofmann, S. M., Schraw, T., Durand, J. L., Li, H., Li, G., Jelicks, L. A., Mehler, M. F., Hui, D. Y., Deshaies, Y., Shulman, G. I., Schwartz, G. J. & Scherer, P. E. 2007. Obesity-associated improvements in metabolic profile through expansion of adipose tissue. *J Clin Invest,* 117, 2621-2637.

Kleinridders, A., Lauritzen, H. P., Ussar, S., Christensen, J. H., Mori, M. A., Bross, P. & Kahn, C. R. 2013. Leptin regulation of Hsp60 impacts hypothalamic insulin signaling. *J Clin Invest*.

Kless, C., Muller, V. M., Schuppel, V. L., Lichtenegger, M., Rychlik, M., Daniel, H., Klingenspor, M. & Haller, D. 2015. Diet-induced obesity causes metabolic impairment independent of alterations in gut barrier integrity. *Mol Nutr Food Res,* 59, 968-978.

Koh, E. H., Park, J. Y., Park, H. S., Jeon, M. J., Ryu, J. W., Kim, M., Kim, S. Y., Kim, M. S., Kim, S. W., Park, I. S., Youn, J. H. & Lee, K. U. 2007. Essential role of mitochondrial function in adiponectin synthesis in adipocytes. *Diabetes,* 56, 2973-2981.

Kraunsoe, R., Boushel, R., Hansen, C. N., Schjerling, P., Qvortrup, K., Stockel, M., Mikines, K. J. & Dela, F. 2010. Mitochondrial respiration in subcutaneous and visceral adipose tissue from patients with morbid obesity. *J Physiol,* 588, 2023-2032.

Kusminski, C. M. & Scherer, P. E. 2012. Mitochondrial dysfunction in white adipose tissue. *Trends Endocrinol Metab,* 23, 435-443.

Le Lay, S., Krief, S., Farnier, C., Lefrere, I., Le Liepvre, X., Bazin, R., Ferre, P. & Dugail, I. 2001. Cholesterol, a cell size-dependent signal that regulates glucose metabolism and gene expression in adipocytes. *J Biol Chem,* 276, 16904-16910.

Lee, M. J., Wu, Y. & Fried, S. K. 2013. Adipose tissue heterogeneity: implication of depot differences in adipose tissue for obesity complications. *Mol Aspects Med,* 34, 1-11.

Lindinger, A., Peterli, R., Peters, T., Kern, B., von Flue, M., Calame, M., Hoch, M., Eberle, A. N. & Lindinger, P. W. 2010. Mitochondrial DNA content in human omental adipose tissue. *Obes Surg,* 20, 84-92.

Lionetti, L., Mollica, M. P., Donizzetti, I., Gifuni, G., Sica, R., Pignalosa, A., Cavaliere, G., Gaita, M., De Filippo, C., Zorzano, A. & Putti, R. 2014. High-lard and high-fish-oil diets differ in their effects on function and dynamic behaviour of rat hepatic mitochondria. *PLoS One,* 9, e92753.

Lopez, M. F., Kristal, B. S., Chernokalskaya, E., Lazarev, A., Shestopalov, A. I., Bogdanova, A. & Robinson, M. 2000. High-throughput profiling of the mitochondrial proteome using affinity fractionation and automation. *Electrophoresis,* 21, 3427-3440.

Lowell, B. B. & Shulman, G. I. 2005. Mitochondrial dysfunction and type 2 diabetes. *Science,* 307, 384-387.

Lu, R. H., Ji, H., Chang, Z. G., Su, S. S. & Yang, G. S. 2010. Mitochondrial development and the influence of its dysfunction during rat adipocyte differentiation. *Mol Biol Rep,* 37, 2173-2182.

Macotela, Y., Emanuelli, B., Mori, M. A., Gesta, S., Schulz, T. J., Tseng, Y. H. & Kahn, C. R. 2012. Intrinsic differences in adipocyte precursor cells from different white fat depots. *Diabetes,* 61, 1691-1699.

Martin, S. D. & McGee, S. L. 2014. The role of mitochondria in the aetiology of insulin resistance and type 2 diabetes. *Biochim Biophys Acta,* 1840, 1303-1312.

Montague, C. T. & O'Rahilly, S. 2000. The perils of portliness: causes and consequences of visceral adiposity. *Diabetes,* 49, 883-888.

Montague, C. T., Prins, J. B., Sanders, L., Digby, J. E. & O'Rahilly, S. 1997. Depot- and sex-specific differences in human leptin mRNA expression: implications for the control of regional fat distribution. *Diabetes,* 46, 342-347.

Montgomery, M. K. & Turner, N. 2015. Mitochondrial dysfunction and insulin resistance: an update. *Endocr Connect,* 4, R1-R15.

Müller, S., Kulenkampff, E. & Wolfrum, C. 2015. Adipose Tissue Stem Cells. *Handb Exp Pharmacol*.

Nawrocki, A. R., Rajala, M. W., Tomas, E., Pajvani, U. B., Saha, A. K., Trumbauer, M. E., Pang, Z., Chen, A. S., Ruderman, N. B., Chen, H., Rossetti, L. & Scherer, P. E. 2006. Mice lacking adiponectin show decreased hepatic insulin sensitivity and reduced responsiveness to peroxisome proliferator-activated receptor gamma agonists. *J Biol Chem,* 281, 2654-2660.

Olswang, Y., Cohen, H., Papo, O., Cassuto, H., Croniger, C. M., Hakimi, P., Tilghman, S. M., Hanson, R. W. & Reshef, L. 2002. A mutation in the peroxisome proliferator-activated receptor gamma-binding site in the gene for the cytosolic form of phosphoenolpyruvate carboxykinase reduces adipose tissue size and fat content in mice. *Proc Natl Acad Sci U S A,* 99, 625-630.

Ostermann, J., Horwich, A. L., Neupert, W. & Hartl, F. U. 1989. Protein folding in mitochondria requires complex formation with hsp60 and ATP hydrolysis. *Nature,* 341, 125-130.

Pajvani, U. B., Trujillo, M. E., Combs, T. P., Iyengar, P., Jelicks, L., Roth, K. A., Kitsis, R. N. & Scherer, P. E. 2005. Fat apoptosis through targeted activation of caspase 8: a new mouse model of inducible and reversible lipoatrophy. *Nat Med,* 11, 797-803.

Pardo, R., Enguix, N., Lasheras, J., Feliu, J. E., Kralli, A. & Villena, J. A. 2011. Rosiglitazone-induced mitochondrial biogenesis in white adipose tissue is independent of peroxisome proliferator-activated receptor gamma coactivator-1alpha. *PLoS One,* 6, e26989.

Perevoshchikova, I. V., Sorochkina, A. I., Zorov, D. B. & Antonenko, Y. N. 2009. Safranine O as a fluorescent probe for mitochondrial membrane potential studied on the single particle level and in suspension. *Biochemistry (Mosc),* 74, 663-671.

Pesta, D. & Gnaiger, E. 2012. High-resolution respirometry: OXPHOS protocols for human cells and permeabilized fibers from small biopsies of human muscle. *Methods Mol Biol,* 810, 25-58.

Richelsen, B., Pedersen, S. B., Moller-Pedersen, T. & Bak, J. F. 1991. Regional differences in triglyceride breakdown in human adipose tissue: effects of catecholamines, insulin, and prostaglandin E2. *Metabolism,* 40, 990-996.

Rieusset, J. 2015. Contribution of mitochondria and endoplasmic reticulum dysfunction in insulin resistance: Distinct or interrelated roles? *Diabetes Metab*.

Rogers, G. W., Brand, M. D., Petrosyan, S., Ashok, D., Elorza, A. A., Ferrick, D. A. & Murphy, A. N. 2011. High throughput microplate respiratory measurements using minimal quantities of isolated mitochondria. *PLoS One,* 6, e21746.

Rong, J. X., Qiu, Y., Hansen, M. K., Zhu, L., Zhang, V., Xie, M., Okamoto, Y., Mattie, M. D., Higashiyama, H., Asano, S., Strum, J. C. & Ryan, T. E. 2007. Adipose mitochondrial biogenesis is suppressed in db/db and high-fat diet-fed mice and improved by rosiglitazone. *Diabetes,* 56, 1751-1760.

Rosen, E. D. & Spiegelman, B. M. 2014. What we talk about when we talk about fat. *Cell,* 156, 20-44.

Rospert, S., Looser, R., Dubaquie, Y., Matouschek, A., Glick, B. S. & Schatz, G. 1996. Hsp60-independent protein folding in the matrix of yeast mitochondria. *EMBO J,* 15, 764-774.

Rowe, G. C. & Arany, Z. 2014. Genetic models of PGC-1 and glucose metabolism and homeostasis. *Rev Endocr Metab Disord,* 15, 21-29.

Rutkowski, J. M., Stern, J. H. & Scherer, P. E. 2015. The cell biology of fat expansion. *J Cell Biol,* 208, 501-512.

Ryu, M. J., Kim, S. J., Kim, Y. K., Choi, M. J., Tadi, S., Lee, M. H., Lee, S. E., Chung, H. K., Jung, S. B., Kim, H. J., Jo, Y. S., Kim, K. S., Lee, S. H., Kim, J. M., Kweon, G. R., Park, K. C., Lee, J. U., Kong, Y. Y., Lee, C. H., Chung, J. & Shong, M. 2013. Crif1 deficiency reduces adipose OXPHOS capacity and triggers inflammation and insulin resistance in mice. *PLoS Genet,* 9, e1003356.

Schlieve, C. R., Lieven, C. J. & Levin, L. A. 2006. Biochemical activity of reactive oxygen species scavengers do not predict retinal ganglion cell survival. *Invest Ophthalmol Vis Sci,* 47, 3878-3886.

Schöttl, T., Kappler, L., Braun, K., Fromme, T. & Klingenspor, M. 2015a. Limited mitochondrial capacity of visceral versus subcutaneous white adipocytes in male C57BL/6N mice. *Endocrinology,* 156, 923-933.

Schöttl, T., Kappler, L., Fromme, T. & Klingenspor, M. 2015b. Limited OXPHOS capacity in white adipocytes is a hallmark of obesity in laboratory mice irrespective of the glucose tolerance status. *Molecular Metabolism,* Epub ahead of print 21-JUL-2015.

Shimomura, I., Hammer, R. E., Richardson, J. A., Ikemoto, S., Bashmakov, Y., Goldstein, J. L. & Brown, M. S. 1998. Insulin resistance and diabetes mellitus in transgenic mice expressing nuclear SREBP-1c in adipose tissue: model for congenital generalized lipodystrophy. *Genes Dev,* 12, 3182-3194.

Sivitz, W. I. & Yorek, M. A. 2010. Mitochondrial dysfunction in diabetes: from molecular mechanisms to functional significance and therapeutic opportunities. *Antioxid Redox Signal,* 12, 537-577.

Skurk, T., Alberti-Huber, C., Herder, C. & Hauner, H. 2007. Relationship between adipocyte size and adipokine expression and secretion. *J Clin Endocrinol Metab,* 92, 1023-1033.

Stehling, O., Wilbrecht, C. & Lill, R. 2014. Mitochondrial iron-sulfur protein biogenesis and human disease. *Biochimie,* 100, 61-77.

Sutherland, L. N., Capozzi, L. C., Turchinsky, N. J., Bell, R. C. & Wright, D. C. 2008. Time course of high-fat diet-induced reductions in adipose tissue mitochondrial proteins: potential mechanisms and the relationship to glucose intolerance. *Am J Physiol Endocrinol Metab,* 295, E1076-1083.

Toime, L. J. & Brand, M. D. 2010. Uncoupling protein-3 lowers reactive oxygen species production in isolated mitochondria. *Free Radic Biol Med,* 49, 606-611.

Tormos, K. V., Anso, E., Hamanaka, R. B., Eisenbart, J., Joseph, J., Kalyanaraman, B. & Chandel, N. S. 2011. Mitochondrial complex III ROS regulate adipocyte differentiation. *Cell Metab,* 14, 537-544.

Tran, T. T., Yamamoto, Y., Gesta, S. & Kahn, C. R. 2008. Beneficial effects of subcutaneous fat transplantation on metabolism. *Cell Metab,* 7, 410-420.

Trayhurn, P. & Beattie, J. H. 2001. Physiological role of adipose tissue: white adipose tissue as an endocrine and secretory organ. *Proc Nutr Soc,* 60, 329-339.

Vague, J. 1956. The degree of masculine differentiation of obesities: a factor determining predisposition to diabetes, atherosclerosis, gout, and uric calculous disease. *Am J Clin Nutr,* 4, 20-34.

Valerio, A., Cardile, A., Cozzi, V., Bracale, R., Tedesco, L., Pisconti, A., Palomba, L., Cantoni, O., Clementi, E., Moncada, S., Carruba, M. O. & Nisoli, E. 2006. TNF-alpha downregulates eNOS expression and mitochondrial biogenesis in fat and muscle of obese rodents. *J Clin Invest,* 116, 2791-2798.

Vernochet, C., Damilano, F., Mourier, A., Bezy, O., Mori, M. A., Smyth, G., Rosenzweig, A., Larsson, N. G. & Kahn, C. R. 2014. Adipose tissue mitochondrial dysfunction triggers a lipodystrophic syndrome with insulin resistance, hepatosteatosis, and cardiovascular complications. *FASEB J,* 28, 4408-4419.

Wang, P. W., Kuo, H. M., Huang, H. T., Chang, A. Y., Weng, S. W., Tai, M. H., Chuang, J. H., Chen, I. Y., Huang, S. C., Lin, T. K. & Liou, C. W. 2014. Biphasic Response of Mitochondrial Biogenesis to Oxidative Stress in Visceral Fat of Diet-Induced Obesity Mice. *Antioxid Redox Signal*.

Whelan, S. P. & Zuckerbraun, B. S. 2013. Mitochondrial signaling: forwards, backwards, and in between. *Oxid Med Cell Longev,* 2013, 351613.

WHO 2015. Diabetes fact sheet N°312.

Wilson-Fritch, L., Nicoloro, S., Chouinard, M., Lazar, M. A., Chui, P. C., Leszyk, J., Straubhaar, J., Czech, M. P. & Corvera, S. 2004. Mitochondrial remodeling in adipose tissue associated with obesity and treatment with rosiglitazone. *J Clin Invest,* 114, 1281-1289.

Yehuda-Shnaidman, E., Buehrer, B., Pi, J., Kumar, N. & Collins, S. 2010. Acute stimulation of white adipocyte respiration by PKA-induced lipolysis. *Diabetes,* 59, 2474-2483.

Zago, E. B., Castilho, R. F. & Vercesi, A. E. 2000. The redox state of endogenous pyridine nucleotides can determine both the degree of mitochondrial oxidative stress and the solute selectivity of the permeability transition pore. *FEBS Lett,* 478, 29-33.

Zhang, Y., Proenca, R., Maffei, M., Barone, M., Leopold, L. & Friedman, J. M. 1994. Positional cloning of the mouse obese gene and its human homologue. *Nature,* 372, 425-432.

Zhao, Q., Wang, J., Levichkin, I. V., Stasinopoulos, S., Ryan, M. T. & Hoogenraad, N. J. 2002. A mitochondrial specific stress response in mammalian cells. *EMBO J,* 21, 4411-4419.

Zhou, M., Diwu, Z., Panchuk-Voloshina, N. & Haugland, R. P. 1997. A stable nonfluorescent derivative of resorufin for the fluorometric determination of trace hydrogen peroxide: applications in detecting the activity of phagocyte NADPH oxidase and other oxidases. *Anal Biochem,* 253, 162-168.

This list includes references of (1) Introduction (2) Methodology to assess white adipocyte mitochondrial bioenergetics and (4) Discussion. References of (3) Publications and Manuscripts, and (6) Appendix are listed separately.

6 APPENDIX

6.1 MOUSE MODELS

Experiments were in accordance with the German guidelines for animal care and with permission of the government of Upper Bavaria, Germany (Regierung von Oberbayern, AZ 55.2.1.54-2532-148-13 and AZ 55.2-1-54-2532-12-12).

Experiments were performed on male C57BL/6 inbred mice which were housed in groups in individually ventilated cages (IVC, type II 540 cm^2) in a specific pathogen-free environment. Mice were kept on a 12h:12h light-dark photocycle at 22 ± 1°C (relative humidity of 50-60%) with ad libitum access to water and food. Chow diet (V1124) was fed until mice were assigned to feeding experiments. Diets were purchased from Ssniff Spezialdiäten GmbH or LASVendi, both Soest, Germany (Table 6-11, Figure 6-2). Hygiene status of the mice was checked within a three-months-cycle according to criteria of the Federation of European Laboratory Animal Science Associations (FELASA). At the end of the respective experiment, mice were anesthetized by CO_2 and killed by exsanguination.

6.1.1 COMPARISON OF MITOCHONDRIAL BIOENERGETICS IN WHITE ADIPOCYTES FROM DIFFERENT FAT DEPOTS OF LEAN WILDTYPE MICE

Ten weeks old wildtype C57BL/6N mice were purchased from Charles River and kept on chow until killing at the age of 12 weeks.

6.1.2 METABOLIC CHALLENGES

High-fat diet feeding and diet-induced obesity

At the age of seven weeks, wildtype C57BL/6N mice (bred in house, founder breeding pairs originally purchased from Charles River Laboratories, Inc.) were switched from chow to a purified research control diet (CD, 12 kJ% fat, SS745-E702, Table 6-1, Figure 6-1). After acclimatization for one week, mice were matched by body weight into a control and a high-fat diet group (HFD, 48 kJ% fat SS745-E712; Ssniff, Table 6-11, Figure 6-2). Feeding duration differed between one week and six months (Table 6-1). During experimental feeding, body weight was controlled every two weeks. At the beginning and the end of each experiment, body composition and glucose tolerance were determined. Mice of the high-fat-recovery experiment (HF-recovery) additionally underwent body composition and glucose tolerance determination before refeeding CD after 24 weeks HFD exposure.

Table 6-1. Overview of high-fat diet versus control diet feeding studies

Experiment	Feeding duration
Short-term high-fat exposure	One week: HFD versus CD feeding
Long-term high-fat exposure	24 weeks: HFD versus CD feeding
HF-recovery feeding	One week CD feeding subsequent to 24 weeks HFD versus CD feeding

Abbreviations: HF(D) high-fat (diet), CD control diet

Genetic obesity

Mice with mutations in the obese (*ob*) and the melanocortin-4 receptor (*Mc4r*) gene were used as murine models of monogenetic obesity. Both mutant strains were on a C57BL6/J background and bred in house (C57BL6/J founder breeding pairs were purchased from Charles River Laboratories Inc.). Body mass development was controlled every two weeks. Body composition and glucose tolerance were assessed prior to dissection.

Leptin deficient Lep$^{ob/ob}$ mice

Founder breeding pairs (B6.V-Lep^{ob}/J) were originally purchased from the Jackson Laboratory Inc. Experimental mice derived from heterozygous breeding pairs and were homozygous for the wildtype (wt, Lep$^{wt/wt}$) or the mutated allele (Lep$^{ob/ob}$). Genotyping was performed according to Table 6-2 and 6-4. Mice were maintained on chow until killing at the age of 14 weeks.

Mc4r W16X knockin mice

Mice carrying the human obesity-associated *Mc4r* nonsense mutation W16X (Marti *et al.*, 2003) were generated by gene targeting by Dr. Florian Bolze (Bolze *et al.*, 2013). Experimental mice derived from heterozygous breeding pairs and were homozygous for the wildtype (wt, Mc4r$^{wt/wt}$) or the mutated allele (Mc4r$^{X16/X16}$). Genotyping was performed according to Table 6-2 and Table 6-5. At the age of seven weeks Mc4r$^{X16/X16}$ mice and Mc4r$^{wt/wt}$ littermates were switched from chow to CD. Mice were killed at the age of 32 weeks.

Generation of *Hspd1*$^{flox/flox}$-*AdipoQ*CreER^{T2+} mice

Hspd1$^{flox/flox}$ and *Adipoq*CreER^{T2+} mice, both on C57Bl/6N background, were mated. Breeding was conducted in close cooperation with the group of Prof. Dr. Dirk Haller (Chair of Nutrition and Immunology, Technische Universität München). Genotyping was performed as demonstrated in Table 6-3, 6-6, 6-7.

Hspd1$^{flox/flox}$

The *Hspd1*$^{flox/flox}$ mouse was generated by Taconic-Artemis in collaboration with Prof. Dr. Dirk Haller. In this model exon 4-8 of *Hspd1* (encoding HSP60) are flanked by *loxP* sites leading to a frameshift downstream exon 3 upon induction of Cre-*loxP* site-specific recombination, removing parts of the GroEL chaperone, the ATPase domain, and by generating a frameshift downstream of exon 3. This should result in loss-of-function of the *Hspd1* gene (Berger, 2014).

*Adipoq*CreER^{T2+}

The *Adipoq*CreER^{T2+} mouse was created and kindly provided by Univ. Prof. Dr. Christian Wolfrum (Eidgenössische Technische Hochschule Zürich). Mice are hemizygous for the transgene CreER^{T2} (Cre, causes recombination, fused to a mutated human estrogen

receptor binding domain, ER^{T2}). The mutated receptor is highly sensitive to 4-hydroxytamoxifen, the active metabolite of the synthetic prodrug tamoxifen (Feil *et al.*, 1997).

Tamoxifen-induced genomic recombination and monitoring

At the age of 16 weeks *Hspd1*$^{flox/flox}$-*Adipoq*CreER^{T2+} mice and respective -CreER^{T2-} controls were subjected to experimental feeding for 6 weeks (Figure 6-1).

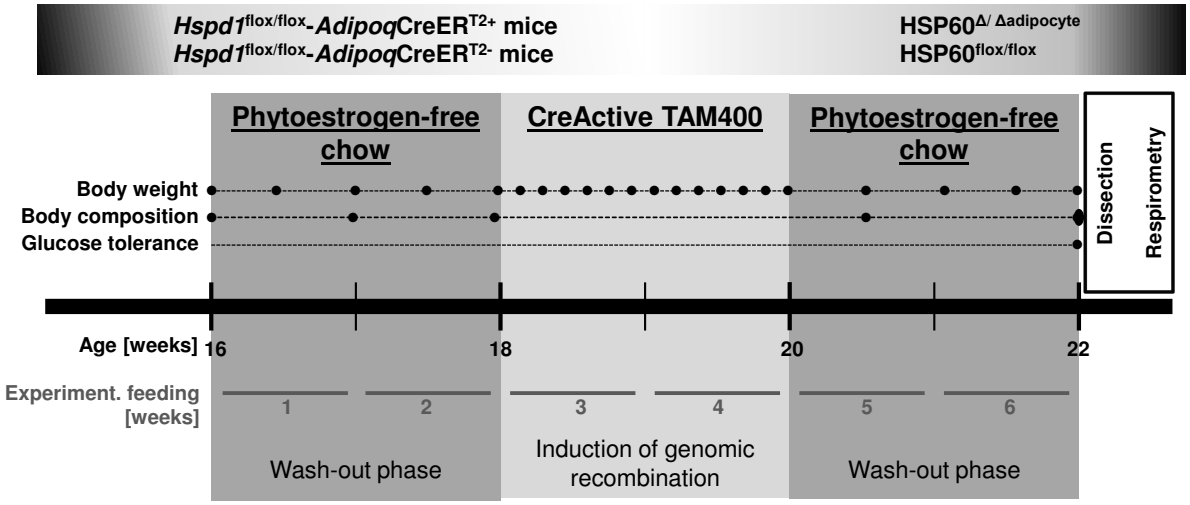

Figure 6-1. Experimental design and metabolic monitoring of *Hspd1*$^{flox/flox}$-*Adipoq*CreER^{T2+} mice and -CreER^{T2-} controls (nomenclature at the beginning of the experiment)/ HSP60$^{\Delta/\Delta adipocytes}$ and HSP60$^{flox/flox}$ controls (nomenclature at the end of the experiment). CreActive TAM400= tamoxifen containing diet (400 mg/kg).

In week 1 and 2 mice received phytoestrogen-free chow (PEF, V1154-300), to exclude effects of phytoestrogens on the outcome of our study. In week 3 and 4 mice received tamoxifen containing CreActive TAM400 diet (400 mg/kg tamoxifen, LASvendi), to induce Cre-mediated recombination. After successful knockout induction, mice were termed HSP60$^{\Delta/\Delta adipocytes}$ and HSP60$^{flox/flox}$ controls. In week 5 and 6 mice again received PEF, to avoid effects of both tamoxifen and phytoestrogens on the outcome of our study (Hesselbarth, 2015), and to provide enough time for the development of any metabolic alterations associated with HSP60 knockout. Over the whole period, body weight and body composition were monitored. At the end of experimental feeding (end of week 6) oral glucose tolerance was assessed and mice were killed.

6.1.3 GENOTYPING

Mutant mice were genotyped by polymerase chain reaction (PCR). Ear punches were lysed in genotyping-buffer at 65°C and 1,000 rpm overnight. Following, Proteinase K was inactivated by heat (95°C, 5 min). Buffer containing digested tissue was directly applied for PCR analysis (Table 6-2 to 6-7).

Genotyping-buffer 10 mM TRIS pH 8.3, 50 mM KCl, 0.45% Nonidet P40, 0.45% Tween 20, 0.2 mg/ml Proteinase K

Table 6-2. Standard genotyping PCR Mix 1 (one reaction)

Substance	Volume [µl]
2 x Immomix	10
Forward primer [10 pmol/µl]	1
Reverse primer [10 pmol/µl]	1
Nuclease-free water	7
Sample	1
∑	20

Table 6-3. Standard genotyping PCR Mix 2 (one reaction)

Substance	Volume [µl]
5x Crimson Taq Puffer	4
dNTPs [10 mM each]	0.4
$MgCl_2$ [25mM]	1.2
Forward primer [10 pmol/µl]	0.4
Reverse primer [10 pmol/µl]	0.4
CrimsonTaq [5U/µl]	0.1
Nuclease-free water	12.1
Sample	1
∑	20

Table 6-4. PCR program for B6.V-Lep^{ob}/J mutant line genotyping

PCR Program			
Step	**Temperature [°C]**	**Time [s]**	**Cycles**
Initial denaturation	94	180	
Denaturation	94	30	35
Anealing	62	60	
Elongation	72	45	
Final elongation	72	120	
Forward primer 5‘-TGTCCAAGATGG ACCAGACTC-3‘ Reverse primer 5‘-ACTGGTCTGAGGCAGGGAGCA-3‘			
Following PCR: digestion of PCR products by 10 U/µl Dde I, 3h, 37°C Program and primers adopted from the Jackson Laboratory, Bar Harbor, ME, USA			

Table 6-5. PCR program for Mc4r W16X mutant line genotyping

Step	Temperature [°C]	Time [s]	Cycles
Initial denaturation	95	420	
Denaturation	95	10	
Anealing	60	10	35
Elongation	72	25	
Final elongation	72	180	
Forward primer 5‘-CCTATGCCAAATGATACCCCACC-3‘			
Reverse primer 5‘-CTCTAAGATGAAATGAACGCTGGACC-3‘			

Table 6-6. PCR program for HSP60$^{flox/wt}$ mutant line genotyping

PCR Program			
Step	**Temperature [°C]**	**Time [s]**	**Cycles**
Initial denaturation	95		
Denaturation	95		
Anealing	58		35
Elongation	68		
Final elongation	68		
Forward primer 5‘-ACCAAGACCCTGTACTCTTAACC-3’			
Reverse primer 5‘-AACTTGACCTAGATGTTGTGTGG-3‘			

Table 6-7. PCR program for *Adipoq*CreER$^{T2\ Tg/wt}$ mutant line genotyping

PCR Program			
Step	**Temperature [°C]**	**Time [s]**	**Cycles**
Initial denaturation	94	420	
Denaturation	94	15	
Anealing	57	15	34
Elongation	72	30	
Final elongation	72	300	
Forward primer 5‘-GCGGTCTGGCAGTAAAAACTATC-3‘			
Reverse primer 5‘-GTGAAACAGCATTGCTGTCACTT-3‘			

6.1.4 METABOLIC PHENOTYPING

Determination of body mass and body composition

Body mass was measured regularly using a commercial balance. Body composition was measured with nuclear magnetic resonance spectroscopy (NMR, Bruker). Time points differed between mouse models and are indicated in 6.1.2.

Determination of oral glucose tolerance

After food deprivation for six hours (from 8 am to 2 pm), mice received 2.66 mg glucose per [g lean mass + (0.2 * g fat mass)] by single oral gavage (Even & Nadkarni, 2012). Blood glucose was monitored before, as well as 15, 30, 60, and 120 minutes after glucose administration using a standard glucometer (Abbott Diabetes Care). Therefore, blood droplets were obtained by careful incision of the tail tip using a commercial scalpel (Aesculap Inc.). Glucose tolerance was judged by both, absolute blood glucose levels at respective time points, and total area under the curve (AUC, calculated using the trapezoidal rule (Andrikopoulos *et al.*, 2008)), as suggested by Bowe *et al.* (Bowe *et al.*, 2014).

Analysis of plasma insulin, leptin, and adiponectin

For plasma preparation, cardiac blood was sampled from CO_2 anesthetized, non-fasted mice in heparin-coated tubes and centrifuged for 2 min at 2,000g. Supernatants were collected and frozen at -20°C. Plasma levels of insulin, leptin, and adiponectin were ascertained by commercial Enzyme Linked Immunosorbent Assay kits (ELISA, Christal Chem) validated for murine plasma samples. Procedures were conducted as described in the manufacturer's instruction (including dilution factors for determination of leptin and adiponectin). For determination of insulin levels, plasma was diluted as follows: $Lep^{ob/ob}$ 1:20, $Mc4R^{X16/X16}$ 1:10, HFD: 1:10, and undiluted plasma for lean controls and HF-recovery mice.

6.1.5 DISSECTION OF TISSUES AND ORGANS BEYOND WHITE ADIPOSE TISSUE

Interscapular brown adipose tissue, brain, kidney, heart, liver, and skeletal muscle (quadriceps) were dissected and weighed. Specimen of approximately 30 mg were frozen in liquid nitrogen and subsequently stored at -80°C.

6.2 STANDARD METHODS

6.2.1 DETERMINATION OF ADIPOCYTE SIZE – HEMATOXYLIN AND EOSIN STAINING OF HISTOLOGICAL SECTIONS

Immediately after dissection, posterior-subcutaneous and epididymal fat depots were transferred into fixing solution and incubated for 3-4 days at RT. Following, samples were dehydrated in an increasing ethanol/xylene series and infiltrated and embedded in paraffin (Leica, Table 6-8). Sections of 5 µM (rotary microtome, Leica) were mounted on microscope slides (Carl Roth) and dried for 24 h at 37°C.

Table 6-8. Programs for tissue dehydration, paraffin embedding, rehydration, and hematoxylin and eosin staining

Dehydration and paraffin embedding			Rehydration and H&E staining		
Step	**Substance**	**Time [min]**	**Step**	**Substance**	**Time [min]**
1	70% EtOH	60	1	Xylene	3
2	70% EtOH	60	2	Xylene	3
3	80% EtOH	60	3	100% EtOH	2
4	96% EtOH	60	4	96% EtOH	2
5	96% EtOH	60	5	70% EtOH	1
6	100% EtOH	60	6	dH_2O	1
7	100% EtOH	60	7	Hematoxylin	4
8	100% EtOH	60	8	dH_2O (running)	2
9	Xylene	60	9	Eosin	2
10	Xylene	60	10	70% EtOH	1
11	Paraffin	60	11	96% EtOH	1
12	Paraffin	60	12	100% EtOH	1
			13	100% EtOH	1.5
			14	Xylen+100% EtOH	1.5
			15	Xylene	2
			16	Xylene	2

After rehydration, tissue was automatically stained with hematoxylin and eosin (H&E) (Leica, Table 6-8). Stained sections were covered with a glass slip (Carl Roth). Adipocyte diameters were analyzed automatically on microscopic photographs (Leica) using WimAdipose, a macro specifically developed for image analysis of adipose tissue.

Fixing solution	4% para-formaldehyde, 2.4‰ picric acid in PBS

6.2.2 IMMUNOBLOT ANALYSIS

Protein extraction from cells and tissues

Snap-frozen tissue (~30 mg) and isolated adipocyte and SVF specimen (30 µl) were homogenized (ULTRA-TURRAX® IKA) in 200 µl iced Radioimmunoprecipitation assay buffer (RIPA). Homogenates were centrifuged at 16,000g for 10 min at 4°C. The protein containing supernatant was transferred into new tubes (in case of adipocytes, insulin syringes were used to punctuate the fat layer and harvest supernatants). Centrifugation was repeated at 10,000g for 10 min at 4°C. Supernatants were collected as described above. Protein concentration was determined using a commercial BCA kit (Thermo Scientific) according to the manufacturer's instructions (protein extracts from adipocytes and SVFs were used directly, protein extracts from brown adipose tissue, brain, heart, kidney, liver, skeletal muscle were diluted 1:15 in H_2O). Samples were stored at -20°C until further processing.

RIPA buffer	50 mM TRIS-HCl, NP-40 1%, 0.25% deoxycholic acid sodium salt, 150 mM NaCl, 1mM EDTA; pH 7.4 Freshly added: Protease Inhibitor Cocktail, Phosphatase Inhibitor Cocktail, both 1:200

Sample preparation

Protein extracts from tissues and cells (30 or 37.5 µg protein) were diluted in water to a final volume of 25 µl and filled up with sample buffer to 50 µl. Isolated mitochondria (25 µg protein) were diluted in water to a volume of 8 µl and filled up with denaturing buffer to 16 µl. For OXPHOS immunoblot analysis samples were incubated for 5 min at 50°C under agitation (500 rpm) referring to manufacturer's information. In all other cases protein denaturation was achieved by incubation for 5 minutes at 95°C and agitation of 500 rmp.

Denaturing buffer (2x)	17.75 ml H_2O 17.75 ml, 6.25 ml 0.5M TRIS-HCl, 12.5 ml Glycerin, 10 ml 10% SDS, 0.5% Bromphenol blue Freshly added: 5% β-Mercaptoethanol

Sodium dodecyl sulfate polyacrylamide gel electrophoresis, western blot, and immunodetection

Proteins were separated by sodium dodecyl sulfate polyacrylamide gel electrophoresis (SDS-PAGE). Following separation, proteins were transferred from SDS gels onto nitrocellulose membranes (LI-COR Biosciences). Two different vertical electrophoresis and transfer systems were used depending on the number of samples analyzed (Table 6-9). Unspecific binding sites of immunoblots were blocked by incubation in 3% BSA in TBS for 2 hours at RT. Afterwards, membranes were incubated with primary antibody solution overnight, 4°C (Table 6-14). Membranes were washed 5 times in TBST before incubation with infrared dye-conjugated secondary antibody solution (LI-COR Biosciences) for 1h at RT (Table 6-14). After washing twice with TBS and three times with TBST, proteins of interest were analyzed using the Odyssey infrared imaging system (LI-COR Biosciences).

Table 6-9. Electrophoresis and transfer systems used for immunoblot analysis

	≤ 15 samples	**>15 samples**
Resolving Gel [12.5%]	Mini-Protean System®	Perfect blue™ double gel system
Reagent	Volume [ml]	Volume [ml]
Rotiphorese® Gel 30	4.17	12.52
Resolving gel buffer	1.25	3.76
H_2O	4.43	0.30
SDS (10%)	0.1	0.15
AMPS (10% in H_2O)	0.05	0.015
TEMED	0.005	
Resolving Gel [7.5%]		
Reagent	Volume [ml]	
Rotiphorese® Gel 30	2.5	
Resolving gel buffer	1.25	
H_2O	6.1	
SDS (10%)	0.1	
AMPS (10% in H_2O)	0.05	
TEMED	0.005	
Stacking gel [5%]		
Reagent	Volume [ml]	Volume [ml]
Rotiphorese® Gel 30	0.8	2.4
Stacking gel buffer	1.25	3.75
H_2O	3.16	8.58
SDS (10%)	0.05	0.15
AMPS (10% in H_2O)	0.03	0.09
TEMED	0.01	0.03
Transfer system	Tank system	Semi-dry system
	100 V, 60 min	0.8 mA*cm^2, 45 min

Electrophoresis buffer (10x)	2.5 M Glycine, 0.25 M TRIS, 1% SDS
Transfer buffer	48 mM TRIS, 21 mM Glycine, 1.3 mM SDS, 20% Methanol, pH 9.2
TBST	TBS pH 7.6 + 1% Tween 20

6.3 STATISTICS AND DATA PRESENTATION

Statistical significance was assessed by two-tailed Student's t-test, One-Way ANOVA, Two-Way ANOVA, and Two-Way repeated measures ANOVA (Table 6-10).

Table 6-10. Statistical tests used for data analysis

Statistical test	Data	Software
Two-tailed Student's t-test	RCRs, body mass and composition, AUC, organ and tissue masses, protein and mRNA levels, CS activity, mDNA/nDNA	GraphPad Prism6
One-Way ANOVA (Tukey's multicomparison test)	HF-recovery mice before and after refeeding CD vs. controls: body mass, body composition, AUC	SigmaStat 12.5
Two-Way ANOVA (Bonferroni correction)	Plasma leptin, adiponectin, insulin	SigmaStat 12.5
Two-Way repeated measures ANOVA (Bonferroni correction)	Bioenergetic profiles, glucose clearance rates, body weight development	SigmaStat 12.5

When data failed the normality test, log-transformation was performed [log (x+1)] prior to statistical testing. Data are presented as means ± standard deviation (SD). All diagrams were generated using GraphPad Prism 6. Significance was accepted at p-values < 0.05.

Significance levels: $p < 0.05$ = *, $p < 0.01$ = **, $p < 0.001$ = ***.

REFERENCES (APPENDIX 6.1 - 6.3)

Andrikopoulos, S., Blair, A. R., Deluca, N., Fam, B. C. & Proietto, J. 2008. Evaluating the glucose tolerance test in mice. *Am J Physiol Endocrinol Metab,* 295, E1323-1332.

Berger, E. 2014. Impact of unfolded protein responses on intestinal epithelial homeostasis in genetically modified mouse models. *Verlag Dr. Hut*.

Bolze, F., Rink, N., Brumm, H., Kuhn, R., Mocek, S., Schwarz, A. E., Kless, C., Biebermann, H., Wurst, W., Rozman, J. & Klingenspor, M. 2013. Characterization of the melanocortin-4-receptor nonsense mutation W16X in vitro and in vivo. *Pharmacogenomics J,* 13, 80-93.

Bowe, J. E., Franklin, Z. J., Hauge-Evans, A. C., King, A. J., Persaud, S. J. & Jones, P. M. 2014. Metabolic phenotyping guidelines: assessing glucose homeostasis in rodent models. *J Endocrinol,* 222, G13-25.

Even, P. C. & Nadkarni, N. A. 2012. Indirect calorimetry in laboratory mice and rats: principles, practical considerations, interpretation and perspectives. *Am J Physiol Regul Integr Comp Physiol,* 303, R459-476.

Feil, R., Wagner, J., Metzger, D. & Chambon, P. 1997. Regulation of Cre recombinase activity by mutated estrogen receptor ligand-binding domains. *Biochem Biophys Res Commun,* 237, 752-757.

Hesselbarth, N. P., C; Kunath, A; Böge, E; Kern, D; Kern, M; Klöting, N 2015. Tamoxifen: how it influences adipocyte biology in vivo. *Keystone Symposia 2015,* Beige and Brown Fat: Basic Biology and Novel Therapeutics, 56.

Marti, A., Corbalan, M. S., Forga, L., Martinez, J. A., Hinney, A. & Hebebrand, J. 2003. A novel nonsense mutation in the melanocortin-4 receptor associated with obesity in a Spanish population. *Int J Obes Relat Metab Disord,* 27, 385-388.

6.4 MATERIAL

6.4.1 DIETS

Table 6-11. Experimental diets

Name	Product code	Company
Chow type M-Z	V1124	Ssniff, Soest, Germany
Phytoestrogen-free chow	V1154-300	Ssniff, Soest, Germany
Purified control diet (Figure 6-2A)	S5745-E702	Ssniff, Soest, Germany
Purified high-fat diet (Figure 6-2B)	S5745-E712	Ssniff, Soest, Germany
LASCRdiet™ CreActive TAM400	---	LASvendi, Soest, Germany

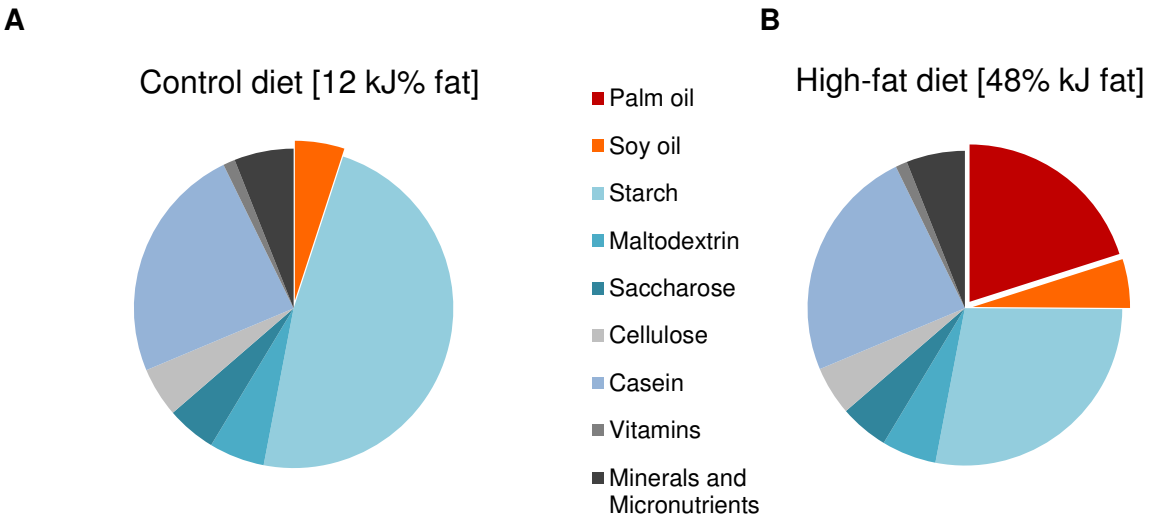

Figure 6-2. Composition of purified experimental diets.
(A) Control diet (#S5745-E702)
(B) High-fat diet (#S5745-E712). Diets were custom-made by Ssniff Spezialdiäten GmbH, Soest, Germany.

6.4.2 CHEMICALS

Table 6-12. List of chemicals

Name	Product code	Company
Acetyl-CoA (Acetyl coenzyme A sodium salt)	A2056	Sigma-Aldrich, St.Louis, MO, USA
ADP (Adenosine 5'-diphosphate sodium salt bacterial)	A2754	Sigma-Aldrich, St.Louis, MO, USA
Agarose	114046	Serva, Heidelberg, Germany
Amplex® Red	A12222	Invitrogen, life technologies, Carlsbad, CA, USA
AMPS (Ammoniumperoxide disulfate)	9593.2	Carl Roth, Karlsruhe, Germany
Antimycin A	A8674	Sigma-Aldrich, St.Louis, MO, USA
Bromphenol blue	A512.1	Carl Roth, Karlsruhe, Germany
BSA (Albumin fraction V)	8076.2	Carl Roth, Karlsruhe, Germany
BSA (bovine serum albumin essentially fatty acid free, ≥98%)	A 3803	Sigma-Aldrich, St.Louis, MO, USA
Collagen A solution (1mg/ml)	L7220	Biochrom, Berlin, Germany
Deoxycholic acid sodium salt	3484.1	Carl Roth, Karlsruhe, Germany
Digitonin	D1415	Sigma-Aldrich, St.Louis, MO, USA
DMSO	2189.2	Carl Roth, Karlsruhe, Germany
DNA-Ladder 100 bp	T833	Carl Roth, Karlsruhe, Germany
DTNB (5,5'dithiobis(2-nitrobenzoic acid)	D21800	Sigma-Aldrich, St.Louis, MO, USA

EDTA	8043.2	Carl Roth, Karlsruhe, Germany
EGTA	3054.2	Carl Roth, Karlsruhe, Germany
Ethanol >99.8%	9065	Carl Roth, Karlsruhe, Germany
Ethanol 70%	T913.3	Carl Roth, Karlsruhe, Germany
FCCP (Carbonyl cyanide-4-trifluoromethoxy)phenylhydrazone)	C2920	Sigma-Aldrich, St.Louis, MO, USA
Glucose solution 20%	03158931	B. Braun, Melsungen, Germany
Glycerin	3783.1	Carl Roth, Karlsruhe, Germany
HBSS (Hank's balanced salt solution, 1x)	14025-092	Gibco®, live technologies, Carlsbad, CA, USA
HEPES ((4-(2-hydroxyethyl)-1-piperazineethanesulfonic acid)	H 7523	Sigma-Aldrich, St.Louis, MO, USA
Hydrogen peroxide (H_2O_2)	8070	Carl Roth, Karlsruhe, Germany
ImmoMix	BIO-25020	Bioline, Luckenwalde, Germany
Lactobionic acid	L2398	Sigma-Aldrich, St.Louis, MO, USA
Malate	M9138	Sigma-Aldrich, St.Louis, MO, USA
Magnesiumchlorid Hexahydrat ($MgCl_2$ x $6H_2O$)	2189.2	Carl Roth, Karlsruhe, Germany
2-Mercaptoethanol	4227	Carl Roth, Karlsruhe, Germany
Methanol	4627.5	Carl Roth, Karlsruhe, Germany
MOPS 3-(N-morpholino)propanesulfonic acid)	6979	Carl Roth, Karlsruhe, Germany
Nonidet®P40	74385	Fluka Analytica, via Sigma Aldrich
Nuclease-free water	P119c	Promega, Madison, Wi, USA
Oligomycin	O4876	Sigma-Aldrich, St.Louis, MO, USA
Oxaloacetate	O4126	Sigma-Aldrich, St.Louis, MO, USA
Palmitoyl-L-carnitine chloride	P1645	Sigma-Aldrich, St.Louis, MO, USA
Phenol:Chloroform-Isoamylalcohol (25:24:1)		Carl Roth, Karlsruhe, Germany
Phosphatase inhibitor cocktail	P5726	Sigma-Aldrich, St.Louis, MO, USA
Potassium chloride (KCL)	6781	Carl Roth, Karlsruhe, Germany
Potassium hydroxide (KOH)	P1767	Sigma-Aldrich, St.Louis, MO, USA
Potassium lactobionate	153516	Sigma-Aldrich, St.Louis, MO, USA
Potassium phosphate monobasic (KH_2PO_4)	3904.1	Carl Roth, Karlsruhe, Germany
Protease inhibitor cocktail	P8340	Sigma-Aldrich, St.Louis, MO, USA
Rotiphorese® Gel 30	3029	Carl Roth, Karlsruhe, Germany
Roti®-Quant	K015	Carl Roth, Karlsruhe, Germany
Roti®-Histokitt	6638.1	Carl Roth, Karlsruhe, Germany
Rotenone	R8875	Sigma-Aldrich, St.Louis, MO, USA
Safranin O	S884	Sigma-Aldrich, St.Louis, MO, USA
SDS (sodium dodecyl sulfate)	4360.2	Carl Roth, Karlsruhe, Germany
SensiMix SYBR No-ROX	QT650-05	Bioline GmbH, Luckenwalde,Germany
Sodium chloride	T879.2	Carl Roth, Karlsruhe, Germany
Sodium dithionite	13351	Riedel-de Häen, Honeywell, Seelze, Germany
Sodium phosphate dibasic	255793	Sigma-Aldrich, St.Louis, MO, USA
Sodium phosphate monobasic	S3139	Sigma-Aldrich, St.Louis, MO, USA
Sodium pyruvate	P2256	Sigma-Aldrich, St.Louis, MO, USA
D(+)-Sucrose	4621	Carl Roth, Karlsruhe, Germany
Succinate	S3674	Sigma-Aldrich, St.Louis, MO, USA
Taurine	4721.1	Carl Roth, Karlsruhe, Germany
TEMED	2367	Carl Roth, Karlsruhe, Germany
TRIS	4855.2	Carl Roth, Karlsruhe, Germany
TRIS-HCl	9090	Carl Roth, Karlsruhe, Germany
Tween 20	9127	Carl Roth, Karlsruhe, Germany

6.4.3 ENZYMES

Table 6-13. List of enzymes

Name	Product code	Company
Collagenase A	10103586001	Roche Diagnostics, Unterhaching, Germany
Peroxidase from horseradish (HRP)	P8375	Sigma-Aldrich, St.Louis, MO, USA
Proteinase K (20 mg/ml)	EO0491	Thermo Scientific, Waltham, MA, USA
Superoxide dismutase (SOD)	S5639	Sigma-Aldrich, St.Louis, MO, USA

6.4.4 ANTIBODIES

Table 6-14. List of antibodies

Target	MW [kDa]	Host	Dilution factor	Product Code	Company
Primary antibodies					
Actin	43	Mouse	5000	MAB1501	Millipore
Porin (VDAC)	~31	Rabbit	900	PC548T	Calbiochem
COXIV	17	Rabbit	5000	4844	Cell Signaling
Citrate synthase	~52	Rabbit	1000	ab96600	Abcam
Histone H3		Rabbit	2000	4499	Cell Signaling
HSP60 (N20)	60	Goat	2000	Sc-1052	Santa Cruz
OXPHOS		Mouse	250	MS604	MitoSciences
SOD2	25	Mouse	10000	Ab16956	Abcam
UCP1	32	Rabbit	10000		
Secondary antibodies					
IRDye® 680 Donkey anti-Mouse IgG		Donkey	20000	926-32222	LI-COR Biosciences
IRDye® 680 Goat anti-Rabbit IgG (H + L)		Goat	20000	926-32221	LI-COR Biosciences
IRDye® 800 Donkey anti-Mouse IgG (H + L)		Donkey	20000	926-32212	LI-COR Biosciences
IRDye® 800 IgG Donkey anti-Goat IgG (H+L)		Donkey	20000	926-32214	LI-COR Biosciences

MW molecular weight, COXIV cytochrome c oxidase subunit 4, HSP60 heat shock protein 60, OXPHOS oxidative phosphorylation, SOD2 superoxide dismutase 2, UCP1 uncoupling protein 1, VDAC voltage-dependent anion channel.

6.4.5 EQUIPMENT & MATERIAL

Table 6-15. List of equipment and material

Item	Name	Company
Balances	Precision TP-214	Denver Instrument, Brentwood
	Laboratory balance PB Präpraum	Kern, Bailingen, Germany
Blood glucose monitoring system	Freestile lite	Abbott Diabetes Care, Alamenda, CA, USA
Blotting paper	GB003	Whatman – part of GE Healthcare, Stockholm, Sweden
Centrifuges	Centrifuge 5810R	Eppendorf, Hamburg, Germany
	Centrifuge 5417R	Eppendorf, Hamburg, Germany
	Sorvall Evolution RC	Thermo Scientific, Waltham, MA, USA
	Sorvall Discovery 90	Thermo Scientific, Waltham, MA, USA
	Zellkulturzentrifuge	
Centrifuge tubes	Oak Ridge Centrifuge Tubes,	Nalgene Thermo Scientific,

	50 ml	Waltham, MA, USA
Electrophoresis chamber	Mini-Protean® System	Bio-Rad, Hercuels, CA, USA
	PerfectBlue™ double gel system	PEQLAB B
Gas chamber	Custom-made	
Glass-glass homogenizer	S 15 ml	Sartorius, Göttingen, Germany
Heparin-coated tubes	Microvette® CB300CH	Sarstedt, Nürnberg, Germany
Imaging system	Odyssey® infrared imaging system	LI-COR® Biosciences, Lincoln, NE, USA
Incubator	WiseCube® WIS-20	Wisd laboratory instruments, Witeg, Wertheim, Germany
Insulin syringe	Myjector 1ml	Terumo Corporation, Shibuya, Yapan
Respirometer	Oxygraph-2k	OROBOROS INSTRUMENTS, Innsbruck, Austria
	XF96 Extracellular Flux Analyzer with XF96 FluxPak	Seahorse Bioscience, MA, USA
Magnetic stirrer	RCT basic IKAMAG® safety control	IKA®, Staufen, Germany
Microplate reader	Infinite® 200	Tecan, Männedorf, Switzerland
Microtome	RM2255 rotary microtome	Leica Mikrosysteme Vertrieb GmbH, Wetzlar, Germany
Microscope	Leica DMI4000B	Leica Mikrosysteme Vertrieb GmbH, Wetzlar, Germany
Microscope coverglasses		Carl Roth, Karlsruhe, Germany
Microscope slides		Carl Roth, Karlsruhe, Germany
Multistainer	Multistainer ST5020	Leica Mikrosysteme Vertrieb GmbH, Wetzlar, Germany
Multi-well plates	FLUOTRAC™ 200	Greiner Bio-One, Frickenhausen, Germany
	FrameStar 384	4titude, Surrey®, UK
	Infinite® 200 NanoQquant	Tecan, Männedorf, Switzerland
	LightCycler® Multiwell plate 96	Roche, Basel, Switzerland
	NUNC F96 transparent	Thermo Fisher Scientific, Waltham, MA, USA
	XF96-PS Cell Culture Microplates	Seahorse Bioscience, MA, USA
Nitrocellulose membrane		LI-COR® Biosciences, Lincoln, NE, USA
NMR spectrometer	The minispec mq7.5POY Live Mice Analyzer	Bruker, Billerica, MA, USA
Nylon mesh	250 µM	Schwegmann Filtrations-Technik Grafschaft-Gelsdorf, Germany
pH meter	CyberScan pH 510	Eutech Instruments, Singapore
Pipets	Multipette® stream	Eppendorf, Hamburg, Germany
	Pasteur pipettes	Brand, Wertheim, Germany
	Research®	Eppendorf, Hamburg, Germany
Power supply	PowerPAC™ Basic	Bio-Rad, Hercuels, CA, USA
Ultra-Turrax	ULTRA-TURRAX® T8	IKA®, Staufen, Germany
Scalpel	Stainless Steel 5518040	Aesculap Inc., Center Valley, PA, USA
Semi-dry transfer cell	Trans-Blot® SD Semi-Dry	Bio-Rad, Hercuels, CA, USA
Shaker	VXR basic Vibrax®	IKA®, Staufen, Germany
Syringes	Microliter™ Syringe #701	Hamilton, Reno, NV, USA
Thermocycler	Mastercycler® ep realplex epgradient S	Eppendorf, Hamburg, Germany

	LightCycler® 96, 480	Roche, Basel, Switzerland
Tissue Processor	Semi-enclosed Benchtop Tissue Processor (TP1020)	Leica Mikrosysteme Vertrieb GmbH, Wetzlar, Germany

6.4.6 KITS

Table 6-16. List of kit systems

Name	Product code	Company
BCA Protein assay kit	23227	Pierce™, Thermo Scientific, Waltham, MA, USA
Bradford Roti®-Quant	K015.1	Carl Roth, Karlsruhe, Germany
Mouse Adiponectin ELISA kit	80569	Chrystal Chem, Downers Grove, IL, USA
Mouse Insulin ELISA kit		Chrystal Chem, Downers Grove, IL, USA
Mouse Leptin ELISA kit	90030	Chrystal Chem, Downers Grove, IL, USA
Wizard® SV Genomic DNA Purification System	A2360	Promega, Fitchburg, WI, USA

6.4.7 SOFTWARE

Table 6-17. List of software

Name/Version	Company
DatLab 5	OROBOROS INSTRUMENTS, Innsbruck, Austria
GraphPad PRISM 6	GraphPad Software, Inc. La Jolla, CA, USA
LightCycler® 480 SW 1.5	Roche, Basel, Switzerland
Office 2010	Microsoft Corporation, Redmond, WA, USA
Seahorse *XF96* Software	Seahorse Bioscience, MA, USA
SigmaPlot 12.5	Systat Software, Inc. San Jose, CA, USA
Tecan i-control 1.4	Tecan, Männedorf, Switzerland
Tecan Magellan	Tecan, Männedorf, Switzerland
WimAdipose	Wimasis GmbH, Munich, Germany

6.5 PROTOCOL EXTRACELLULAR FLUX ANALYZER

Table 6-18. Bioenergetic profiling of isolated mitochondria

Protocol Steps			
Start Protocol			
	Command	**Time (min)**	**Port (Substance)**
	Calibrate	0,0	
	Mix	1,0	
	Wait	3,0	
	Mix	0,5	
	Measure	3,0	
	Mix	0,5	
	Measure	3,0	
	Mix	0,5	
	Inject		**A (ADP)**
	Mix	1,0	
	Measure	3,0	
	Mix	0,5	
	Measure	3,0	
	Mix	0,5	
	Inject		**B (Oligomycin)**
	Mix	1,0	
	Measure	3,0	
	Mix	0,5	
	Measure	3,0	
	Mix	0,5	
	Inject		**C (FCCP)**
	Mix	1,0	
	Measure	3,0	
	Mix	0,5	
	Measure	3,0	
	Mix	0,5	
	Inject		**D (Antimycin A, Rotenone)**
	Mix	1,0	
	Measure	3,0	
	Mix	0,5	
	Measure	3,0	
	Mix	0,5	
End Protocol			

6.6 LETTERS OF APPROVAL

6.6.1 LETTER OF APPROVAL - ENDOCRINOLOGY, 2015 MAR;156(3):923-33

publication-based dissertation, letter of approval

ANTWORTEN ALLEN ANTWORTEN WEITERLEITEN

Kelly, Rebecca <RKELLY@ENDOCRINE.ORG>
Di 24.02.2015 16:15

Als ungelesen markieren

An: Schöttl, Theresa;

Dear Dr. Schottl,

The Endocrine Society allows authors to reproduce their own works in full for the purposes of inclusion in a PhD dissertation. It will be fine for you to use the data-set in this way.

Best wishes,
Rebecca Kelly

ENDOCRINE SOCIETY

Rebecca Kelly Managing Editor
2055 L STREET NW, SUITE 600, WASHINGTON, DC 20036
T. 202.971.3636 F. 202.736.9705 D. 202.971.3675
rkelly@endocrine.org endocrine.org

6.6.2 LETTER OF APPROVAL – MOLECULAR METABOLISM, 2015 JUL 21

[EPUB AHEAD OF PRINT]

Elsevier · Rosenstrasse 2 · 10178 Berlin · Germany

Theresa Schöttl
Molecular Nutritional Medicine,
Technische Universität München
Gregor-Mendel-Str. 2
D-85356 Freising-Weihenstephan
GERMANY

Elsevier GmbH

Executive Publisher
Thomas Schwarz-Romond
Dr. rer. nat.; MBA
Tel. +49 30 | 243 102 215
Fax +49 30 | 243 102 22
t.schwarz-romond@elsevier.com

Berlin, 15.07.2015

ELSEVIER

To whom it may concern,

In my role as Executive Publisher of Molecular Metabolism, I herewith and formally approve that the CC BY-NC-ND 4.0 license under which the article 'Limited OXPHOS capacity in white adipocytes is a hallmark of obesity in laboratory mice irrespective of the glucose tolerance status', authored by Schöttl et al. (doi 10.1016/j.molmet.2015.07.001) grants the rights to be included in a publication-based dissertation. This Elsevier Open Access license requires appropriate reference, citation of the original article source and restricts reuse, in whole or in parts, to an entirely non-commercial framework.

Please do not hesitate to contact me in case of remaining questions.

Yours truly,

Thomas Schwarz-Romond, PhD/MBA
Elsevier Journals,
Berlin office

Elsevier GmbH · Das Plus im Web: www.elsevier.com
Hackerbrücke 6 · 80335 München · Tel. +49 | 89 | 53 83-0 · Fax +49 | 89 | 53 83-609
Elsevier GmbH, München· HRB 152680 · USt.-ID. DE 180607607
Geschäftsführung: Olaf Lodbrok, Martin Beck

7 ACKNOWLEDGEMENTS

An allererster Stelle möchte ich mich bei Prof. Martin Klingenspor für die großartige Unterstützung während meiner Doktorarbeit, aber auch für die tolle Zusammenarbeit am Lehrstuhl für Molekulare Ernährungsmedizin im Allgemeinen bedanken. Seine wissenschaftliche Expertise war essentiell für diese Arbeit. Die Begeisterung für die Thematik, das kontinuierliche Interesse am Fortschritt dieses Projekts, sowie das Vertrauen und die Entfaltungsmöglichkeiten, die ich darin genießen durfte weiß ich wirklich sehr zu schätzen.

Als nächstes bedanke ich mich bei Dr. Tobias Fromme. Unsere zahlreichen Diskussionen über meine Projektplanung und Ergebnisinterpretation, sowie die stets konstruktive (!) Kritik von Tobis Seite waren und sind sehr wertvoll für mich und meine Arbeit.

Ich danke meinen Kooperationspartnern vom Lehrstuhl für Ernährung und Immunologie, Prof. Dr. Dirk Haller, Dr. Emanuel Berger, sowie Sandra Hennig für die hervorragende Zusammenarbeit im HSP60-Projekt.

ALLEN (aktuellen und ehemaligen) Kollegen am Lehrstuhl für Molekulare Ernährungsmedizin gebührt mein herzlicher Dank für die positive Arbeitsatmosphäre und die fruchtbaren Diskussionen. Besonderer Dank geht an: Monja, Flo, und Nadine für alle Antworten auf meine Fragen hinsichtlich Mauszucht; Tobi und Kerstin für Rat und Tat in Mitoangelegenheiten; meinen drei Masterstudentinnen Lisa, Delia und Kathi für ihren bemerkenswerten Einsatz und die tolle Zusammenarbeit.
Vielen lieben Dank an das Expertenteam Flo & Tobi für das Korrekturlesen meiner Arbeit!
Anika, Sabine und Philipp, sowie alle Tierpfleger vom Kleintierforschungszentrum Weihenstephan haben mich sehr unterstützt und mir den Alltag im Labor und Tierhaus erleichtert.

Der letzte Dank geht an meine Lieben, die mich auf verschiedenste Art und Weise unterstützt und geduldig begleitet haben. Das gilt nicht nur für die Zeit meiner Doktorarbeit, sondern auch für die Zeiten davor, in denen der Grundstein dafür gelegt wurde. Ihr habt es wunderbar hinbekommen, dass immer jemand da war.
Für all die kleinen und großen Hilfestellungen auf meinem Weg sage ich von ganzem Herzen DANKE!

Diese Arbeit wurde teilweise durch das Bildungsministerium für Bildung und Forschung finanziert (BMBF AZ 0315674).

8 CURRICULUM VITAE

9 DECLARATION OF AUTHORSHIP

EIDESSTATTLICHE ERKLÄRUNG

Ich erkläre an Eides statt, dass ich die bei der promotionsführenden Einrichtung Wissenschaftszentrum Weihenstephan für Ernährung, Landnutzung und Umwelt der TUM zur Promotionsprüfung vorgelegte Arbeit mit dem Titel:

Novel experimental strategies to assess the interplay between White adipocyte mitochondrial bioenergetics and systemic glucose homeostasis in C57BL/6 mice

am Lehrstuhl für Molekulare Ernährungsmedizin unter der Anleitung und Betreuung durch Univ.-Prof. Dr. Martin Klingenspor ohne sonstige Hilfe erstellt und bei der Abfassung nur die gemäß § 6 Abs. 6 und 7 Satz 2 angegebenen Hilfsmittel benutzt habe.

Ich habe keine Organisation eingeschaltet, die gegen Entgelt Betreuerinnen und Betreuer für die Anfertigung von Dissertationen sucht, oder die mir obliegenden Pflichten hinsichtlich der Prüfungsleistungen für mich ganz oder teilweise erledigt.

Ich habe die Dissertation in dieser oder ähnlicher Form in keinem anderen Prüfungsverfahren als Prüfungsleistung vorgelegt.

Die vollständige Dissertation wurde noch nicht veröffentlicht.

Ich habe den angestrebten Doktorgrad **noch nicht** erworben und bin **nicht** in einem früheren Promotionsverfahren für den angestrebten Doktorgrad endgültig gescheitert.

Die öffentlich zugängliche Promotionsordnung der TUM ist mir bekannt, insbesondere habe ich die Bedeutung von § 28 (Nichtigkeit der Promotion) und § 29 (Entzug des Doktorgrades) zur Kenntnis genommen. Ich bin mir der Konsequenzen einer falschen Eidesstattlichen Erklärung bewusst.

Mit der Aufnahme meiner personenbezogenen Daten in die Alumni-Datei bei der TUM bin ich einverstanden.

Freising, den .....

…..……
Unterschrift